THE UNIVERSITY OF WESTERN ONTARIO
DEPARTMENT OF CIVIL AND
ENVIRONMENTAL ENGINEERING

Water Resources Research Report

An Integrated System Dynamics Model for Analyzing Behaviour of the Social-Energy-Economic-Climatic System: Model Description

By:
M. K. Akhtar
S. P. Simonovic
J. Wibe
J. MacGee
And
J. Davies

Report No: 075
Date: August 2011

ISSN: (print) 1913-3200; (online) 1913-3219;
ISBN: (print) 978-0-7714-2896-8; (online) 978-0-7714-2903-3;

ABSTRACT

The feedback based integrated assessment model ANEMI represents the society-biosphere-climate-economy-energy system of the earth and biosphere. The development of ANEMI model is done using the system dynamics simulation approach that (a) allows understanding and modeling of complex global change and (b) assists in the investigation of possible policy options for mitigating, and/or adopting to global changing conditions, within an integrated assessment modeling framework. This report presents ANEMI model and its nine individual sectors: climate, carbon cycle, land-use, population, food production, hydrologic cycle, water demand, water quality, and energy-economy. Two versions of the model are developed and presented in the report. The first one represents the society-biosphere-climate-economy-energy system on a global level. The second one is developed for regional presentation of Canada. The development of Canada model is based on the top down approach and various disaggregation techniques. To evaluate market and nonmarket costs and benefits of climate change, ANEMI model integrates an economic approach, with a focus on the international energy stock and fuel price, with climate interrelations and temperature change. The market clearance mechanism of economy sector introduces optimization within the simulation framework, which makes the model unique and different from any other integrated assessment model available in the published literature. The model takes account of all major greenhouse gases (GHG) influencing global temperature and sea-level variation.

Several of the model sectors are built from the basic structure of the previous version of ANEMI. However, they are integrated in a novel way, the water sectors in particular. The integration of optimization within the simulation framework of the ANEMI model is timely, as recognition of the importance of energy based economic activities in determining long-term Earth-system behaviour grows. Experimentation with different policy scenarios demonstrated their consequences on future behaviour of the society-biosphere-climate-economy-energy

system through feedback based interactions. The use of ANEMI model improves both, scientific understanding and socio-economic policy development strategy.

This report describes the model structure in details and illustrates its use through the analysis of three policy scenarios.

Keywords: system dynamics simulation; feedback; climate change; integrated assessment modeling; society-biosphere-climate-economy-energy system ; Earth-system model; water resources management; disaggregation

ACKNOWLEDGEMENTS

We are grateful for the support of NSERC (Natural Sciences and Engineering Research Council of Canada) through its Strategic Research Grant to Professor Slobodan P. Simonovic and his collaborators, which funded development of the ANEMI model. We are also grateful for the input provided by the representatives of the federal Departments of Environment, Finance, Natural Resources, Fisheries and Oceans, and Agriculture, who were research partners in this work.

CONTENTS

LIST OF FIGURES

LIST OF TABLES

1 INTRODUCTION

This report presents the second version of a dynamic integrated assessment model of the social-economic-climatic system - ANEMI. It builds on the previous version of ANEMI model (Davies, 2007; Davies and Simonovic, 2008; 2009; 2010; 2011). The model development is done using the feedback based system dynamics simulation package, Vensim DSS (Ventana System, 2010a). In this version a very significant modeling change has been implemenetd in order to integrate a new economy-energy sector with other model sectors. System dynamics simulation with imbedded optimization is used that makes ANEMI an original integrated assessment tool. Integration process is supported through the use of MATLAB (Math Works, 2011) and Visual studio (Microsoft, 1998) programming tools.

Chapter 2 describes all individual model sectors in terms of theory, causal loop diagram and mathematical formulation. This chapter also holds a nice and brief description of the energy-economy sector and its own calibration procedure which is based on the use of optimization approach within the simulation model. The inter connections between different sectors with feedback loops are also presented in this part of the report. The model simulation results are compared with available literature and field measurements data in order to verify model performance.

Chapter 3 presents the regionalization of the global model. Both, temporal and spatial disaggregation methods are introduced. This chapter reviews each model sector from the disaggregation point of view.

Chapter 4 describes the implementation of the ANEMI model in policy analyses. The first section describes the policy scenarios with their background information. The second section describes the use of ANEMI for policy analyses. The global version of the ANEMI model is used first. The third section discusses the same policy experimentation in the context of Canada regional version of the model.

The detailed ANEMI user's manual is provided as a separate document (Akhtar et al, 2011).

2 GLOBAL MODEL DESCRIPTION

This model is an integrated assessment model, which describes the major characteristics of the climate, carbon cycle, land-use, water demand, water quality, natural hydrologic cycle, food production, energy-economy, and population subsystems of the larger society-biosphere-climate-economy-energy system.

In this version of the ANEMI model, all of the key processes of model sectors, whether socio-economic or physical, are modelled at the global scale. The simulated values are based on the spatially aggregated behaviour of model components. Caution is required in downscaling simulated aggregate behaviour to local or regional scales. It is clear that global population, economic growth, temperature change, and atmospheric carbon dioxide concentration are global variables in the ANEMI and therefore they do not capture important regional or local differences.

Within each individual sector or sub-sector, the model describes the relevant dynamics of individual system elements. At the intersectoral level of ANEMI, the individual model sectors are linked through mathematical feedbacks in order to describe the existing important dynamics of the Earth-system. The model simulation period starts from 1980 to 2100. The model time step is one year, providing a long-term view of the feedback effects of global change, sacrificing daily and seasonal variation. Several components of the model are original and several are based on available relevant models.

2.1 Individual Model Sectors

The main focus of ANEMI model is to capture the level of behavioural complexity by combining different sectors of socio-economic-climatic system through feedback mechanisms. The representation of all these sectors follows a structural approach, reproduces the important elements or processes of the physical system in question rather than simulating its behaviour

through mathematical, pattern-matching type behaviour. The structural approach allows for representation of the feedback relationships in a more scientific fashion.

Version 2 of the ANEMI model represents each sector either in zero-dimension or one-dimensional form. Dimensionality refers to the degree of aggregation in a sector. Zero-dimensional sectors model important characteristics and processes at a global-aggregate level, while one-dimensional sectors have one spatial direction. For example, the food production and population sectors produce single, global-aggregate values, and so are considered zero-dimensional. The oceans are modelled using vertical layers, and the terrestrial biomes are separated into six components, and so are one-dimensional sectors of the model.

The model consists of nine sectors: climate, carbon cycle, energy-economy, land-use, food production, population, hydrologic cycle, water demand, and water quality, which are of various levels of complexity. For example, the land-use and population sectors are relatively simple, while the carbon cycle and water-related sectors have much more complex structure. A very sophisticated energy-economy sector makes the model quite different from the conventional integrated assessment models. All the sectors of the ANEMI model are shown in Figure 2.1. The detailed description of all sectors follows.

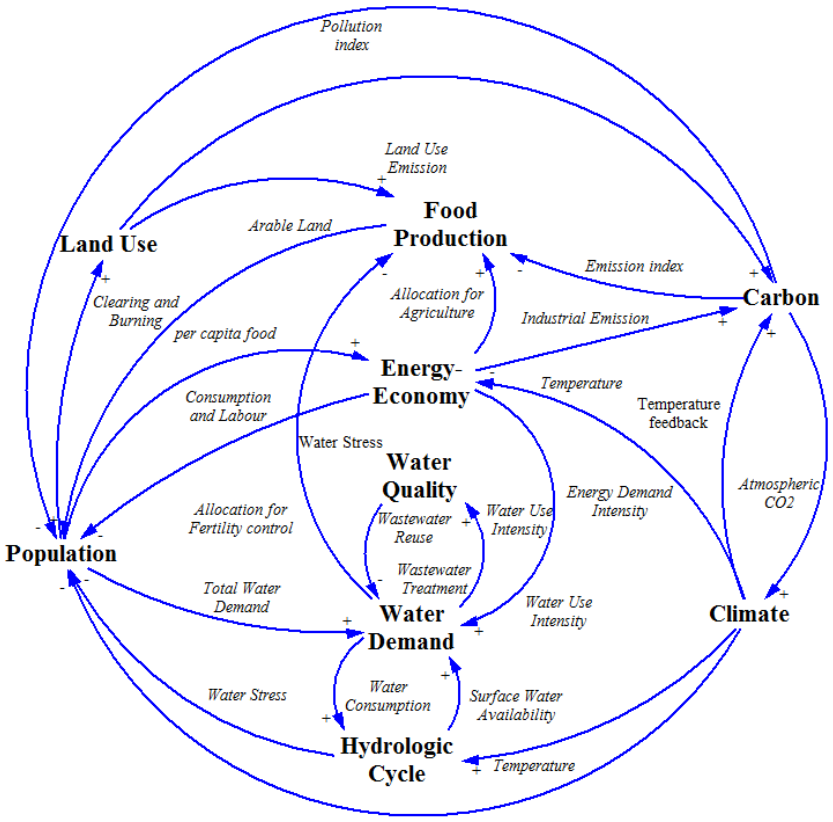

Figure 2.1: ANEMI model structure

2.1.1 The Climate Sector

The climate sector of the ANEMI model simulates the atmospheric and oceanic temperature changes due to the increase in anthropogenic CO_2 concentration. The climate sector is based on the upwelling-diffusion energy-balance model (UD/EBM) that builds on the Box Advection-Diffusion (BAD) model of Harvey and Schneider (1985a). Similar to other box-diffusion models, the BAD model focuses on the role of oceans in determining the global surface temperature response to climatic forcing, such as changes in anthropogenic greenhouse gas (GHG) emissions. The basic principles behind the energy balance model and box-model is available in McGuffie and Henderson-Sellers (2005).

The BAD model includes the important solar and terrestrial radiative energy exchanges between outer space, the atmosphere, and the oceanic surface layer; the infrared radiative,

and latent and sensible heat flows between the earth's surface and the atmosphere; and the diffusive and advective energy transfers within the ocean. As one dimensional model, BAD calculates energy transfers, and thus temperature differences, between the atmosphere, ocean surface (mixed layer), and various ocean depths. The temperature profile it generates at steady state – when external forcing are assumed equal to zero – matches that of the observed oceanic profile quite well. The BAD model also matches closely to the global surface temperature changes, which are predicted by GCMs and other complex models under climatic forcing (Harvey and Schneider, 1985a). For example, BAD has a climate sensitivity of roughly 1.8°C for atmospheric doubling of CO_2, or $2xCO_2$, concentrations, and uses a value of 4 W/m^2 for radiative forcing at $2xCO_2$. This climate sensitivity lies near the middle of a 1.0°C - 4.1°C temperature-change spectrum (Forster and Gregory, 2006). Therefore, if necessary, the forcing response in the climate sector can be adjusted easily through the model's reaction to radiative forcing. For example, the climate sensitivity becomes 2.0°C for a radiative forcing value of 4.37 W/m^2, as used in the IPCC SAR, or 1.7 °C for forcing of 3.7 W/m^2 or 3.80 ± 0.33 W/m^2, as recommended by the IPCC TAR (Houghton et al., 2001), and the IPCC AR4 (Meehl et al., 2007), respectively.

The version of BAD used in this research applies the constant values of oceanic thermal diffusivity, *K*, and advection velocity, *w*, suggested by Harvey and Schneider (1985a). There is one important difference between this version of the model and the original: the system dynamics-based stock-and-flow structure of the model necessitates the conversion of the climate sector from Harvey and Schneider's (1985a) temperature based equations, using *dT/dt*, to an energy-based approach, with energy stocks and flows, or *E* and *dE/dt*, measured in Joules, and Joules yr^{-1}. Several modifications to *K* and *w* are described in Harvey and Schneider (1985a), while structural changes exist in other upwelling-diffusion models (see Harvey and Huang, 2001, and Joos et al., 1997, for example). However, they are significantly more complicated than BAD and prove essentially irrelevant to the behaviour of the model as a whole, as determined by a Monte Carlo sensitivity analysis described in Davies and Simonovic (2008; 2010).

Climate sector of the ANEMI model version 2 described in this report has a 'switch', by which modeller can choose the complexity of the climate sector setup. The comprehensive one is adopted from the BAD model and includes detailed information, such as: longwave radiation, shortwave radiation, temperature at different depth of the ocean, latent heat fluxes and so on (Figure 2.2). The second option includes simplified setup (Figure 2.3) for computing atmospheric and oceanic temperature, based on DICE model (Nordhaus, 1994).

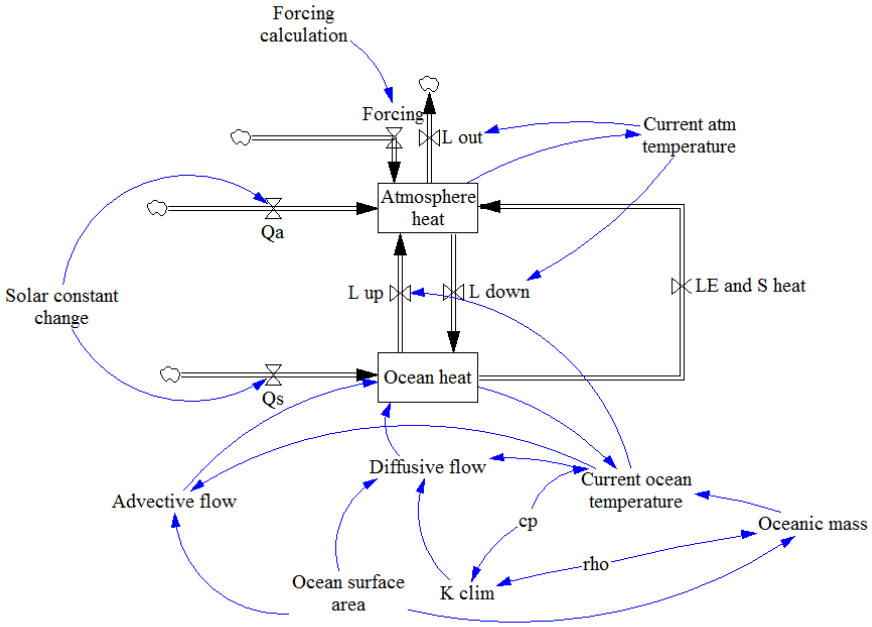

Figure 2.2: Model structure of the comprehensive climate sector

Nordhaus (1994) used a second-order, linear system, with three negative feedback loops. The first loop describes worming of the ocean while the remaining two transmit heat from the atmosphere and ocean surface. Deep ocean warming is a slow process, because the ocean has a large heat capacity. In this model structure radiative forcing from CO_2 is expressed as a logarithmic function of the atmospheric CO_2 concentration, while forcing from other gases are considered as exogenous variables based on the IPCC assumptions from the DICE model

(Nordhaus, 1994). The equilibrium temperature response to a change in radiative forcing is determined by the radiative forcing coefficient and the climate feedback parameter.

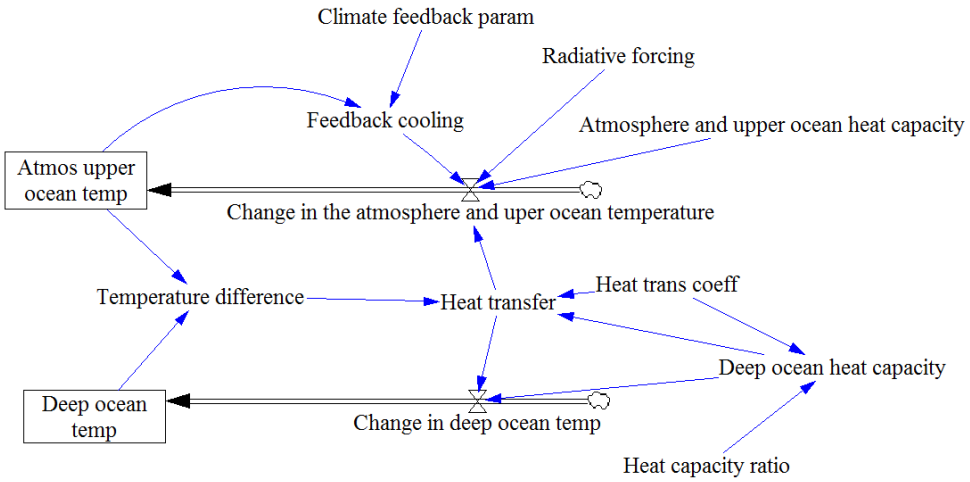

Figure 2.3: Model structure of the simplified climate sector (after Nordhaus, 1994)

Causal Structure of the ANEMI Model Climate Sector

The causal loop diagram for the climate sector is presented in **Error! Reference source not found.** (Comprehensive version) and Figure 2.5 (simplified version). In the ANEMI model, the comprehensive climate structure computes the atmospheric temperature from radiation absorbed by earth surface, latent heat flux, upward surface radiation. In this setup the ocean has 20 layers and the heat is transmitted through advective (heat flow represents global water upwelling) and diffusive (flow carries heat downwards into colder parts) processes.

The simpler structure of the climate sector transmits the heat from the atmosphere and upper ocean layer to the deep ocean based on temperature gradient and heat absorption capacity of the deep ocean. For the simplicity, here the model consists of only 2 layers, one for the atmosphere and upper ocean and the other for the deep ocean. In both cases the forcing/radiative forcing is one of the main contributors of atmospheric and upper ocean layer's temperature change, where the radiative forcing is produced from CO_2 and other GHG gas including CH_4 (methane), NO_2 (nitrous oxide), and CFC (chlorofluorocarbon).

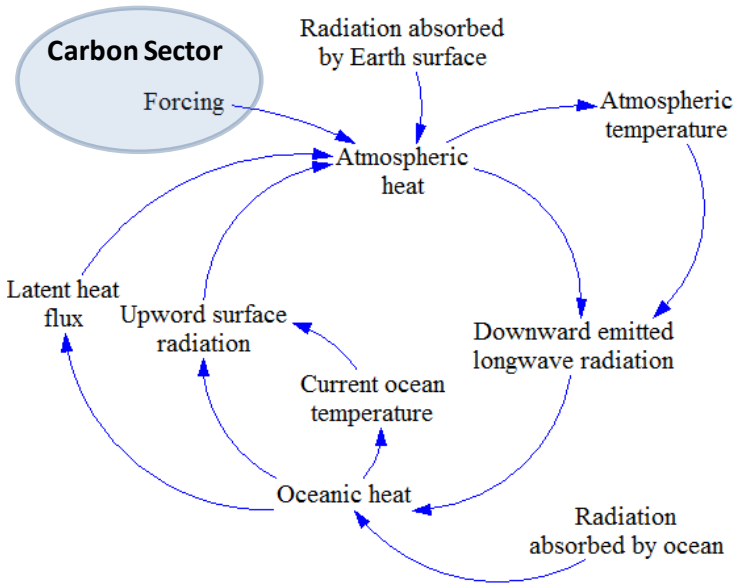

Figure 2.4: Causal loop diagram of the comprehensive climate sector

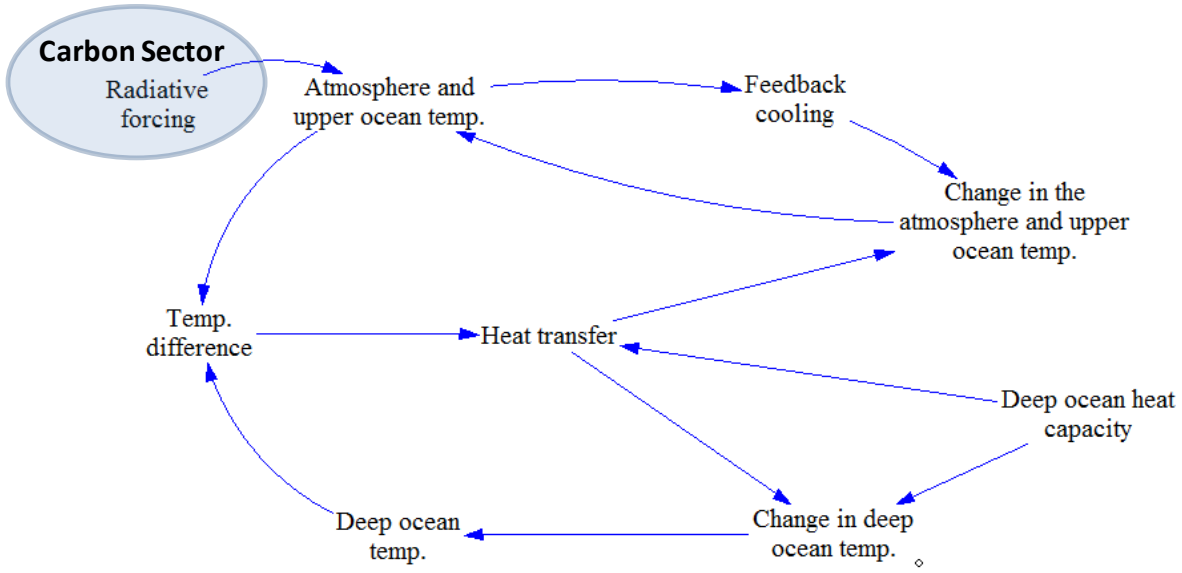

Figure 2.5: Causal loop diagram of the simplified climate sector

Mathematical Description of the ANEMI Climate Sector

The major equations of the ANEMI climate sector, and the values of their associated parameters, are provided in this section. The comprehensive version of climate sector description is based on the work of Harvey and Schneider (1985a).

The governing equation for the heat content of the *atmosphere* is:

$$H_A = \int (Q_A^* + L_\uparrow - L_\downarrow - L_{out} + H + LE + F) \cdot dt \qquad (2.1)$$

where H_A is the heat content of the atmosphere measured in Joules, with an initial value given by $R_A \cdot SA_E \cdot T_{A,0}$, or the atmospheric heat capacity R_A, 1.02 x 10^7 J m^{-2} K^{-1}, multiplied by the surface area of the Earth SA_E, 5.1 x 10^{14} m^2, and the initial temperature of the atmosphere $T_{A,0}$, 287.5 K. The other variables are the shortwave (solar) radiation absorbed by the atmosphere, Q_A^*, the upward emitted surface longwave (planetary) radiation, $L_\uparrow$, the downward emitted longwave radiation, $L_\downarrow$, the longwave radiation emitted to space from the top of the atmosphere, L_{out}, and the turbulent sensible and latent heat fluxes, *H* and *LE*, respectively. The value used for the shortwave radiation is a constant 66.9 W/m^2, while the other flows are calculated according to the following equations. All flows are measured in J yr^{-1}. Note that the last term, *F,* represents the radiative forcing from anthropogenic greenhouse gases, given by,

$$F = S\left(C_A / C_{A0}\right) - S \qquad (2.2)$$

where *F* is the climate forcing in W/m^2, *S* is a 'climate sensitivity' constant that relates the change in atmospheric CO_2 concentrations to *F*, and is set to 4 W/m^2, and C_A and C_{A0} represent the current and initial atmospheric carbon dioxide concentrations, respectively. Since equation (2.2) represents an intersectoral feedback, its full explanation is provided in the intersectoral feedback section of the text.

For the downward longwave radiation emitted by the atmosphere, Harvey and Schneider (1985a) use the Angström formula, which has the following form,

$$L_{\downarrow} = \sigma {T_A}^4 [0.89 - 0.2(10^{-0.07 e_a})] \quad (2.3)$$

where σ is the Stefan-Boltzman constant, 5.67 x 10^{-8} J m^{-2} K^{-2}, T_A is the current atmospheric temperature in Kelvin, and e_a is the atmospheric vapour pressure, measured in mbar.

The upward longwave radiation calculation is modelled as the blackbody radiation from the Earth's surface,

$$L_{\downarrow} = \sigma {T_S}^4 \quad (2.4)$$

where T_S is the surface temperature, also referred to as an 'equivalent mixed layer'(EML). Harvey and Schneider (1985a) used an EML depth of 30 m as the surface thermal inertia; this value is obtained by choosing a globally averaged mixed layer depth of 70 m (based on Manabe and Stouffer, 1980) and a thermal inertia equivalent to 1.7 m of water (Harvey and Schneider, 1985b), and taking an approximately equal weighting of the arithmetic and harmonic means of these two depths (for more details see Thompson and Schneider, 1979).

The longwave radiation to space is given by,

$$L_{out} = A + B \cdot T_A - C \cdot F_{CL} \cdot \Delta T_{S,CL} \quad (2.5)$$

which, is a parameterization of the more complex blackbody form. Here, A is set to -251 W/m^2, B equals 1.8 W/(m^2 K), C is 1.73 W/(m^2 K), F_{CL} represents the area-weighted mean annual cloud amount, set to 0.531, and $\Delta T_{S,CL}$ is the surface to cloud-top temperature difference, set to 32.34K.

The sensible and latent heat fluxes are based on drag laws, and have the following form,

$$H = C_1(T_S - T_A) \quad (2.6)$$

$$LE = C_2(e_S - e_A) \quad (2.7)$$

where C_1 equals 12.57 W/(m^2 K), C_2 is 11.75 W/m^2 per mbar, e_s is the surface saturation vapour pressure at surface temperature T_S, and e_a is the atmospheric vapour pressure using a fixed relative humidity of 0.71. The vapour pressures, e_s and e_a, are multiplied by factors of 1.39 and 1.31, respectively, to account for nonlinearity in the Clausius-Clapeyron relation. Base values for the two vapour pressures were taken from the "Goff-Gratch exact results" for the Clausius-Clapeyron relation, as suggested by Lowe (1977).

The equation that governs the mixed-layer in the ANEMI model differs slightly from the equation provided by Harvey and Schneider (1985a), although the effect is the same. The heat balance of the mixed-layer is given by,

$$H_M = \int \left(Q_S^* - L_\uparrow + L_\downarrow - H - LE + F_{adv} - F_{diff}\right) \cdot dt \quad (2.8)$$

where H_M is the heat content of the mixed-layer measured in Joules, with an initial value given by, $\rho \cdot c_p \cdot SA_0 \cdot h_M \cdot T_{S,0}$, or the density of sea water ρ , 1030 kg m^{-3}, multiplied by the specific heat capacity of water at constant pressure C_p, 4218 J kg^{-1} K^{-1}, the surface area of the ocean SA_0, 3.8 x 10^{14} m^2, the equivalent mixed-layer depth, 30 m, and the initial surface temperature $T_{S,0}$, 289.1 K. The new flows included in the equation are the solar radiation absorbed at the Earth's surface, Q_S*, with a constant value of 168.95 W/m^2, the upward advective heat flow in the oceans, F_{adv}, and the downward diffusive heat flow in the oceans, F_{diff}.

In the oceans, advective heat flow represents global water upwelling, while the diffusive flow carries heat downwards into colder layers. Essentially, diffusive flow would homogenize the temperature of the oceans over a long period of time, so that the bottom and surface water

would eventually have the same temperature, while advection maintains a temperature gradient between the surface and the bottom of the ocean. Both, advective and diffusive heat transfers decrease with depth as the temperature gradient between isothermal oceanic 'layers' becomes less steep.

The heat balance for each ocean layer in the model is given by,

$$H_0(h) = \int \left[\left(F_{adv} - F_{diff} \right)_{h+1} + \left(F_{diff} - F_{adv} \right)_{h-1} \right] \cdot dt \tag{2.9}$$

where $H_O(h)$ is the heat content of the selected oceanic layer, *h*, while the subscripts of the brackets around the pairs of flows on the right-hand side represent heat outflows from the current layer, *h*, to the colder, deeper layer, *h+1*, and heat inflows to the current layer, *h*, from the warmer, shallower layer, *h-1*. Recall that advective flows carry heat upwards in the ocean, while diffusive flows transport it downwards.

Advective flows between adjacent isothermal layers take the following general form,

$$F_{adv}(h) = \rho \cdot c_p \cdot SA_0 \cdot w \cdot (\theta(h) - \theta_B) \tag{2.10}$$

where *w* is the constant advection velocity, which is set to 4 m yr^{-1}, $\theta(h)$ is the oceanic temperature at the current depth, *h*, and θ_B is the constant temperature of 'bottom water', set to 274.35 K. Note that a constant advection velocity is assumed in most other upwelling-diffusion models as well – see, for example, Hoffert et al. (1981) and Siegenthaler and Joos (1992).

Diffusive flows between adjacent isothermal layers occur according to the following equation,

$$F_{diff}(h) = -K \cdot SA_0 \cdot \frac{\left(\theta(h+1) - \theta(h)\right)}{d(h)} \tag{2.11}$$

where *K* is a diffusivity constant modified from the version of *κ* used by Harvey and Schneider (1985a) and set here to 2000 m^2 yr^{-1} – the *K* used here equals $\rho \cdot c_p \cdot k$, or 8.224 x 10^9 W/(m^2 K)– while $\theta(h+1)$ is the oceanic temperature in Kelvin for the adjacent, colder, deeper oceanic layer, $\theta(h)$ is the temperature of the current layer, and *d(h)* is the depth of the current layer, which is variable, as explained below. Note that equation (2.11) must be multiplied by the number of seconds per year for correct units.

For calculation purposes, the ocean is represented by twenty layers. Where the temperature gradient is steepest, near the ocean surface, the isothermal layers are made very thin; in the deep ocean, where the temperature change between isothermal layers is small, the layers were left much thicker. Thus, the mixed layer and the next four layers are each 30 m deep, the sixth layer is 50 m deep, bringing the depth to 200 m so far, and then eight layers of 100 m depth followed. From 1000 m-depth, there are two layers of 250 m, three layers of 500 m, and a final layer of 792 m, which gives a total oceanic depth of 3792 m. The behaviour of the diffusion and advection schemes, as modelled here and provided above, is tested by Davies and Simonovic (2008), against an ocean with eighty, equal thickness, isothermal layers to ensure that the equations used did not result in inaccurate oceanic temperatures.

Finally, temperature values are expressed in Kelvin, and their calculations for the atmosphere and the oceans take the following forms. For the atmosphere, temperature is given by,

$$T_A = \frac{H_A}{R_A \cdot SA_E} \tag{2.12}$$

while, the equation for the mixed-layer and ocean temperatures is given by,

$$\theta(h) = \frac{H_0(h)}{RC_p \cdot m_0(h)} \tag{2.13}$$

where $\theta(0)$ equals *TS*, and m_0 *(h)* is the mass of the current oceanic layer, calculated from $\rho \cdot SA_0 \cdot d(h)$

It is already mentioned that there is a switch in the climate sector by which user can choose the level of complexity of the sector. The above equations are adopted from BAD model, which has a higher level of complexity. The remaining section is describing the simplified version of the climate model, adopted from Nordhaus (1994).

The transformation of GHG (specifically CO_2) to equivalent temperature is calculated by,

$$T_{equil} = \frac{k\ ln\left(\frac{C_a}{C_{a,0}}\right)}{\lambda\ ln(2)} \tag{2.14}$$

where T_{equil} refers to equilibrium temperature, C_a is atmospheric CO_2 concentration, $C_{a,0}$ is preindustrial atmospheric CO_2 concentration, k is radiative forcing coefficient, and λ is climate feedback parameter.

While computing the temperature for different layers, unlike BAD model it only consists of two layers (atmosphere and upper ocean, and deep ocean). The temperature of the atmosphere and upper ocean is given by

$$T_{AUO} = \int CT_{AUO} \cdot dt \tag{2.15}$$

where temperature of atmosphere and upper ocean is expressed as T_{AUO} , and CT_{AUO} is the change in atmosphere and upper ocean temperature.

Deep ocean temperature is calculated by Nordhaus (1994) as

$$T_{DO} = \int CT_{DO} \cdot dt \tag{2.16}$$

where T_{DO} is the temperature of the deep ocean and CT_{DO} is the change of temperature in deep ocean.

Temperature change at the atmosphere and upper ocean is computed with the help of radiative forcing, heat transfer and heat capacity of the atmosphere and upper ocean, as below

$$CT_{AUO} = \frac{F - f_H - HT}{HC_{AUO}} \tag{2.17}$$

where CT_{AUO} is the temperature change at the atmosphere and upper ocean, F is for radiative forcing, f_H is the feedback from heating, HT is for heat transfer from the atmosphere and upper ocean to the deep ocean, and HC_{AUO} denotes the heat capacity at atmosphere and upper ocean.

Whereas, temperature change in the deep ocean is only dependent on heat capacity of the deep ocean and heat transfer rate between the atmosphere & upper ocean to the deep ocean

$$CT_{DO} = \frac{HT}{HC_{DO}} \tag{2.18}$$

where CT_{DO} is the temperature change in deep ocean, *HT* is heat transfer from the atmosphere and upper ocean to the deep ocean, and HC_{DO} is the heat capacity of the deep ocean.

Heat capacity of the deep ocean is calculated by the following equation

$$HC_{DO} = R_{HC} \cdot C_{HT} \tag{2.19}$$

where HC_{DO} is the heat capacity of the deep ocean, R_{HC} is the heat capacity ration and C_{HT} stands for heat transfer coefficient.

Heat transfer between the atmosphere and upper ocean and the deep ocean mainly depends on the temperature gradient, heat transfer coefficient and heat absorption capacity, which is computed by

$$HT = (T_{AUO} - T_{DO}) \cdot \frac{HC_{DO}}{C_{HT}} \tag{2.20}$$

where *HT* is the heat transfer from the atmosphere and upper ocean to the deep ocean, T_{AUO} and T_{DO} denotes the temperature at atmosphere & upper ocean and deep ocean respectively. C_{HT} is for heat transfer coefficient and HC_{DO} stands for deep ocean heat capacity.

The initial temperatures for the atmosphere and for each of the ocean layers are given in

Table 2.1, below. The temperature values are given in degrees Celsius for convenience, and depth measurements are in meters.

Table 2.1: Initial temperatures and configuration of ocean layers (°C and m, respectively)

Layer	T_A	T_S	θ(1)	θ(2)	θ(3)	θ(4)	θ(5)	θ(6)	θ(7)	θ(8)	θ(9)
Temperature	14.0	15.90	15.04	14.23	13.47	12.75	11.87	10.44	8.86	7.56	6.48
Depth (top)	N/A	0	30	60	90	120	150	200	300	400	500
Depth (bottom)	N/A	30	60	90	120	150	200	300	400	500	600

Layer	θ(10)	θ(11)	θ(12)	θ(13)	θ(14)	θ(15)	θ(16)	θ(17)	θ(18)	θ_B
Temperature	5.59	4.85	4.23	3.72	3.07	2.44	1.90	1.52	1.32	1.2
Depth (top)	600	700	800	900	1000	1250	1500	2000	2500	3000
Depth (bottom)	700	800	900	1000	1250	1500	2000	2500	3000	3792

2.1.2 The Carbon Sector

The earlier modeling of carbon cycle was primarily focused on the oceanic component. In rare cases both, the ocean and the land surface are included in the model. However, terrestrial modeling within the carbon cycle is becoming important because of the vital role of biosphere as a carbon source and/or sink. Such terrestrial models range in scale from single trees to the entire globe (Harvey, 2000). Some complex form of model like Dynamic Global Vegetation Model (DGVM), focused exclusively on the terrestrial biosphere with high resolution representation of biomass. For more details, see - Quillet et al (2010). At the global scale, the carbon cycle modeling is using simpler representation of carbon exchange process within and between the ocean and terrestrial biomes.

Carbon sector of the ANEMI model version 2 is based on the model developed by Goudriaan and Ketner (1984) and later modified with Fiddaman's (1997; 2002) oceanic component (Figure

2.6). In the ANEMI model, the terrestrial biosphere consists of six biomes: tropical and temperate/boreal forests, grasslands and agricultural lands, deserts/tundra, and settled areas. Living biomass is divided into, leaves, branches, stems, and roots, and dead biomass into three soil-carbon pools, litter, humus, and charcoal/decay-resistant humus. Important biological processes simulated by the carbon cycle include biomass growth, litter fall, and litter and soil decomposition. The model also includes the effects of increased atmospheric carbon dioxide concentrations on biomass growth rates, through the somewhat controversial CO_2-fertilization, or β-factor, approach (Davies and Simonovic, 2008). This model simulates carbon flow among the atmosphere, the terrestrial biosphere, and the oceans.

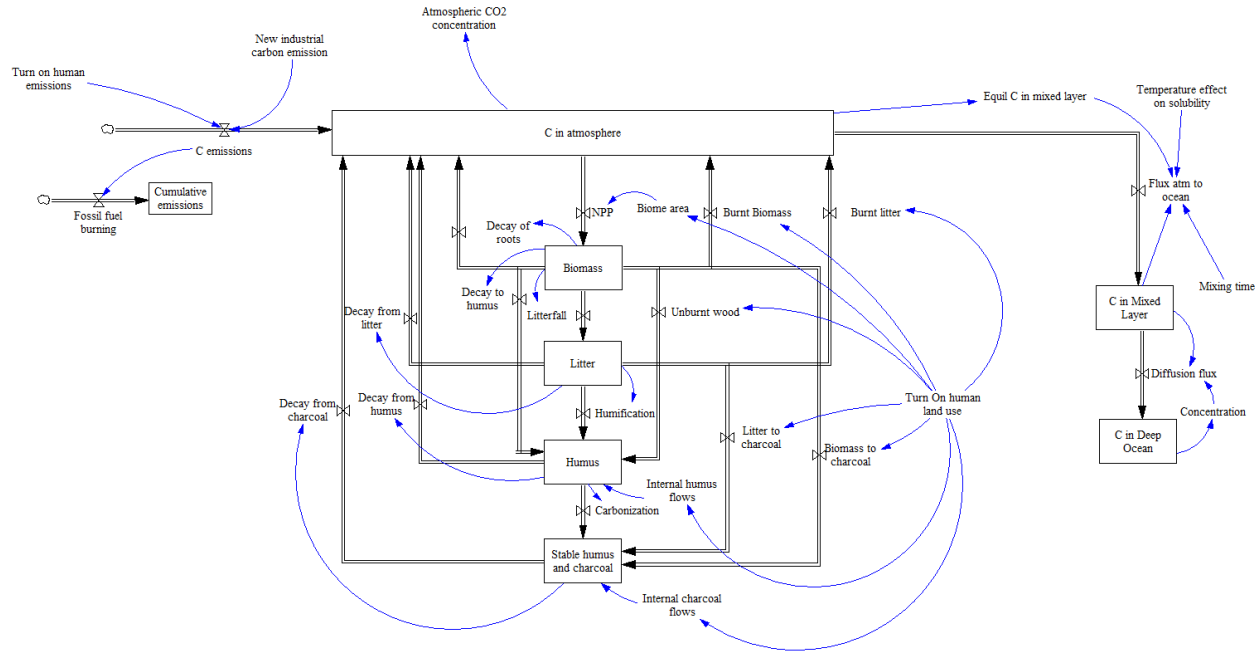

Figure 2.6: Model structure of the ANEMI model carbon sector

Note that, in any model of the carbon cycle, significant uncertainties in the carbon cycle come into play (Falkowski et al., 2000; Geider et al., 2001). Although frequently included in carbon cycle models in the form of Q_{10} factors (Harvey, 2000), the effects of climate change on soil decomposition rates are also controversial, and the model does not by default include the influences of temperature change on microbial respiration – a feedback to the climate sector-

in keeping with the approach used by Goudriaan and Ketner (1984). A Monte Carlo sensitivity analyses performed with the model, which tested different Q_{10}-effect strengths, revealed the greater importance of other factors in determining simulation results.

CO_2 is easily dissolved in seawater and the solubility is temperature dependant. Figure 2.7 illustrates the CO_2 solubility of ocean water between 0.5 to 100MPa, with a wide range of temperature (0 to 10 degree Celsius). Colder water can dissolve more CO_2 and higher water temperature reduces the solubility according to Henry's Law.

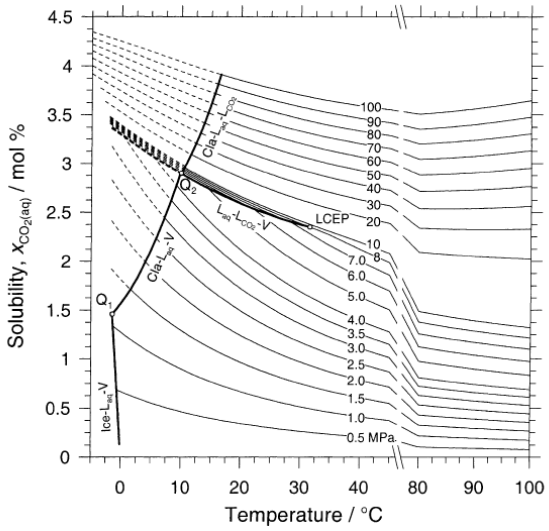

Figure 2.7: CO_2 solubility of ocean water (after Larryn et al., 2003)

Henry's Law says that CO_2 is in equilibrium between air and water at 25 ^{0}C when approximately 1/50 of the gas is in the air and the remaining gas is dissolved in the water. If 50 units of gas are added to the air 49 units will be dissolved into the water. Solubility effect of CO_2 in water due to temperature increase is also implemented in this sector which will influence the carbon absorption rate of ocean.

Causal Structure of the ANEMI Carbon Sector

The causal loop diagram for the climate sector is presented in Figure 2.8, based on Goudriaan and Ketner (1984) with some required modification. In the carbon sector of the ANEMI model,

atmospheric carbon is working as a reservoir where all the major variables are contributing except mixed ocean layer. Change in land-use and human induced emission from fossil fuel and industry is controlling the amount of the atmospheric carbon, which are coming from the other sectors of the ANEMI model. The amount of atmospheric carbon absorbed by the plants are relaying on available biome area through net primary productivity (NPP). Biomass is converted to litter when the leaves are falling from the plants. However those are returning back to the atmosphere by root decay and forest burning. The remaining litter is converted to the humus and stable humus and charcoal. A fraction of these are returning to the atmosphere when they are decayed. Humus stores carbon through unburnt wood and humification from biomass and litter respectively. At the same time humus also looses carbon by decay and carbonization process. Such carbonization process helps stable humus and charcoal layer to accumulate more carbon. Stable humus and charcoal, is also collecting carbon from biomass and litter through burnt/unburnt process and finally releases carbon to the atmosphere with the decay process.

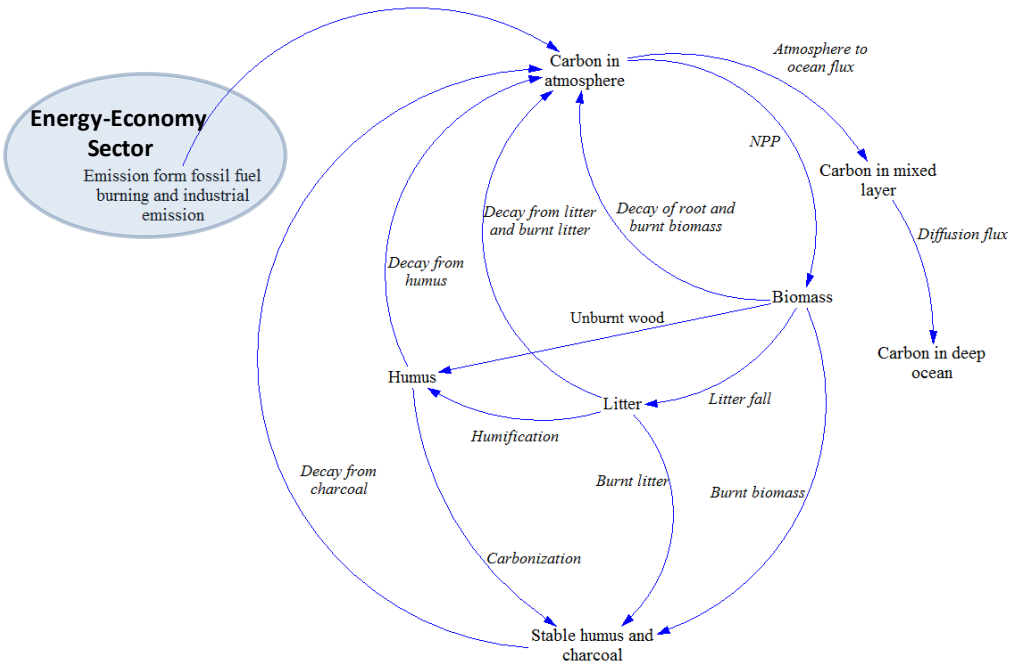

Figure 2.8: Causal loop diagram of the ANEMI carbon sector

Mathematical Description of the ANEMI Carbon Sector

All the equations of the carbon cycle, and the values of their associated parameters, are provided in this section, beginning with the atmosphere. Again, the equations for the terrestrial biosphere and the atmosphere are based on Goudriaan and Ketner (1984), while the oceanic carbon absorption is based on Fiddaman (1997; 2002).

The reservoirs of carbon, or the carbon stocks, in the ANEMI model are measured in gigatons (10^9 t) of carbon, written as Gt C. The corresponding measurement of the carbon flows is Gt C yr^{-1}. To translate the mass of carbon into a parts-permillion-volume (ppmv, or more simply ppm) measurement, the following equation is used,

$$C_A = 0.4754\, N_A \tag{2.21}$$

where C_A is the carbon dioxide concentration in the atmosphere, in ppm, and N_A is the mass of carbon in the atmosphere, in Gt C.

The accumulation of carbon in the atmosphere is governed by the following equation,

$$N_A = \int (D_B + D_L + D_H + D_K - NPP + B_B + B_L + E - F_0) \cdot dt \tag{2.22}$$

where D_B, D_L, D_H, *and* D_K are the releases of organic matter from the terrestrial biomass, litter, humus, and charcoal, respectively, to the atmosphere through decomposition, *NPP* is the net primary productivity (the difference between photosynthesis and respiration, and always positive in value), B_B and B_L are the biomass burning from land-use and land-use change – these two variables are also involved in an intersectoral feedback equation, as described in the intersectoral feedback section below – E is the industrial emission as a result of economic activity, and F_O is the carbon absorption by the oceans.

Industrial emission is calculated in the energy-economic sector of the model, according to the following equation,

$$E = (1 - \mu) \cdot \sigma \cdot Q \quad (2.23)$$

where *E* is the industrial emission level in Gt C yr^{-1}, μ represents the effects of emissions control measures, such as carbon tax, and is expressed as a fraction, σ *is* the ratio of emissions to output, also called the emissions intensity, measured in t/$1000, and *Q* is the global-aggregate economic output, in $\$10^{12}$ yr^{-1}. Further information on industrial emissions is provided in the intersectoral feedbacks section of the report, below.

The equations for the terrestrial biosphere are the most complicated in the carbon cycle model sector, since they incorporate the processes of net primary productivity, litter fall, decomposition, and land-use and land-use change. Net primary productivity drives the model according to the following equation,

$$NPP_{jk} = p_{jk} \cdot \sigma(NPP_j) \cdot A_j \times 10^{15} \quad (2.24)$$

where NPP_{jk} refers to the biome type *(j)* and the biomass component *(k),* p_{jk} is the fraction of biomass partitioned to component *k* of biome *j*, where $(\sum_{k=1}^{4} p_{jk} = 1, \sigma(NPP_j)$ is the surface density of net primary productivity in biome type *j*, measured in g C m^{-2} yr^{-1}, and A_j is the current area of biome *j*, measured in m^2. The last term, 1 x 10^{15} converts between grams and gigatons. In other words, the equation specifies the amount of the total NPP allotted to each component *k* of each biome *j*, so that NPP_{jk} has twenty-four components. Biomass partition values**,** p_{jk}**,** along with other parameters of the carbon flows through the terrestrial biosphere, are given in Table 2.2, which has been reproduced from

Table 2.1 of Goudriaan and Ketner (1984: 178).

To represent the contentious issue of CO_2-fertilization, Goudriaan and Ketner (1984) modify a base *σ(NPP)* value for each biome according to the current atmospheric carbon dioxide concentration as compared with the initial value. The equation used for the variable surface density of net primary productivity in each biome, $\sigma(NPP_j)$, is,

$$\sigma(NPP_j) = \sigma(NPP_j)_0 \times \left(1 + \beta \cdot ln\left({}^{C_A}/_{C_{A0}}\right)\right) \tag{2.25}$$

where $\sigma(NPP_j)_0$ is the base surface density of net primary productivity for biome *j*, β is the CO_2-fertilization factor, set to 0.5, and C_A and C_{A0} are the current and initial carbon dioxide concentrations in the atmosphere, respectively. Values for $\sigma(NPP_j)_0$ are given in **Error! Reference source not found.**.

Table 2.2: Parameters of the flow through the terrestrial biosphere

	Tropical Forest	Temperate Forest	Grassland	Agricultural Land	Human Settled Area	Tundra and Semi-desert
Partitioning (P_{jk})						
Leaf	0.3	0.3	0.6	0.8	0.3	0.5
Branch	0.2	0.2	0	0	0.2	0.1
Stem	0.3	0.3	0	0	0.3	0.1
Root	0.2	0.2	0.4	0.2	0.2	0.3
Life Span (τ)						
Leaf	1	2	1	1	1	1
Branch	10	10	10	10	10	10
Stem	30	60	50	50	50	50
Root	10	10	1	1	10	2
Litter	1	2	2	1	2	2
Humus	10	50	40	25	50	50
Charcoal	550	550	550	550	550	550
Humification Factor (λ)	0.4	0.55	0.55	0.2	0.5	0.55
Carbonization Factor (Ψϕ)	0.05	0.05	0.05	0.05	0.05	0.05
Carbonization factor (ε_k) on burning of leaves is 0.15, of branches 0.25, of stems 0.35 and of litter (ε_L) is 0.3						

Table 2.3: Initial carbon stock and base surface density of NPP, $\sigma(NPPj)_0$, values

	Tropical Forest	Temperate Forest	Grassland	Agricultural Land	Human-Settled Area	Tundra and Semi-Desert
Biomass (Gt C)						
Leaves	8.34	5.2	6.43	5.98	0.06	1.04
Branches	55.6	17.3	0	0	0.4	2.08
Stems	250.2	156.1	0	0	3.0	10.4
Roots	55.6	17.3	4.29	1.5	0.4	1.25
Litter (Gt C)	22.23	13.7	11.5	3.99	0.30	2.92
Humus (Gt C)	111.19	260.0	257.0	37.41	5.0	63
Charcoal (Gt C)	277.97	130.05	160.74	37.41	5.0	31.5
Base Surface Density of NPP (g C m^{-2} Yr^{-1})	770	510	570	430	100	70

In the same fashion as NPP_{jk}, biomass has twenty-four components, in the form of carbon stocks, which consist of the four biomass components in each of the six biome types. The accumulation of biomass in each of these twenty four stocks has the following form,

$$B_{jk} = \int \left(NPP_{jk} - FL_{B\,jk} - FH_{B\,jk} - FK_{B\,jk} - B_{B\,jk} - UB_{B\,jk}\right) \cdot dt \qquad (2.26)$$

where B_{jk} is the biomass in each of component, k, of each of the biomes, j, FL_{Bjk} is the amount of litter falling from the biomass to the litter layer of the soil, FH_{Bjk} is the direct decay of biomass material to humus, FK_{Bjk} is the burning of biomass directly to charcoal, B_{Bjk} is the burning of biomass from human land-use and land-use change, and UB_{jk} is the unburned remainder of biomass after land-use change that becomes part of the humus layer of soil.

The litter stock has only six components, with one component for each of the biomes. Its equation is given by,

$$L_j = \int \left(\sum_{k=1}^{4} FL_{B\,jk} - D_{L\,j} - FH_{L\,j} - B_{L\,j} - FL_{k\,j} \right) \cdot dt \qquad (2.27)$$

where L_j is the mass of litter in each of the six terrestrial biomes, $\Sigma FL_{B\,jk}$ is the total litter fall from all four components, k, of biome j to litter stock j (some of these flows are clearly zero, since roots do not create leaf litter, for example), D_{Lj} is the flow of carbon from litter to the atmosphere through decomposition, FH_{Lj} is the decomposition of litter into humus, B_{Lj} is the carbon flow from litter to the atmosphere through litter burning as a result of land-use and land-use change, and FL_{Kj} is the carbon flow from litter directly to charcoal through litter burning, again as a result of land-use and land-use change.

The humus stock also has six components, and its equation is given by,

$$H_j = \int \left(\sum_{k=1}^{4} FH_{B\,jk} + FH_{L\,j} - FK_{H\,j} - D_{H\,j} + \sum_{k=1}^{4} UB_{jk} + FH_{H\,j} \right) \cdot dt \qquad (2.28)$$

where H_j is the mass of humus in each of the six terrestrial biomes, ΣFH_{Bjk} is the direct decay of biomass to humus, FH_{Lj} is the decomposition of litter to humus, FK_{Hj} is the decomposition of humus to charcoal, D_{Hj} is the decay of humus to the atmosphere, ΣUB_{jk} is the unburned remainder of biomass after land-use change that becomes part of the humus layer of soil, and FH_{Hj} is an internal flow of humus from one biome to another that results from land-use change, since humus remains in the soil after a portion of one biome has become part of another biome.

Finally, the stable humus and charcoal stock (generally referred here as the 'charcoal stock') has six components as well, and its equation has the following form,

$$K_j = \int \left(FK_{H\,j} - D_{K\,j} + \sum_{k=1}^{4} FK_{B\;jk} + FK_{L\,j} + FK_{K\,j} \right) \cdot dt \qquad (2.29)$$

where K_j is the mass of charcoal in each of the six biomes, FK_{Hj} is the flow of carbon from humus to charcoal, D_{Kj} is the decay of charcoal to the atmosphere through decomposition, ΣFK_{Bjk} is the

burning of biomass directly to charcoal, FK_{Lj} is the carbon flow from litter directly to charcoal through litter burning, and FK_{Kj} is an internal flow of charcoal from one biome to another that results from land-use change, since charcoal remains in the soil after a portion of one biome has become part of another biome. Initial values for each of the terrestrial stocks are provided in

Table **2.3**, which also gives the base surface density of net primary productivity values from Table 2.2 of Goudriaan and Ketner (1984: 178).

Equations (2.26) to (2.29) deal with the terrestrial biosphere stocks, and list the flows that change these stock values. The equations for the carbon cycle in the oceans are provided later in this section. The subscripts on the flows are *j* and *k*, the flows have twenty-four components; however, when only the subscript *j* is present, there are six flows associated with the equation – one for each of the six biomes.

The computation of NPP is conducted according to Equation (2.24). The presentation of the remainder of the flows that affect the terrestrial biomass in Equation (2.26) begins with litter fall, FL_{Bjk}, which has the form,

$$FL_{Bjk} = \frac{B_{jk}}{\tau B_{jk}} \qquad (2.30)$$

where B_{jk} is the amount of biomass in component *k* of biome *j,* and $\tau(B_{jk})$ is the life-span, or 'residence time', for biomass component *k* of biome *j*. Note that roots, the fourth component of biomass, do not generate litter, so FL_{Bj4} is 0 Gt C yr-1. The values for $\tau(B_{jk})$ are provided in Table 2.2.

The equation for the direct decay of biomass material to humus, FH_{Bjk}, is the same as Equation (2.30) above,

$$FH_{Bjk} = \frac{B_{jk}}{\tau B_{jk}} \qquad (2.31)$$

except that FH_{Bjk} for all above-ground biomass components (k = 1, 2, 3) is 0 Gt C yr^{-1}, and only the decay of roots (k = 4) generates humus directly – in other words, all other biomass components become humus through litter, as in Equation (2.30).

The next member of Equation (2.26), the burning of biomass directly to charcoal, or FK_{Bjk}, is more complicated than the other flows, because it involves a land-use 'transfer matrix'.

This matrix, TM_{ij}, represents clearing and burning *within* a terrestrial biome, and land-use conversions that establish new land-cover in the place of the previous vegetation. A brief description of TM_{ij} follows, although more information is provided in the intersectoral feedbacks section of the report.

In TM_{ij}, the subscripts represent rows i and columns j, where column headings j mean '*from* biome type' and row headings i mean '*to* biome type'. Clearing and burning within a particular biome is represented in equation (2.32) by the diagonal matrix entries, $i = j$, while land-use conversions are represented by the remaining entries. Since there are six terrestrial biomes, the transfer matrix has 6 x 6 = 36 entries. Its equation is given in algorithmic form as,

$\frac{dTm_{ij}}{dt}$ = for all (i,j):

If (i=j)

$r^{1/2}.TM_{ij}$, (2.32)

else ($r.TM_{ij}$)

where TM_{ij} is measured in Mha yr^{-1}, and r is the annual global-aggregate population growth rate. Since the transfer matrix connects the carbon cycle, land-use and population sectors, further details are provided in the next section of the report.

Now the biomass-to-charcoal equation can be formulated. It takes the form,

$$FL_{Bjk} = \mathcal{E}_k.\sigma\,(B_{jk}).\sum_{i=1}^{6} TM_{ji}.1.10^{-5} \qquad (2.33)$$

where ε_k is the carbonization fraction of component k on burning, which has a non-zero value for $k \neq 4$, $\sigma(B_{jk})$ is the surface density of biomass component k of biome j, which is measured in g C m^{-2} yr^{-1}, ΣTM_{ji} represents a flow of burned biomass from all biomes i to the current biome, j, as a result of biomass burning. The idea is that some fraction of the biomass that was part of any of the previous biomes $i \neq j$ prior to their conversion to the new biome, j, burns because of land-use change. The final constant, 1 x 10^{-5}, results from the conversion of g to Gt and m^2 to Mha.

Each $\sigma(X)$ term – for $\sigma(B_{jk})$, $\sigma(L_j)$, $\sigma(H_j)$, and $\sigma(K_j)$, in their respective equations – is a calculated value, which is based on the following equation,

$$\sigma\,(X_{j(k)}) = X_{j(k)}/A_j\,.\,1.\,10^{-5} \qquad (2.34)$$

where $\sigma(X)$ is the surface density of a *B, L, H, or K* component of the terrestrial biosphere, measured in g C m^{-2} yr^{-1}, $X_{j(k)}$ is a carbon stock that has either six (*L*, *H*, and *K*) or twenty-four parts (*B*), and A_j is the current area of biome j, in Mha here. The constant is for unit conversion.

The biomass burning, B_{Bjk}, is related to Equation (2.33), is expresses in the form,

$$FL_{Bjk} = (1 - \mathcal{E}_k).\sigma\,(B_{jk}).\sum_{i=1}^{6} TM_{ji}.1.10^{-5} \text{ for k=1,2}$$

$$FL_{Bj3} = (1 - \mathcal{E}_3 - 0.5).\sigma\,(B_{j3}).\sum_{i=1}^{6} TM_{ji}.1.10^{-5} \quad (2.35)$$

$FL_{Bj4} = 0$

where the fraction of biomass that does not become charcoal (actually much higher than the fraction that does burn to charcoal – see **Error! Reference source not found.**) burns and is released to the atmosphere for *k* = 1 and 2, or the 'leaves and branches'. Variables in the equation include the carbonization fraction, ε_k, from Equation (2.33), the surface density, $\sigma(B_{jk})$, which is based on Equation (2.34), and the transfer matrix ΣTM_{ji} function as in Equation (2.32). In the case of the stems, *k* = 3, some fraction (ε_k) burns to charcoal, another fraction is released to the atmosphere through this equation ($1 - \varepsilon_k - 0.5$), and the last half (0.5) of the stems is left on the land surface after the land-use change and becomes humus. The last biomass component, which is the roots (*k* = 4), does not burn, but is instead transferred directly to the humus pool of the new biome as in Equation (2.36), below.

The last flow in Equation (2.27) pertains to the portion of biomass that does not burn in a land-use change from one biome to another. This unburned biomass, UB_{jk}, is calculated from the following equation,

$$UB_{jk} = 0 \text{ for } k=1,2$$
$$UB_{j3} = 0.5 \cdot \sigma\left(B_{j3}\right) \cdot \sum_{i=1}^{6} TM_{ji} \cdot 1 \times 10^{-5} \quad (2.36)$$
$$UB_{j4} = \sigma(B_{j4}) \cdot \sum_{i=1}^{6} TM_{ji} \cdot 1 \times 10^{-5}$$

where all leaves and branches (*k = 1* and 2) are burned and released to either the atmosphere or to the charcoal layer of the soil, and so the unburned fraction is zero, whereas the unburned fraction (0.5) of the stems (*k* = 3), as well the entire mass of the roots, become humus.

The first flow in Equation (2.27), for the litter stock, is the litter fall from Equation (2.30). The next flow in Equation (2.27) is the decay of litter to the atmosphere, D_{Lj}, which is given by,

$$D_{Lj} = (1-\lambda_j) \cdot L_j / \tau(L_j) \quad (2.37)$$

where λ_j is the humification fraction – or the fraction of litter that becomes humus – for biome j, and $\tau(L_j)$ is the turnover time, or 'residence time', for litter in biome j, which typically has a value of only one to two years. See Table 2.2 for the values for $\tau(L_j)$.

The equation for the decomposition of litter to humus, FH_{Lj}, is the complement to Equation (2.37), and is given by,

$$D_{Lj} = \lambda_j \, L_j / \tau(L_j) \quad (2.38)$$

where the same variable and constant definitions apply as in Equation (2.37).

The carbon flow from litter to the atmosphere as a result of litter burning via land-use and land-use change is analogous to Equation (2.35), for the burning of biomass. For the burnt litter flow, B_{Lj}, the equation is,

$$B_{Lj} = (1 - \varepsilon_l).\sigma\,(L_j).\sum_{i=1}^{6} TM_{ji}.1.10^{-5} \quad (2.39)$$

where ε_L is the carbonization fraction of litter upon burning, $\sigma(L_j)$ is the surface density of litter in biome j, as defined in Equation (2.34), and ΣTM_{ji} represents the transfer matrix measured in Mha, where land-use change results in a flow of burned litter from the area of all the biomes i that was converted to the current biome, j. The final constant is, again, the result of a unit conversion.

The last flow in Equation (2.27), FL_{Kj}, represents the carbon flow from litter directly to charcoal through litter burning, again as a result of land-use and land-use change. Its equation is,

$$FL_{kj} = \varepsilon_l.\sigma\,(L_j).\sum_{i=1}^{6} TM_{ji}.1.10^{-5} \qquad (2.40)$$

which is the complement to Equation (2.39). In other words, the small amount of litter that is not released directly to the atmosphere through burning joins the charcoal stock instead.

Several of the flows associated with the humus stock, as listed in Equation (2.28), have already been defined above: FH_{Bjk}, FH_{Lj}, and UB_{jk}. Equations for the remaining flows are provided below, beginning with the decomposition of humus to charcoal, FK_{Hj},

$$FK_{Hj} = \phi_j \cdot H_j/\tau\left(H_j\right) \qquad (2.41)$$

where φ_j is the carbonization fraction of humus through decomposition, and $\tau(H_j)$ is the turnover time, or 'residence time', for humus in biome *j*.

Decomposition of humus and its release to the atmosphere, D_{Hj}, is the complement to Equation (2.41), so that,

$$D_{Hj} = (1-\phi_j) \cdot H_j/\tau(H_j) \qquad (2.42)$$

where the same variable and constant definitions apply as in Equation (2.41).

The final flow in Equation (2.28) is FH_{Hj}, which represents an internal flow of humus from one biome to another as a result of land-use change. It equation is given by,

$$FH_{Hj} = \sigma\left(H_j\right) \cdot \left[\sum_{i=1}^{6} TM_{ji} - \sum_{i=1}^{6} TM_{ij}\right] \cdot 1 \times 10^{-5} \qquad \forall i \neq j \qquad (2.43)$$

where $\sigma(H_j)$ is the surface density of humus in biome *j*, as defined in Equation (2.34), $\Sigma_i TM_{ji}$ is the sum of all land-use conversions from biome *i* to *j*, and $\Sigma_i TM_{ji}$ is the sum of all land-use conversions from biome *j* to different biomes *i*. The expression in the brackets determines the net change in biome area over the past time step – for tropical forests and some others, the change will be negative, while for agricultural land and others, the change will be positive. The constant is for unit conversions, and the logical statement (for all $i \neq j$) ensures that only land-use conversions are considered here.

In the case of the final stock, charcoal and stable humus from Equation (2.29), only two equations have not been provided. The equation for the decomposition of charcoal to the atmosphere is similar to the other equations for decomposition, and is given by,

$$D_{Kj} = K_j / \tau(K_j) \qquad (2.44)$$

where $\tau(K_j)$ is the turnover time, or 'residence time', for charcoal in biome *j*.

The more complicated equation for FK_{Kj}, which is an internal flow of charcoal from one biome to another that results from land-use change and is analogous to FH_{Hj} in Equation (2.43), takes the following form,

$$FK_{kj} = \sigma(K_j).[\sum_{i=1}^{6} TM_{ji} - \sum_{i=1}^{6} TM_{ij}].1\text{x}10^{-5} \qquad \forall\, i \neq j \qquad (2.45)$$

where $\sigma(K_j)$ is the surface density of charcoal in biome *j*, as calculated in Equation (2.34), and the rest of the terms are the same as in Equation (2.43).

The equations for the *oceanic* component of the carbon cycle are based on work by Fiddaman (1997), and are broken into two parts: the mixed-layer, and the deep oceans.

For the mixed-layer carbon stock, the equation is,

$$C_{ML}=\int\left(FO_A - DF_o(0)\right).dt \qquad (2.46)$$

where C_{ML} is the amount of carbon in the oceanic mixed-layer, with an initial value of 769 Gt C, FO_A is the absorption of carbon dioxide by the mixed-layer from the atmosphere, and $DF_O(0)$ is the diffusive flow of carbon dioxide to the deep ocean. The flows in the ocean are measured in Gt C yr^{-1}.

For the absorption of carbon dioxide from the atmosphere, the equation is,

$$FO_A=(C_{MLeq} - C_{ML})/\tau_{ML} \qquad (2.47)$$

where C_{MLeq} is the equilibrium mixed-layer carbon content, C_{ML} is given by Equation (2.46), and τ_{ML} is the 'mixing time' for the mixed-layer, set to 1.5 yr.

The equation for the diffusive flows takes the following form,

$$DF_o(0) = \frac{2\delta_e\cdot\left({C_{ML}}/{d_{ML}} - conc(0)\right)}{d_{ML}+d(0)}\ for\ mixed\ layer \qquad (2.48)$$

$$DF_o(h) = \frac{2\delta_e\cdot(conc(h+1)-conc(h))}{d_{(h+1)}+d(h)}\ for\ h > 0$$

where the top equation calculates the diffusive flow from the mixed-layer to the first deep ocean layer, *layer 0*, and the bottom equation governs carbon flows between deep ocean layers. Therefore, in Equation (2.48), δ_e is the eddy diffusivity coefficient, which is set to of 4000 m^2 yr^{-1}, d_{ML} is the depth of the mixed-layer, which is 75 m, C_{ML}/d_{ML} is the concentration of

carbon in the mixed-layer, *conc(0)* is the concentration of carbon in the first deep ocean layer, calculated by $C_O(0)/d(0)$, and the denominator (with the '2' moved to the numerator) determines the average distance of heat diffusion from the centre of one oceanic stock to the next. For the bottom equation, *conc(h+1)* is the concentration of carbon in the layer above the current layer, *h*, *conc(h)* is the concentration in the current layer, and *d(h+1)* and *d(h)* are the thicknesses of the two layers. Again, the concentrations are calculated by $C_O(h)/d(h)$.

The equilibrium mixed-layer carbon content, C_{MLeq}, is calculated according to the following equation,

$$C_{ML_{eq}} = C_{ML_0} \cdot \left({}^{C_A}/_{C_{A0}} \right)^{1/\xi} \tag{2.49}$$

where C_{ML0} is the pre-industrial mixed-layer carbon content, set to the initial value for C_{ML}, C_A is the current atmospheric carbon dioxide concentration, from Equation (2.21), and C_{A0} is the initial carbon dioxide concentration, from equation (2.25). The buffer factor, ξ, is also a calculated value, and comes from the following equation,

$$\xi = \xi_0 + \xi_0 \cdot \ln\left({}^{C_A}/_{C_{A\xi}} \right) \tag{2.50}$$

where all the terms are parameters, except for C_A. The reference buffer value, ξ_0, is set to 10, while buffer coefficient, ξ_c, is set to 4.05. Finally, the reference carbon dioxide in the atmosphere at the base buffer value, $C_{A\xi}$, is 760 Gt C.

For the deep ocean carbon stock, the equation is,

$$C_0(h) = \int [DF_0(h) - DF_0(h+1)] \cdot dt \tag{2.51}$$

where $C_O(h)$ represents the carbon content of ocean layer h, $DF_O(h)$ is the diffusive flow of carbon from the layer above to the current layer, and $DF_O(h+1)$ is the diffusive flow to the layer below from the current layer – see Equation (2.48), above. In this model of the ocean based on Fiddaman (1997), there are ten layers of unequal depth, with each of the top five layers having a thickness of 200 m, and the bottom five layers having a thickness of 560 m each.

2.1.3 The Energy-Economy Sector

The energy-economy sector of the ANEMI model version 2 describes the world's energy resources, and how prices move to equate the global demand and supply of energy. It's an extension of the traditional (Solow) neoclassical growth model. The novel part of the model is the energy piece governing the allocation of energy production across fossil fuels, hydro, nuclear, and alternative energy sources.

The model follows common practice in macroeconomics, assuming that the global economy consists of a representative household and a representative firm. The household has preferences over an aggregate consumption good and supplies labour services inelastically to the firm each period. The firm takes labour, capital, and energy services as inputs in a Cobb-Douglas production function, and produces the final good which is used for consumption and investment. Investment is determined by a Solow rule where a fraction s of output is invested into new capital each period. There is no trade in the model.

'Energy services' is modeled as a composite good aggregated from heat energy and electric energy. Heat energy is produced from fossil fuels and alternative energy sources. Electric energy is produced from fossil fuels, nuclear, and hydro power.

The production of output is negatively affected by climate damages. The global mean temperature represents a negative impact to the economic system from industrial emissions through climate damages.

The energy data for the global energy economy is from the U.S. Energy Information Administration (EIA) and the World Bank's World Development Indicators (WDI). Fossil fuel reserves, fossil fuel discoveries, total energy produced from fossil fuel, and total electricity produced from nuclear and hydro power data are collected from EIA database (EIA, 2006). WDI database (http://databank.worldbank.org, last accessed August 2011) is used for the production of electricity from fossil fuels. An important input into the model is the path of future discoveries for oil and natural gas. The uncertainty associated with the size of undiscovered reserves in the Arctic is but one factor. Perhaps of greater uncertainty is the future developments in technology and prices which may allow for extraction of resources considered unrecoverable today. The U.S. Geological Survey estimates that there are about 3.4 trillion barrels of heavy oil in the world; however, only 450 billion barrels are recoverable given today's technology and price level. For the benchmark calibration it is assumed that future 'discoveries' will be around 1.3 trillion barrels. Similar assumption is made for natural gas. The implicit assumption is that higher fossil fuel prices will motivate technological progress and make extraction of heavy oil and shale gas economically viable.

Causal Structure of the ANEMI Energy-Economy Sector

The causal structure diagram for the energy-economy sector is presented in **Error! Reference source not found.**. In the ANEMI model version 2, the energy-economy sector takes global mean temperature and population as inputs. The climate damage relationship is from Nordaus (2000), and is represented by a quadratic function in global mean temperature. Changes to population levels and demographics impacts the productive capacity of the economy as the labour input for the firm is assumed to be the working age share of the world population.

The available energy resources are primitives in the model. In this model the available fossil fuel reserves and the technology available to produce nuclear, hydro, and alternative energy are presumed. The output produced from the energy-economy sector is industrial emissions and the world's gross domestic product. Industrial emissions are calculated from the burning of

fossil fuels in producing energy services. Gross domestic product is equal to final output, and depends on the world's capital stock, labour force, and energy resources. It may be noted that energy production in the model is an intermediate good.

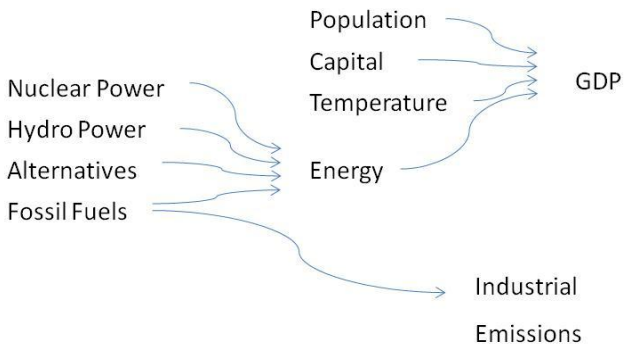

Figure 2.9: Causal loop diagram of ANEMI energy-economy sector

Mathematical Description of the ANEMI Energy-Economy Sector

Under this sub-section a detailed description of the variables and equations of the energy-economy sector are presented. The assumptions made about the representative household, the representative firm, and the choices available to them, given the world's energy resources are presented too.

The world's population is assumed to be represented by a stand-in household whose preferences can be represented by the utility function

$$U(C) = \ln(C) \qquad (2.52)$$

where C is a generic consumption good. The household supplies labour, L, inelastically to the market. It is assumed that the household owns the world's capital stock and natural resources.

Thus, the consumer rents the capital to the firm, earning income rK, where r is the interest rate and K is the aggregate capital stock in the economy. The consumer also sells energy services to the firm, earning income $P_E E$, where *E* is aggregate of energy services, and P_E is the price of aggregate energy services.

Investment, I, is assumed to follow a Sollow investment rule where a fraction s of output, Y, is invested into new capital each period. Given prices, the household tries to maximize the utility subject to its budget constraint. Each period the household's optimization problem is:

$$\max \log(C)$$

$$subject\ to$$

$$rK + wL + P_E E - \overline{T} \geq C + I \qquad (2.53)$$

$$I = sY$$

$$T = \sum_i \tau_i F_i$$

The world's production of final output is represented by a stand-in firm which employs a Cobb-Douglas production technology. The firm hires labour, capital, and energy services from the stand in household and produces the generic consumption goods.

The aggregate production function is:

$$Y = \Omega A K^{\alpha} L^{\beta} E^{1-\alpha-\beta} \qquad (2.54)$$

$$\Omega = \frac{1}{1 + \theta_1 T + \theta_2 T^2} \qquad (2.55)$$

where $A,$ is total factor productivity (TFP), K is the aggregate capital stock in the economy, L is the labour force, and Ω is the Nordhaus damage coefficient. θ_1 and θ_2 are the parameters of damage function. The damage coefficient is a function of T, global mean temperature. TFP is assumed to increase at a decreasing rate. TFP growth in 2005 is 1.6%, 0.9% in 2050, and 0.6% in 2100. The sum of the share parameters from the aggregate production function, α and β, are assumed to decrease over time. This assumption implies that the share of energy services in final output is decreasing. The assumption here is that technology improvements reduce the energy intensity of the economy as a whole.

The formulation used in this report assumed that there is a government in the model that can implement carbon taxes on energy consumption. The government is exogenous to the model, and tax revenues are transferred as a lump-sum to the household. We assume a set of fuel specific taxes, τ_i, which depend on the emission intensity of each fuel type i. Finally, $\overline{T}$ is the sum of tax revenues from carbon emission. Then, $P_E E - \overline{T}$ is the household's income from selling energy services to the firm net of taxes.

It is assumed that representative firms produce heat energy and electric energy from CES production functions. Aggregate energy services, E, is modeled as a composite good produced from heat energy and electric energy.

Electric energy is produced from fossil fuels, nuclear and hydro power. Here, nuclear and hydro power are assumed policy variables, and are exogenous to the firm. For each period the representative firm solves the following optimization problem:

$\min_{F_{El,i}} ATC_{El}(F_{El,Coal}, F_{El,Oil}, F_{El,Nat.Gas})$

subject to

$E_{El} \geq \overline{E_{El}}$

$P_{El} = ATC_{El}$ (2.56)

K_{Coal}, K_{Oil}, $K_{Nat.Gas}$ given.

where

$$E_{El} = A_{El}\left(a_1 {F_{El,Coal}}^{\vartheta} + a_2 {F_{El,Oil}}^{\vartheta} + a_3 {F_{El,Nat.Gas}}^{\vartheta} + a_4 {\bar{E}_{El,Nucl.}}^{\vartheta} + a_5 {\bar{E}_{El,Hydr.}}^{\vartheta}\right)^{1/\vartheta}.$$

and

$a_i = \left(\frac{1}{\omega}\right)\left(g_i - \left(\frac{F_{El,i}}{K_i}\right)^2\right)$, *for i=1,2,3.*

That is, given the capital stocks for fossil fuels and the nuclear and hydro power available, the representative firm chooses $\{F_{El,Coal}, F_{El,Oil}, F_{El,Nat.Gas}\}$ to minimize the average total cost of electricity. Here, A_{El} is a productivity term specific to electricity production, $F_{El,i}$ is the fuel input used for fuel type i in electricity production, ATC_{El} is the average total cost of electric energy, $\overline{E_{El}}$ is the threshold value for electric energy, P_{El} is the price of electric energy and ϑ is the CES elasticity parameter (implies elasticity of substitution of $E_S = {1}/{(1-\vartheta)}$).

The functions a_i, for the fossil fuels, are decreasing in the fuel-to-capital ratio. Inside a period this assumption implies diminishing returns, as capital is a fixed factor. The parameters a_4 and a_5 are fixed. The parameters ω and g_i are used to calibrate the relative levels of fossil fuels in electricity production.

The structure for production of heat energy is symmetric to the production of electric energy. It is assumed that heat energy is produced from fossil fuels and alternative energy sources. In each period the representative firm solves the following optimization problem:

$$\min_{F_{H,i}} ATC_H\left(F_{H,Coal}, F_{H,Oil}, F_{H,Nat.Gas}, F_{H,Alt.}\right)$$

subject to

$$E_H \geq \overline{E_H}$$

$$P_H = ATC_H \tag{2.57}$$

where,

$$E_H = A_H\left(b_1 {F_{H,Coal}}^{\mu} + b_2 {F_{H,Oil}}^{\mu} + b_3 {F_{H,Nat.Gas}}^{\mu} + b_4 {F_{H,Alt}}^{\mu}\right)^{1/\mu}$$

There is no capital in the heat energy sector. The capital for heat energy comprises part of the aggregate capital for the economy. The firm chooses $\{F_{H,Coal}, F_{H,Oil}, F_{H,Nat.Gas}, F_{H,Alt.}\}$ to minimize the average total cost of heat energy. Here, A_H is a productivity term specific to heat energy production, $F_{H,i}$ is the input of fuel type *i* for heat energy production, b_i is the CES weight for fuel type *i*, ATC_H is the average total cost of heat energy, $\overline{E_H}$ is the threshold value for heat energy, E_H is the heat energy service, P_H is the price of heat energy services, and μ is the CES elasticity parameter.

A_{El} and $A_H$is assumed to grow linearly. Implicit productivity increases are embedded in the assumptions on fossil fuel discoveries, the price function of alternative heat energy, and the share parameters in the aggregate production function. Currently, μ and ϑ are arbitrarily set equal to 0.5.

The fossil fuel price functions are increasing in the ratio of the reserve value at its base year relative to its current value.

$$P_{F_{i,t}} = \tau_{i,t} + P_{F_{i,t=1980}} \left(\frac{R_{i,t} + D_{i,t} - F_{El_{i,t}} - F_{H_{i,t}}}{R_{i,t=1980}} \right)^{\rho} \tag{2.58}$$

where subscripts *i* and *t* refer to the fossil fuel type and the year respectively. $P_{F_{i,t}}$ is the fuel price, $\tau_{i,t}$ is the fuel specific carbon tax, $P_{F_{i,t=1980}}$ is the price of fuel at the base year (1980), $R_{i,t}$ is the current reserve level, $R_{i,t=1980}$, is the base year reserve level, and $D_{i,t}$ is the new discovery value. $F_{El_{i,t}}$and $F_{H_{i,t}}$is extraction of fuel for electricity and heat energy production respectively. $\rho < 0$ is an elasticity parameter.

It is clear that the fossil fuel price decreases when the current reserve value falls relative to the base year. That is, the more fuel extracted the higher the price becomes. New discoveries of fossil fuel reduce the price of fossil fuel, holding everything else constant. The paths for new fossil fuel discoveries are prescribed. The elasticity parameter for the fossil fuel price functions, ρ, is set to -0.4. A lower value would make fossil fuel prices more responsive to depletion of the fossil fuel reserves. The parameter value and the functional form for the price functions are from the ANEMI version 1.2 energy-economy sector (Davies and Simonovic, 2009).

The price of alternative heat energy is represented by the function:

$$P_{F_{Alt.,t}} = \mu_{1,t} + {F_{H,Alt.,t}}^{\mu_{2,t}} \tag{2.59}$$

where $P_{F\,Alt}$ is the price, and $F_{H,Alt.}$ is the quantity of alternative fuel used in heat energy production. μ_1 and μ_2 are parameters. It is assumed that they are decreasing, representing decrease of the alternative fuel price over time.

The initial values for the parameters for the alternative energy price function, μ_1 and μ_2, are assumed equal to 3 and 5 respectively. The parameters decrease linearly over time representing decrease in the price of alternative energy over time as technology improves. For the calibration we had a target of 3% alternative heat energy in 2005. The energy demand side is derived from the aggregate production function.

For one period problem the capital and labour inputs are fixed. Demand for aggregate energy services can be expressed as:

$$E = \left(\frac{(1-\alpha-\beta)AK^{\alpha}L^{\beta}}{P_E}\right)^{1/(\alpha+\beta)} \tag{2.60}$$

where E is the representative firm's demand for aggregate energy services, K is aggregate capital, L is the world's labour force, and P_E is the price of aggregate energy services. α and β are the share parameters from the aggregate production function.

Heat energy and electric energy are combined into aggregate energy services by a CES function:

$$E = \left(\gamma E_H^{\theta} + (1-\gamma)E_{El}^{\theta}\right)^{1/\theta} \tag{2.61}$$

where E_H is the total heat energy produced, and E_{El} is the total electricity produced. The elasticity of substitution is determined by the parameter θ, and γ is the CES share parameter. The elasticity parameter in aggregation of electricity and heat energy, θ, is also set to 0.5, whereas the share parameter γ in the CES aggregator for heat an electric energy is set to 0.9.

Investment into new capital for electricity production follows an average cost investment rule and is allocated by a built-in function of the Vensim system dynamics simulation software called 'Allocate-by-priority' (Ventana, 2010b).

The available supply of investments funds for electricity production is assumed to follow a Solow rule. That is, each period I_{El} is available to invest in new electricity capital:

$$I_{El} = sY\left(\frac{\sum_i K_i}{K + \sum_i K_i}\right) \tag{2.62}$$

where K_i is the current capital stock used to produce electricity from energy source i, which could be either a fossil fuel, nuclear or hydro power. K without a subscript i is the aggregate capital stock for the economy.

For the investment into electricity capital in the energy sector, the allocate-by-priority (ABP) function serves the purpose of a market clearing mechanism. The ABP function in Vensim is based on the William T. Wood algorithm for allocating a resource in scarce supply to competing orders or 'requests' (Ventana Systems, 2010b). The allocate-by-priority function takes as inputs the supply of available investment funds to be allocated, and the 'capacity' and the 'priority' of each order, representing the size and competitiveness of the orders respectively.

The ABP function has a 'width' parameter which determines how exclusively the available investment funds will be allocated. The width-parameter can take any positive value. The lower the value of the width the more responsive is the allocation to differences in order priority. For example, if two orders have similar capacitates and priorities, then a high width will produce a very even allocation. On the other hand, as the width parameter decreases, the allocation of investment funds will be shifted towards the order with the higher priority.

Given the fixed quantity of investment funds available inside a period, the market allocation depends on (a) the size of the request, (b) the relative priority given to each sector, and (c) the width parameter. After testing multiple approaches, it has been decided to set the priorities for the sectors equal to each other, and only focus on the request dimension. The intention behind this decision is to simplify the calibration and to make the investment function more transparent. More information about the ABP function in Vensim can be found in the Vensim manual and the supporting documentation online (http://www.vensim.com/allocp.html, last accessed August 2011).

The demand for new investment funds for each energy source used in electricity production is based on an average cost investment rule where the allocation is determined by the ABP function. Given a fixed priority across energy sources, the 'request' function takes the following form:

$$Req_i = \varphi_i \delta_i K_i + \left(\frac{K_i}{\sum_i K_i}\right)\left(\frac{ATC_{El}}{ATC_i}\right) \quad (2.63)$$

The request for new investment funds (Req_i) is a function of 'replacement capital' and the current capital share of the sector scaled by its relative average total cost. Each period a share δ of existing capital depreciates, and an assumption is made that all sectors will ask for that capital to be replaced. The parameter φ is a weighting factor that will reduce the request for replacement capital if the average total cost exceeds some threshold value. The second term is the relative size of the current capital stock (K_i) for energy source i multiplied by its relative average cost. This implies that sectors with a lower average cost will have higher requests. ATC_{El} is the average total cost of electricity, and ATC_i is the average total cost of energy source i.

The value of φ is set to 0.5 which means that if the condition is true, then the request for replacement capital is only half of the depreciated capital. The intuition behind this parameter is to improve the adjustment process of the capital stock in electricity production from fossil fuels in response to average cost changes.

Note that as the path for nuclear and hydro power is given exogenously, the capital stock used in production of nuclear and hydro power is also prescribed. The amount needed for new capital for nuclear and hydro power is first subtracted from the total amount available for investment into electricity capital; what is left over is allocated to the fossil fuel capital stocks using the ABP function.

In the ANEMI model, the consumed portion of the fossil fuel specific energy resources is converted into the respective carbon emission mass. This approach is in-line with the recommendations from the IPCC (2006: Vol. 2, Ch. 2, Pg. 2.11) for calculating tier one emissions.

Carbon emissions are calculated as follows:

Coal:

The energy content of coal is, on average, 21.213 GJ t_{coal}^{-1}, which means that combustion of 1 ton of coal releases:

1. 0.518 tons of carbon, for an emission factor of 0.518 t_C t_{coal}^{-1} (EIA, 2008); or
2. 0.541 tons of carbon, for an emission factor of 0.541 t_C t_{coal}^{-1} (IPCC, 2008 [using 26 t_C TJ^{-1}, 98% combustion].

$$E_{coal} = k_{combust} . \varphi_{coal} . \frac{R_{depl_{coal}}}{1000} = 0.99 * 0.518 . \frac{R_{depl_{coal}}}{1000} \quad (2.64)$$

where E_{coal} is the emission for the coal, $k_{combust}$ is the combustion amount out of 1 unit, φ_{coal} is the emission factor of coal. $R_{depl_{coal}}$ represents the amount of coal depleted from the reserve or used in energy production.

Oil:

The energy content of oil is, on average, 6205 MJ bbl^{-1}, which means that combustion of 1 barrel of crude oil releases;

1. 0.119 tons of carbon, for an emission factor of 0.119 t_C bbl^{-1} (EIA, 2008); or
2. 0.125 tons of carbon, for an emission factor of 0.125 t_C bbl^{-1} (IPCC, 2008) [using 20.5 t_C TJ^{-1}, 99% combustion].

$$E_{oil} = k_{combust} . \varphi_{oil} . \frac{R_{depl_{oil}}}{1000} = 0.99 * 0.119 . \frac{R_{depl_{oil}}}{1000} \quad (2.65)$$

where $\mathrm{E}_{\mathrm{oil}}$ is the emission for the oil, $\mathrm{k}_{\mathrm{combust}}$ is the combustion amount out of 1 unit, φ_{oil} is the emission factor of oil. $\mathrm{R}_{\mathrm{depl}_{\mathrm{oil}}}$ represents the amount of oil depleted from the reserve or used in energy production.

Natural gas:

The energy content of natural gas is, on average, 38.264 MJ m^{-3}, which means that combustion of 1 m^3 of natural gas releases

1. 5.246 x 10-4 tons of carbon, for an emission factor of 0.0005246 t_C m^{-3} (EIA, 2008); or
2. 5.796 x 10-4 tons of carbon, for an emission factor of 0.0005796 t_C m^{-3} (IPCC, 2008) [using 15.3 t_C TJ^{-1}, 99% combustion].

$$E_{nat\ gas} = k_{combust} \cdot \varphi_{nat\ gas} \cdot R_{depl_{nat\ gas}} = 0.99 * 0.000525 * R_{depl_{nat\ gas}} * 10^3 \qquad (2.66)$$

where $\mathrm{E}_{\mathrm{nat\,gas}}$ is the emission for the Natural Gas, $\mathrm{k}_{\mathrm{nat\,gas}}$ is the combustion amount out of 1 unit, $\varphi_{\mathrm{nat\,gas}}$ is the emission factor of Natural Gas. $\mathrm{R}_{\mathrm{depl}_{\mathrm{nat\,gas}}}$ represents the amount of natural gas depleted from the reserve or used in energy production.

ANEMI model used the first-listed emission factors for each of the three fossil fuels, because they give the closest correspondence to historical emission values, as shown in the next section. The combustion factor, which states that the combustion process uses 99% of the fuel, also corresponds to the data.

For simplicity it is assumed that future fossil fuel discoveries are known at the beginning of the time horizon. The sum of the total discoveries is added to the initial reserve value in the base year. This assumption makes global fossil fuel price movement smooth, which is helpful as the price paths are used as inputs to the energy-economy sector of the Canada regional model.

The initial reserve values for the base year are noted in the Table 2.4 **Error! Reference source not found.**, where, the first column shows the initial reserve value used in the baseline model. It is calculated as the sum of observed 1980 reserves, observed discoveries from 1980-2005 of EIA (2006), and assumed discoveries after 2006.

Table 2.4: Initial fossil fuel reserve (in trillion GJ)

	1980 Assumed Initial Reserves	1980 Reserves (EIA)	1980-2005 Discoveries (EIA)	2006 - Assumed Discoveries
Coal	20	20	-	-
Oil	21	3.9	6.8	10.3
Natural Gas	18	2.7	5.7	9.6

Numerical Solution of the ANEMI Energy-Economy Sector

The ANEMI model version 2 is developed using Vensim system dynamics simulation software (Ventana Systems, 2010a). The model structure allows for analyses of numerous feedback relationships within each sector and between different sectors. However, the economic model presented above involves optimization of problems in Equations (2.53), (2.56) and (2.57). In macroeconomics, the most common way to solve these optimization problems computationally is by employing various iterative nonlinear optimization algorithms.

The scope for optimization within Vensim, the system dynamics simulation software package, is limited. As a consequence, the energy-economy sector is employing MATLAB software otpimization package subroutine. In each simulation time step, Vensim sends information to MATLAB which solves the one-period optimization problem for the energy-economy. Specifically, at each time-step, Vensim sends the global mean temperature, the capital stocks of energy production, and the population data to MATLAB. MATLAB is then used to solve a non-linear system of equations which represents the optimal solution to the one-period

optimization problem in the energy-economy sector. The solution to that problem is the production allocation, the optimal energy use across energy sources in production, which then is sent back to the Vensim simulation model. Based on the energy consumption Vensim can run the next time-step, calculating emissions based on energy consumption which then is used to calculate global mean temperature. This value is then used by other sectors of the ANEMI model.

The current modeling approach allows for a market clearing mechanism in the energy-economy, where energy prices move to equate supply and demand. The main drawback of this approach is the increase in the model's computation time.

2.1.4 The Food Production Sector

The fundamental assumption of the food production sector is that the global amount of food that can be produced each year is limited. It's proven that the proper allocation of the physical resources (water, fertilizer, suitable land and etc) can enhance the food production, but they are not abundant. One can argue that the technological innovations may lead to a very high yield within the same agricultural area. However, it's evident that there are decreasing returns to technology's ability to increase land yield by diverting other limited resources input into the agriculture sector (Meadows et al., 1974).

Food is not only produced by cultivation of arable land, although land cultivation is at present by far the most important source of food production for human consumption. Other sources of food are the oceans and the world's grazing lands. However, the analyses of FAO data (AQUASTAT, 2010) established that only 7.4% of the total amount of food product is coming from animal product (Figure 2.10).

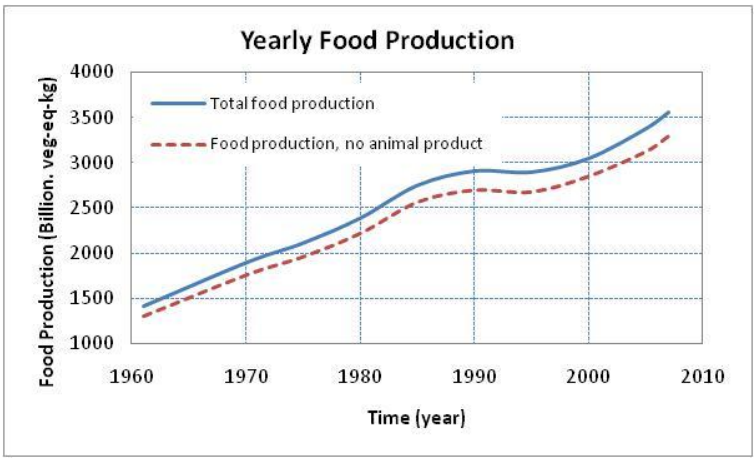

Figure 2.10: Yearly food production (billion veg-eq-kg)

Besides, the current and potential food output, from fisheries and from livestock feeding on grazing land, is small compared to the food output from the cultivation of arable land (Meadows et al., 1992). Therefore, these other sources of food are relatively insignificant and will remain so. It has been decided to neglect food obtained from oceans and grazing lands in the ANEMI model version 2. The world's grazing lands currently cover 3.6 billion hectares, an area somewhat larger than the potentially arable land of 3.2 billion hectares. The average carrying capacity of the world's grazing lands is roughly 1 animal unit per 20 hectares, where 1 animal unit is equivalent to the production of 100 kilograms of meat per year (Meadows et al., 1974). If it is assumed that 7 kilograms of vegetable crops are needed to produce 1 kilogram of meat, this yield amount of 35 vegetable-equivalent kilograms per hectare-year. Thus the vegetable-equivalent food yield from grazing lands is low when compared with the traditional yield of 600 vegetable-equivalent kilograms per hectare-year that can typically be obtained from arable land without the use of modern agricultural inputs. The grazing land yield is only about 2 percent of the world average cultivated land yield of around 2,000 vegetable-equivalent kilograms per hectare-year. In summary, the food output from grazing land is of relatively lower importance (Meadows et al., 1974).

Food production sector of the ANEMI model version 2 (Figure 2.11) is developed based on the WORLD3 model (Meadows et al., 1974). In the model, the capital investments in agriculture can increase total food production in two ways: (a) by increasing the stock of arable land through land development, and (b) by increasing land yield through the application of modern agricultural inputs. The agriculture sector also distinguishes between two phenomena that can reduce overall food production. The first one, 'land erosion' is included, as an irreversible process taking place over centuries, that physically removes land from production. The rate at which land erodes can be large or small, depending on the human actions taken to control the erosion rate, but it is assumed that the direction of land movement cannot be changed. The erosion rate could be zero, but it will never become negative. The second assumption is that the total food output can be reduced through a reduction in land yield caused by lower land fertility, a reduction in the humus and nutrient content of the soil. This is a reversible process, as degradation of the land's fertility occurs only when insufficient resources are allocated to the enhancement of the natural soil regeneration mechanisms; thus the regeneration forces do not manage to keep up with the continually occurring degradation forces. In the ANEMI model all types of arable land are included in a single stock, so the model reflects in a single quantity, the aggregate of all different lands with the varying cultivation characteristics.

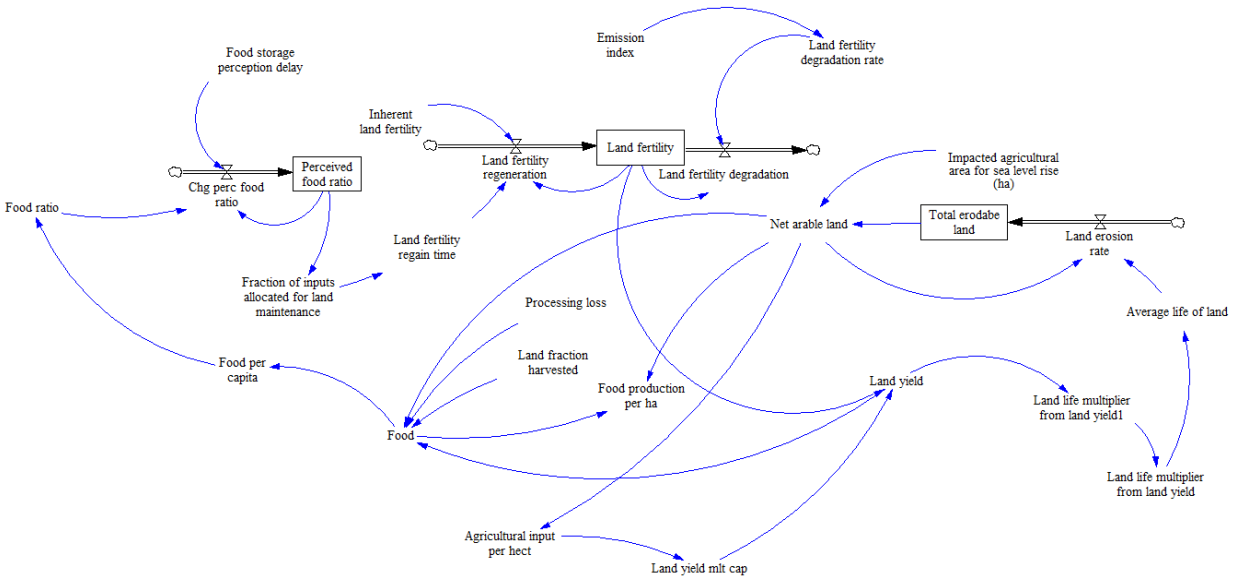

Figure 2.11: Model structure of the ANEMI food production sector

Technological change affects relationships in the agriculture sector in a variety of ways. Some of the effects of advances in technological capability are included endogenously in the food production sector. For instance, it is assumed that the allocation of more investment to increasing land yield will have roughly the same success in the total global agricultural system. Such an assumption implies that the regional variations posed by different soils, climates, and traditional cultivation procedures will be eliminated by the advancement of technology. In the same manner it is also assumed that the investment in land maintenance, regeneration of land fertility, will always succeed.

Causal Structure of the ANEMI Food Production Sector

The causal loop diagram for the food production sector is presented in Figure 2.12 based on the WORLD3 model of Meadows et al. (1974). This figure represents a simplified representation of the causal loop structure of the food production sector. The complex land yield is obtained from the land fertility, water-stress, capital investment, where all of these variables are connected with positive polarity. The total amount of produced food depends on the land yield, availability of the agricultural land, availability of the water for irrigation, and so on. In this diagram food ratio is working as a thermostat, by which extra investment is pumped in the food production sector, when the ratio is below the threshold level. The extra investment is used to improve the land fertility and technological development is used to enhance the food production by increasing the land yield. Unplanned agricultural activity increases the land erosion and decreases the land fertility. They are controlled by decrease in the suitable agricultural activity. Two most essential parameters of this sector; water-stress and arable land are coming from the other sectors of the ANEMI model. Population, which is the product of the population sector, is used in the computation of the per capita food production to assess the requirements for further investment.

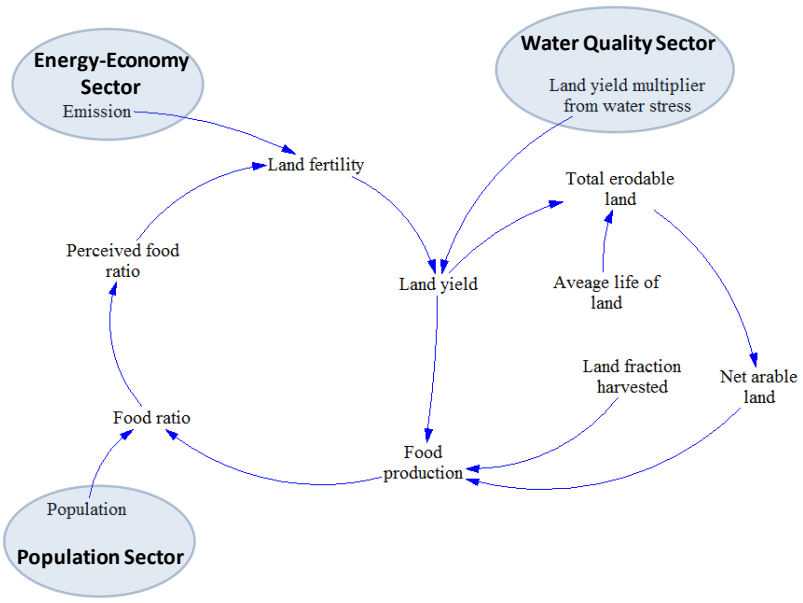

Figure 2.12: Causal loop diagram of the ANEMI food production sector

Mathematical Description of the ANEMI Food Production Sector

The important equations of the food production sector, and the values of their associated parameters, are provided in this section. The food production sector description is based on the work of Meadows et al. (1974).

The total annual food production is assumed to be the function of cultivated land and land yield. Labour force is not included in this calculation assuming that there will not be any shortage of labour force. Moreover, with the technological improvement the requirement for the labour force will be decreased day-by-day. Thus the food output is calculated simply as the output per hectare of harvested land times the total cultivated land area.

$$F_p = L_y \cdot A_l \cdot L_{fh} \cdot (1 - P_l) \tag{2.67}$$

where F_p is the amount of food production, L_y is the land yield. The net arable land, land fraction under harvesting and processing loss is denoted by A_l , L_{fh} and P_l respectively. Here, the processing loss is assumed as 10%.

The land yield L_y is the average total weight of crop production on a hectare of land per year. In the ANEMI version 2 model land yield is partly computed by the land fertility, which is defined as the weight of crop that land will produce using only traditional inputs such as human or animal energy and natural fertilizers, such as manure. The land yield, L_y, can be increased significantly above the land fertility by the use of modern agricultural inputs.

$$L_y = L_{yf} \cdot L_{fert} \cdot L_{ymc} \cdot L_{ymw} \tag{2.68}$$

where L_{yf} is the land yield factor, L_{fert} is the land fertiality, and L_{ymc} is the land yield multiplier from capital. Availability of water resources is a vital component of the land yield, therefore water-stress to land yield factor (L_{ymw}) is introduced in the Equation (2.68).

The land fertility (L_{fert}) is the average ability of one hectare of net arable land (A_l) to produce crops without the use of modern agricultural input. The fertility of the land is a complex function of the organic and inorganic content of the soil, the climate, and the incident solar radiation. Any process that interferes with soil chemistry, water holding capacity of the soil is likely to change the soil fertility. There are many such processes, some with positive influence tending to regenerate soil fertility and some tending to degrade it. In a simplified way the land fertility can be defined as:

$$L_{fert} = \int \left(L_{fr} - L_{fd}\right) \cdot dt \tag{2.69}$$

where L_{fr} and L_{fd} stand for land fertility regeneration and land fertility degradation, respectively.

Calculation of the net arable land (A_l) combines different inputs including impacted agricultural land due to sea-level rise. It represents the net cultivated area which is dedicatedly used for the direct human food production. Therefore, it excludes the land area used for the production of fodder and animal crop (L_{fa}), and can be expressed as:

$$A_l = (L_{ar} - L_{ero}) \cdot L_{obs} - L_{slr} - L_{fa} \quad (2.70)$$

where $L_{ar}$and L_{ero} represent the arable land and net erodible land, respectively. Obstacle to land conversion is defined as L_{obs} and impacted agricultural land is denoted as L_{slr}.

2.1.5 The Land-Use Sector

Land-use change can be considered one of the factors contributing to the increase in CO_2 concentration in the atmosphere. Therefore, the land-use change plays a key role in determining the atmospheric level of carbon dioxide over the long period of time. It is estimated that an added extra 1.6 ± 0.8 Gt C/year was released in the atmosphere in 1990's due to conversion of forests to agricultural land (Watson et al., 2000), while anthropogenic greenhouse emissions contributed 6.7 Gt C (Marland et al, 2008) in 2000.

The ANEMI model version 2 represents land-use and land-use change in the same fashion as in Goudriaan and Ketner (1984), as shown in Figure 2.13. The transfer matrix simulates both conversions of one of the six biome-types to another (such as the conversion of tropical forest

to agricultural land), and human interference within a single biome type (such as forest fire, burning of grassland or agricultural land after harvesting). The transfer matrix is only considering the human intervention, assuming that the ecosystem is resilient to natural disturbance.

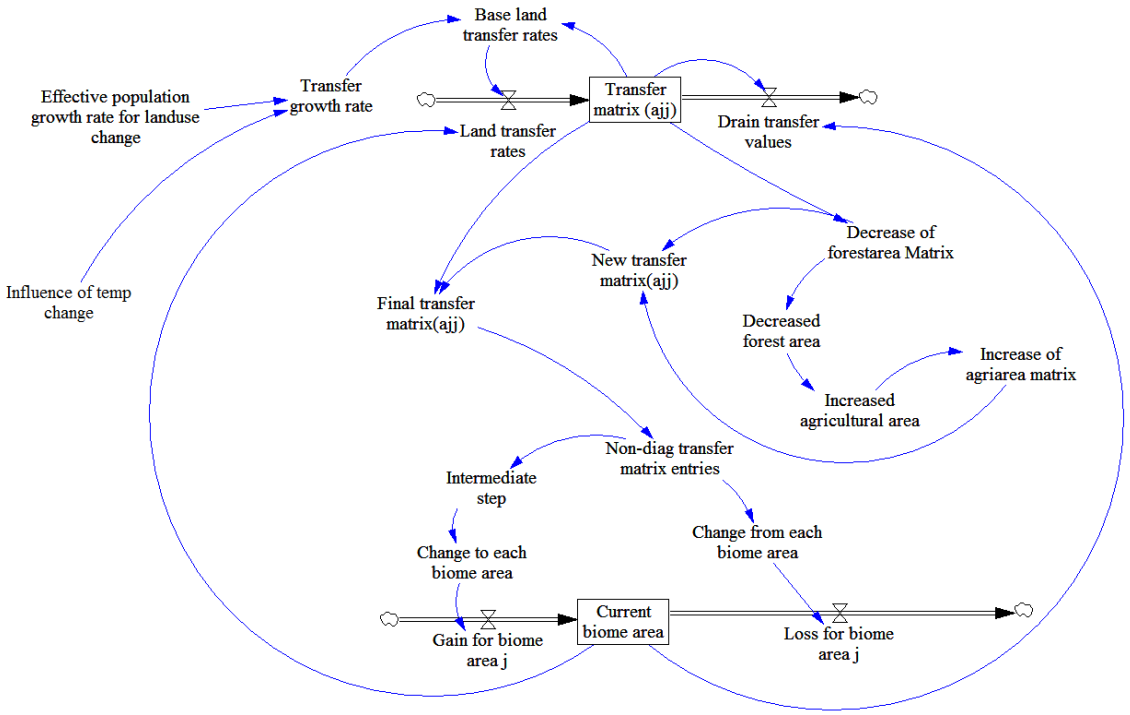

Figure 2.13: Model structure of the ANEMI land-use sector

The transfer matrix does not include actual spatial data. It describes the total extent of one biome and its change over time in an abstract fashion. Finally, it also does not specify the actual cause of change in biome area. Any change is modelled simply as a result of population change – an intersectoral feedback. However, despite its simplicity, the approach models human impacts on biome extent acceptably, given the limited understanding of the direct impacts of land-use change (Lambin et al., 2001; Veldkamp and Lambin, 2001).

The initial values for the transfer matrix and biome areas are shown in Table 2.5. Note, that these values match 1980 values in Table 2.2 and Table 2.5 in Goudriaan and Ketner (1984: 178,180), when the model incorporates a feedback from the population sector.

Table 2.5: Transfer matrix of area between ecosystems (Mha yr^{-1}) in 1980

From (j): / To (i):	Tropical Forest	Temperate Forest	Grassland	Agricultural Land	Human Area	Semi-Desert and Tundra
Tropical Forest	15	0	0	0	0	0
Temperate Forest	0	2	0	0	0	0
Grassland	6	1	400	0	0	0
Agricultural Land	6	0	0	400	0	2
Human Area	0.5	0.5	1	1	0	0
Semi-Desert and Tundra	0	0	0	0	0	0
1980 Area	3610	1705	1880	1745	200	2970

Causal Structure of the ANEMI Land-Use Sector

The causal structure of the land-use sector is presented in **Error! Reference source not found.** based on Goudriaan and Ketner (1984). This is a simplified representation of the basic causal loop structure of the land-use sector. The intensity of shifting cultivation and burning are related to human population size, but this relationship is less than proportional, because of increased urbanization. Temperature change is also treated as a minor factor of land transfer, as in many places increased temperature could make desertification more rapid but at the same time it could open the opportunity for the agricultural activities in the northern hemisphere. In the ANEMI, the main driving force, population growth, is the outcome of the population sector, whereas temperature change is computed in the climate sector. However, loss or gain of the each biome area in each year is determined on the basis of the transfer matrix. The current biome area is basically the total area under each biome type at any specific time. So it's a current balance of biome accounting system. Current biome area serves as a checking mechanism for the unrealistic land transfer, when any of the biome types reaches almost zero value by completely converting to other types of biome.

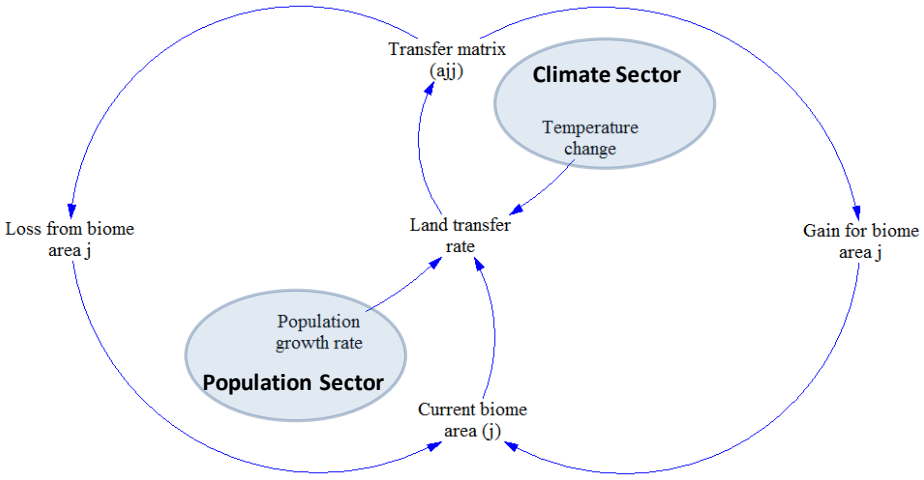

Figure 2.14: Causal loop diagram of the ANEMI land-use sector

Mathematical Description of the ANEMI Land-Use Sector

The land-use sector is represented by a very simple model structure, where the provided land transfer matrix (by Goudriaan and Ketner, 1984) is only influenced by the population growth and minor impact of temperature change.

It is assumed that the land transfer rate outside the diagonal direction of the transfer matrix (see Table 2.5) is proportional to the population growth rate, but that burning and shifting cultivation which represented by the diagonal direction, grow with the square root of 'population growth rate'. Therefore, the land transfer rate can be expressed as:

$$L_{trans\ (non\_dia)} = L_{tm} \cdot r \qquad (2.71a)$$

where the land transfer rate in non-diagonal direction is $L_{trans(non\_dia)}$, L_{tm} is transfer matrix and r denotes population growth rate.

In case of land transfer along diagonal direction, the transfer rate ($L_{trans\ (dia)}$) can be describes as:

$$L_{trans\ (dia)} = L_{tm} \cdot (r)^{1/2} \qquad (2.71b)$$

Transfer matrix is working as a reservoir where inflow is land transfer rate and outflow is drain transfer value (L_{tdr}). The drain transfer value is used in the model to avoid negative term. The following equation represents the generic form of 'transfer matrix' calculation, which can be used for both diagonal and non-diagonal matrix entities.

$$L_{tm} = \int (L_{trans} - L_{tdr}) \cdot dt \qquad (2.72)$$

The area A_j of ecosystem *j* changes as:

$$\frac{dA_j}{dt} = \sum_{i=1}^{6} (a_{ij} - a_{ji}) \qquad (2.73)$$

where A_j is the area of ecosystem *j*, a_{ij} is the rate of transition of area from ecosystem *j* to ecosystem *i*.

2.1.6 The Population Sector

Two basic dynamics of the society-biosphere-climate-economy-energy system of the Earth and biosphere are exhibited by all human populations tendency towards exponential growth, and a long delay in the population's adaptive response to changing external conditions (Meadows et al., 1974). The actual rate of growth, the nature of the adaptive response, and the length of delay, vary, depending on many factors in the total system. When any biological population grows, the pattern of growth over time tends to be exponential. In the twentieth century, rapid exponential growth has been exhibited not only by the global human population but by nearly every national and regional population as well (Meadows et al., 1974). The total increase in the population during any time period must be at least partially determined by the size of the population of reproductive age in that time period. For the global population, migration is not a factor, as there is no consideration of spatial distribution of the population.

Demographic responses to new external conditions, through changed birth and death rates, are often significantly delayed. The two major sources of the delay are the age structure of the population and the inherent slowness of social change. It takes at least 15 years for a newborn child to mature and become a parent (Figure 2.15). There is a delay of more than 50 years before the child reaches the age of highest probability of death. The long delays inherent in the biological processes of maturation and aging give every human population a strong momentum - a tendency to keep following the same dynamic behaviour it has followed in the past (Meadows et al., 1974). Because of the momentum, a population that has been growing rapidly will continue to grow for decades, even after fertility has fallen to the equivalent of two surviving children per married couple. Similarly, a population that has experienced fertility lower than the replacement level may continue to decrease for some time after fertility has risen to the replacement level.

The population sector includes a four-level population model, which means the population is divided into 4 age groups (0 to 14 yr; 15 to 44yr; 45 to 60yr; and 60 to 60 plus). As initial stocks values, the UN data (DESA, 2011) of 1980 is used.

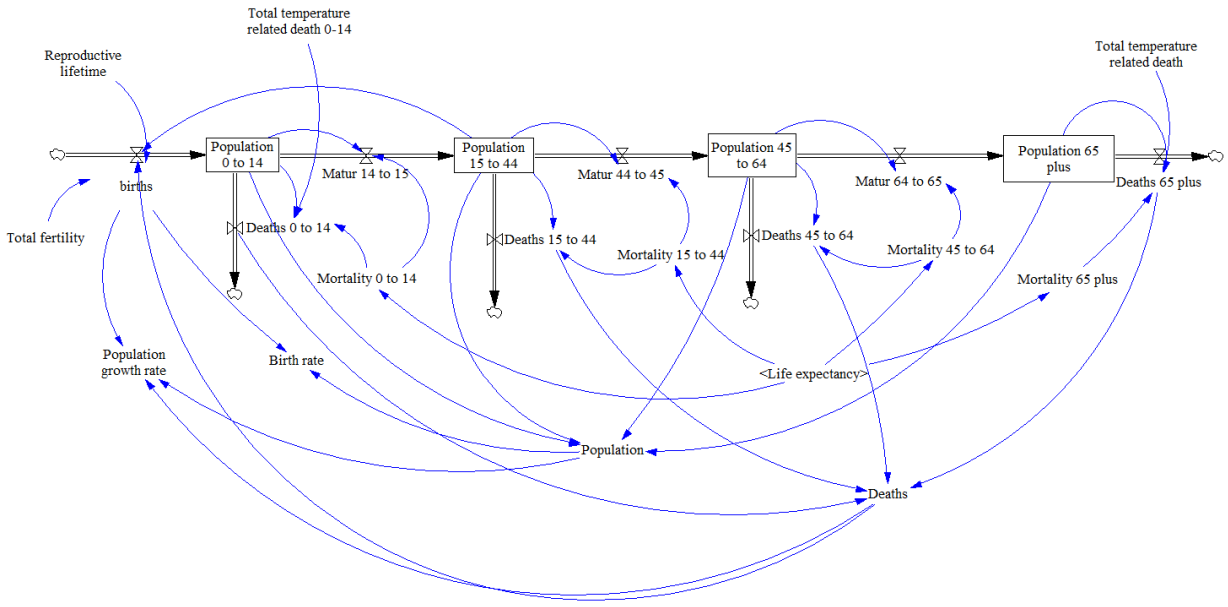

Figure 2.15: Model structure of the ANEMI population sector

Causal Structure of the ANEMI Population Sector

The population sector of the ANEMI model version 2 is based on the WORLD3 population model (Meadows et al., 1974). It represents continuous dynamic interactions among the human population, climate and global resources (Figure 2.16). The population sector model contains numerous feedback loops representing demographic and technological-economic means of achieving a favourable balance between the population size and the supply of resources. In this model crowding, pollution, availability of food, and household income are affecting the life expectancy. The life expectancy and extreme temperature are determining the population death rate. Fertility is determined based on the fertility control effectiveness, the capital allocation, desired family size, and so on. Birth and death rates are only two direct variables used in the population computation.

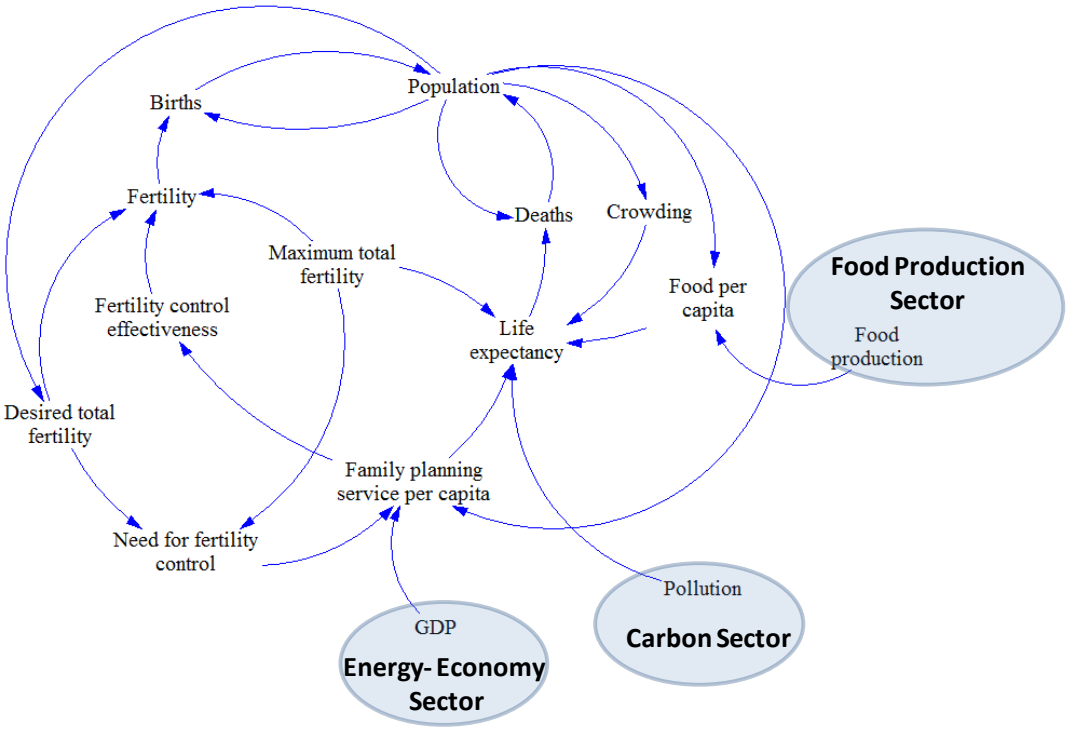

Figure 2.16: Causal loop structure of the ANEMI population sector

Mathematical Description of the ANEMI Population Sector

Many factors are affecting the population's average level of health or life expectancy. It is by no means easy to assess the role of various factors that are working to increase or decrease the mortality. When one variable of interest seems to depend on a number of other variables, statistical interface techniques are usually required to find out the relative importance of each individual contributing factor. In case of life expectancy, Kusukawa (1967) carried out a statistical analysis. The empirical relationship between food per capita, and life expectancy is adopted from Meadows et al (1974); and Keyfitz and Flieger (1971).

Four factors: (i) food, (ii) health services, (iii) crowding, and (iv) pollution are incorporated in the equation for life expectancy as modifiers, or multipliers, of a 'normal' life expectancy. The normal life expectancy can be set at any arbitrary value as long as the four multipliers are all defined properly with respect to that value.

$$L_E = L_{EN} \cdot L_{MF} \cdot L_{MHS} \cdot L_{MP} \cdot L_{MC} \quad (2.74)$$

where L_E is the life expectancy, L_{EN} is the life expectancy normal, and L_{MF} is the lifetime multiplier from food. Lifetime multiplier from health service, persistent pollution, and crowding are represented as L_{MHS}, L_{MP}, and L_{MC} , respectively.

In the population sector the number of deaths per year (D_{er}) is expressed as the total number of people of a specific age group (P_{agr}) multiplied by the mortality (P_{mor}) of the same group.

$$D_{er} = P_{agr} \cdot P_{mor} \quad (2.75)$$

where mortality is a function of life expectancy and the functional relationship is available from Meadows et al (1974, page 170-172) as:

$$P_{mor} = f(L_E) \quad (2.76)$$

The thermal stress related mortality should increase due to the climate change. It has been established that 16 to 30 degree Celsius is the comfortable temperature zone. One percent increase in the death rate could happen for 1 degree drop in temperature below 16 degree Celsius. On the other hand 1.4 percent increase in the death rate may be experienced per degree temperature rise above 30 degree Celsius. As children's and aged people (above 65 years of age) are mainly vulnerable to extreme climate, so the temperature related death is

incorporated in the ANEMI model for 2 age categories (0-14 and 65 plus). So the Equation (2.75) changes as follows:

$$D_{er} = P_{agr} \cdot P_{mor} + D_{heat} \tag{2.77}$$

The Equation (2.75) is still valid for the population between 15 to 64 years of age. The number of births per year (B_{er}) is calculated from a purely demographic factor, the number of fertile women in the population (assumed, half of the total population between 15 to 44 age group), and from a socio-economic factor, the average number of births per women per year.

$$B_{er} = F_{total} \cdot \frac{0.5 \cdot P_{15-44}}{R_{life}} \tag{2.78}$$

where F_{total} is the total fertility, R_{life} is the reproductive lifetime of 30 years, and P_{15-44} is the total population between age 15 and 44.

Total fertility is computed from the maximum total fertility (F_{Mtotal}), desired total fertility (F_{Dtotal}) and fertility control effectiveness (F_{econt}):

$$F_{total} = MIN\left(F_{Mtotal}, F_{Mtotal} \cdot (1 - F_{econt}) + F_{econt} + F_{Dtotal}\right) \tag{2.79}$$

2.1.7 The Water Resources Sectors

The representation of the global water resources in the ANEMI model version 2 includes: hydrologic cycle, water demand, and water quality sectors. Global hydrologic cycle and water demand sectors can be found in many models like: WaterGAP2 (Alcamo et al, 2003a), Water balance model (Vörösmarty, 2002b), Macro-PDM (Arnel, 1999a) and etc. Simonovic (2002), also enhanced the existing WORLD3 (Medows et al., 1992) by adding the water sectors. Even though with those improvements, the water sectors of those models are not dynamic in nature. Davies and Simonovic (2008) for the first time, successfully introduced a detailed water resources component in the ANEMI model version 1. The version 2 of ANEMI model extends the work of Davies and Simonovic (2008; 2010; 2011) in an attempt to capture the dynamics of the water resources in respect to both, quality and quantity of water.

2.1.7.1 Hydrologic Cycle Sector

Water is the only natural resource that exists in three forms: liquid, solid (snow, ice) and gas (clouds). Unlike most mineral resources, it is renewable. Water reservoirs in the global hydrologic cycle include the oceans, the land surface, groundwater, ice sheets, and the atmosphere, which can be separated into marine and terrestrial components (Chahine, 1992). Transfers between these reservoirs include the processes of evaporation and evapotranspiration, advection, precipitation (both solid and liquid), snow and ice melting, groundwater percolation into, and base flow from aquifers, and surface runoff to the oceans (Chahine, 1992; Gleick, 2000b; Shiklomanov, 2000). Being a cycle, it has no specific beginning or ending. Rather, liquid water from the Earth's surface, particularly the oceans, is evaporated into a gaseous form and enters the atmosphere as water vapour (clouds). The atmospheric moisture is eventually returned to the Earth's surface in the form of rain or snow. The liquid fresh water moves over the land surface on its journey back to the ocean (Figure 2.17). During its overland journey, it creates rivers, lakes, wetlands and/or groundwater aquifers. This cycle comprises nature's method of replenishing, redistributing and purifying the world's natural water resources (William D. Williams, 2001).

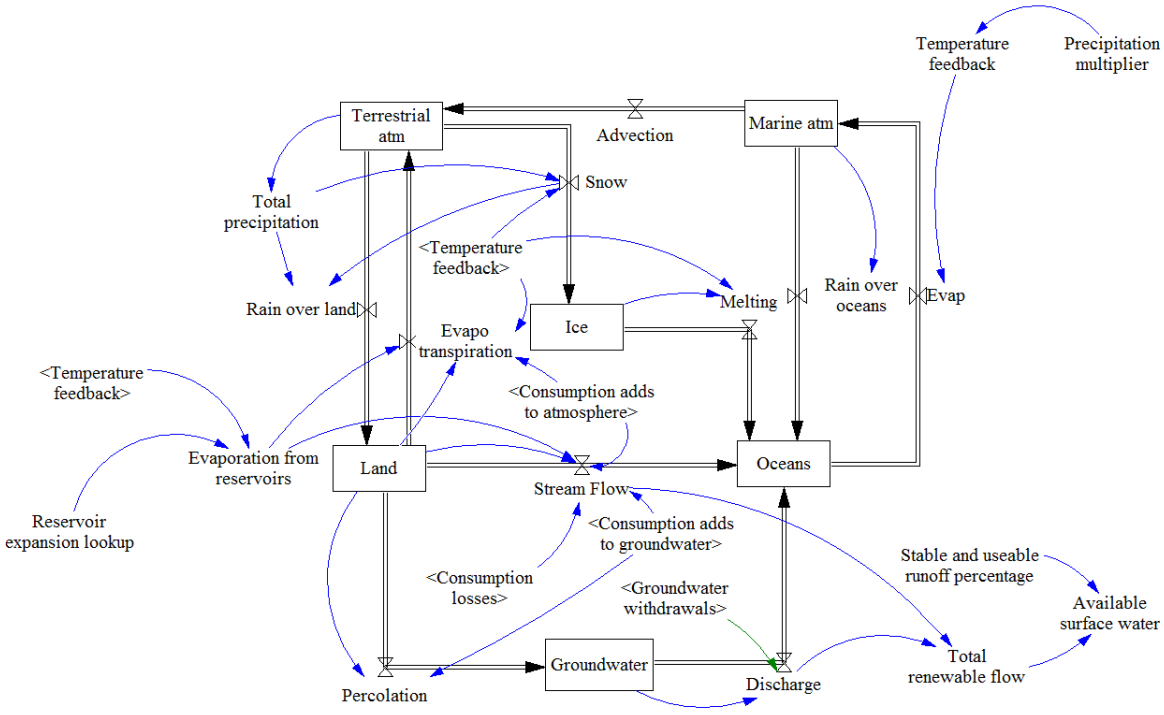

Figure 2.17: Model structure of the ANEMI hydrologic cycle sector

Shiklomanov (2000) estimates the annual runoff of close to 42,750 km^3/year. All the water is not stable or controlled by the natural hydrologic cycle because of human interception. The ANEMI model reaches a steady-state at the stock and flow values given in Table 2.6 and Table 2.7, which lie within the range of values provided by Shiklomanov and Rodda (2003: 13), Gleick (2000b: 21) and Chahine (1992). Table 2.6 compares the range of stock values provided in the literature with the values used in the ANEMI model; where values differ between the sources, the most recent figures available have been used.

The initial, steady-state flow values used in the ANEMI model simulations are close to the values available in the literature, as shown in Table 2.7, where no values are available, the flow in question is marked as 'Not available'.

Table 2.6: Major stocks of water, and values used in the ANEMI model (in km^3)

Name of Stock	Literature Value	Model Values
Marine Atmosphere	9.4-11 x 10^3	9.4 x 10^3
Terrestrial Atmosphere	4.0-4.5 x 10^3	4.0 x 10^3
Oceanic Water Content	1338 x 10^6	1338 x 10^6
Land Surface Water	118-360 x 10^3	200 x 10^3
Ice and Permanent Snow	24-43 x 10^6	24.5 x 10^6
Groundwater Content	10.5-23.4 x 10^6	10.6 x 10^6

Table 2.7: Hydrologic flows and initial flow values used in the ANEMI model (in $km^3\ yr^{-1}$)

Name of Flow	Literature Value	Model Values
Rainfall over Land	107000-180151	115019
Terrestrial Evapotranspiration	71000-126631	73320
Snowfall over Ice Sheets	2474	2625
Advection (Marine to Terrestrial)	36000-53520	45375
Precipitation over Oceans	398000-481680	489825
Evaporation from Oceans	434000-535200	535200
Melting of Ice Sheets (to Oceans)	2474	2625
Percolation to Groundwater	*Not available*	2312
Groundwater Discharge	*Not available*	2002
Streamflow	36000	39090
Total Renewable Flow	42750	41091

Note that the most sensitive values in the model are the base flows rather than stock values. However, the terrestrial atmosphere is an exception. It has the smallest volume of any of the stocks, and is affected by very large flow values. Particularly uncertain values in the model are the groundwater recharge, base flow, ice melt, and snowfall over ice sheets.

Causal Structure of the ANEMI Hydrologic Cycle Sector

Ocean is the vast reservoir of water and it works as a collector. Ocean receives water by rainfall, snow melt, surface flow and ground water discharge from marine atmosphere, land ice, land surface and ground water reserve respectively (**Error! Reference source not found.**). Ocean also releases water to the marine atmosphere through the evaporation process. This water travels to the terrestrial atmosphere through the advection process. While traveling over the land the

water vapour condense and produce either snow or rainfall. Over the years the snow hardens and converts into ice. On the other hand, after touching the land surface raindrops flow over the land into the river as a surface flow. Some part of the rainwater is absorbed by the soil through a percolation process and recharges the groundwater reserve. However, a portion of the rainfall is stored in low-lying areas and reservoirs. Plants also use water for food production and release the excess water through transpiration. Through evaporation some water returns to the atmosphere mainly from open water bodies.

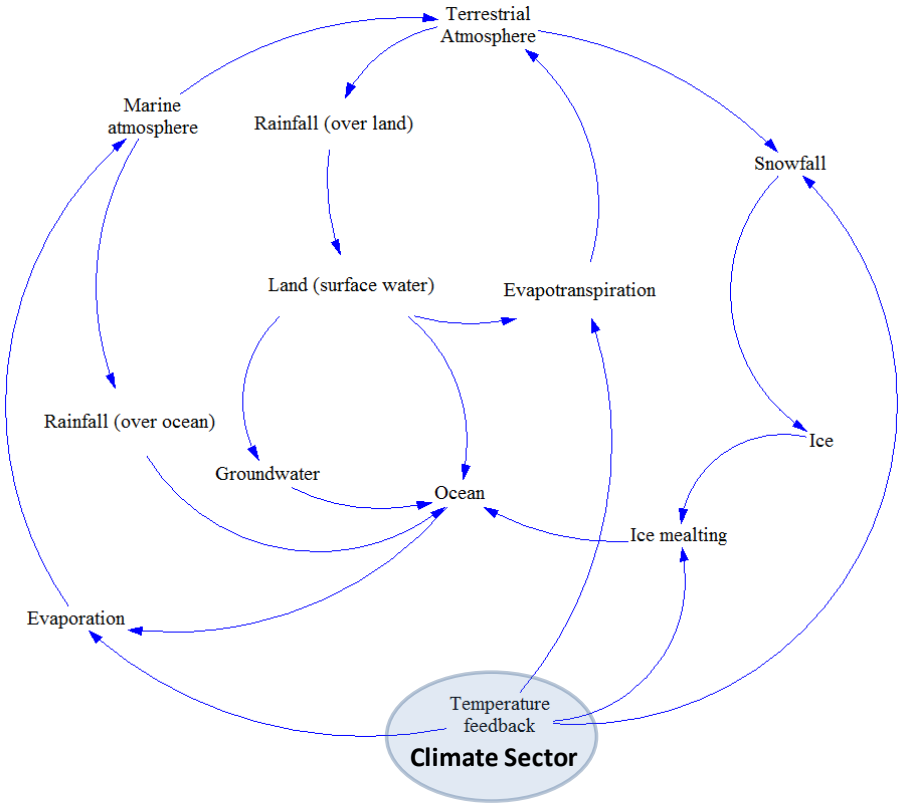

Figure 2.18: Causal loop diagram of the ANEMI hydrologic cycle sector

Mathematical Description of the Hydrologic Cycle Sector of ANEMI Model

The main process of the natural hydraulic cycle is already discussed, whereas this section lists the major stock and flow equations of the hydrologic cycle sector.

The equations for the marine and terrestrial atmospheric components are given by,

$$A_M = \int (E_M - Adv - P_0) \cdot dt \quad (2.80)$$

and,

$$A_L = \int (Adv + ET - P_R - P_s) \cdot dt \quad (2.81)$$

where A_M and A_L are the atmospheric water contents over the ocean and land, respectively, measured in km^3 and with the initial values given in Table 2.6. E_M is the evaporation from the oceans to the marine atmosphere, *Adv* is the advective flow of moisture from the marine atmosphere to the terrestrial atmosphere, P_O is precipitation over the oceans, *ET* is evapotranspiration from the land surface to the terrestrial atmosphere, P_R is precipitation over land in the form of rain, and P_S is precipitation in the form of snow, which accumulates on ice sheets and in glaciers.

The equation for the land surface has the following form,

$$LS = \int (P_R - ET - SF - GP) \cdot dt \quad (2.82)$$

where *LS* represents the water storage in the terrestrial environment, *SF* is the surface flow of water to the oceans, and *GP* is percolation of water from the land surface into longer-term storage in groundwater.

The oceans are governed by the following equation,

$$O = \int (SF + GD + P_0 + M - E_M) \cdot dt \quad (2.83)$$

where *O* is the water storage in the oceans, *GD* is the discharge of groundwater to surface flow, which then flows to the oceans, and *M* is the melting of ice sheets into the oceans.

Groundwater storage, GS, is determined by,

$$GS = \int (GP - GD) \cdot dt \tag{2.84}$$

and ice storage, *IS*, is given by,

$$IS = \int (P_S - M) \cdot dt \tag{2.85}$$

The evaporation from the ocean to the marine atmosphere is provided as:

$$E_M = E_{M0} \cdot T_{feedback} \tag{2.86}$$

where E_{M0} is the initial evaporation, set to 535,200 km^3 yr^{-1}, as in Table 2.7, and $T_{feedback}$ is a multiplier that represents the effect of climate change on the global hydrologic cycle. $T_{feedback}$ increases evaporation, evapotranspiration, snowfall, and melting rates by the fixed percentage for every degree of warming, and its value is based on two equations,

$$T_{feedback} = 1 + \left({}^{P_{mult}}/_{100} \right) \tag{2.87}$$

$$P_{mult} = P_{mult,base} \cdot \Delta T_S \tag{2.88}$$

where $T_{feedback}$ is the temperature multiplier, and P_{mult} is the percentage increase calculated by equation (2.88), in which $P_{mult,\ base}$ is its base value, set to 3.4% K^{-1}. P_{mult} depends on the change in surface temperature between initial and current conditions, which is represented by the ΔT_S term and is calculated in the model's climate sector. Since these two equations represent the main components of the *intersectoral feedbacks* of the ANEMI model, they are described in greater detail below.

The equation for advection from the marine atmosphere to the terrestrial atmosphere is given by,

$$Adv = Adv_0 \cdot \left(1 + {}^{\delta_{adv}}/_{100}\right) \tag{2.89}$$

where Adv_0 is the initial advection value, set to 45,375 km^3 yr^{-1}, as in Table 2.7, and δ_{adv} is the percent change in advection due to changes in the gradient that drives moisture from the marine atmosphere into the terrestrial atmosphere. The calculation of the percent change in advection, δ_{adv}, is given by,

$$\delta_{adv} = 100 \cdot \frac{\left[\left({}^{A_M}/_{SA_{0\%}} - {}^{A_L}/_{SA_{L\%}}\right) - \left({}^{A_{M0}}/_{SA_{0\%}} - {}^{A_{L0}}/_{SA_{L\%}}\right)\right]}{\left({}^{A_{M0}}/_{SA_{0\%}} - {}^{A_{L0}}/_{SA_{L\%}}\right)} \tag{2.90}$$

where A_{M0} and A_{L0} are the initial water contents of the marine and terrestrial atmospheres, respectively, as in Table 2.6, $SA_{O\%}$ is the percent of the Earth's surface that is covered by oceans, and is set to 67%, while $SA_{L\%}$ is the percent of the Earth's surface covered by land.

The equation that governs precipitation over the oceans, P_O, is,

$$P_o = P_{o0}\ {}^{A_M}/_{A_{M0}} \tag{2.91}$$

where P_{o0} is the initial precipitation over the oceans, given in Table 2.7.

From the flows in equation (2.81), the equation for evapotranspiration, *ET*, is

$$ET = ET_0 \cdot {}^{LS}/_{LS_0} \cdot T_{feedback} + E_{res} + C_{wa} \tag{2.92}$$

where ET_0 is the initial evapotranspiration from the earth's surface, given in Table 2.7, LS_0 is the initial water content of the land surface, given in Table 2.6, $T_{feedback}$ is given by equation (2.87), E_{res} is the evaporation from human-made reservoirs, explained below, and C_{wa} is the evaporation from consumptive water uses to the atmosphere, also explained in this section, below.

Precipitation over the land surface is broken into three components, P_R, P_S, and total precipitation, P_L. Precipitation in the form of rain over the land surface is governed by the following equation,

$$P_R = P_L - P_S + C_{wl} \tag{2.93}$$

where P_L is the total precipitation over land, given by equation (2.94), and C_{wl} is the addition to the land surface because of irrigation-based water-logging – note that C_{wl} is added to P_R for convenience only and is not intended to represent a component of the actual physical process of precipitation (recall that stocks can be influenced only through their flows). The total precipitation over land is given by,

$$P_L = P_{L0} \cdot {}^{A_L}/_{A_{Lo}} \tag{2.94}$$

where the initial total precipitation over land, P_{L0}, is given in Table 2.7. Finally, the equation for precipitation in the form of snow is,

$$P_S = \left(P_{S0} \cdot {}^{P_L}/_{P_{Lo}} \right) \Big/ T_{feedback} \tag{2.95}$$

where P_{S0} is the initial precipitation in the form of snow, which is given in Table 2.7. The effect of climate change represented by the division by $T_{feedback}$ rather than multiplication is introduced to decrease the amount of snow.

Several flows to and from the land surface, in equation (2.82), have already been defined. The surface flow equation is more complicated than most in this section, and takes the form,

$$SF = SF_0 \cdot \left({LS}/{LS_0}\right)^2 - E_{res} - C_{wa} - C_{gw} - C_{wl} - C_{loss} \quad (2.96)$$

where SF_0 is the initial surface flow, given in Table 2.7, the land surface content comparison is raised to the exponent 2 to model a non-linear increase in surface flow to the oceans as land storage increases, C_{gw} represents the seepage of withdrawn surface water to groundwater, and C_{loss} is the long-term, or permanent, loss of water from the hydrologic cycle because of its incorporation into manufactured goods, and so on. The other consumptive flows, C_{wa} and C_{wl}, are explained in Equations (2.92) and (2.93), respectively.

The last flow in Equation (2.82) models the percolation of water from the land surface into groundwater storage. The equation for percolation is given by,

$$GP = GP_0 \cdot {LS}/{LS_0} + C_{gw} \quad (2.97)$$

where GP_0 is the initial percolation of land surface water into groundwater, see Table 2.7.

The equation for groundwater discharge is,

$$GD = GD_0 \cdot {GS}/{GS_0} + GW \quad (2.98)$$

where GD_0 is the initial groundwater discharge from Table 2.6, GS_0 is the initial groundwater storage also from Table 2.6, and *GW* is the groundwater withdrawal, explained below. Note that, like C_{wl} in Equation (2.93), *GW* is added to *GD* for convenience only and is not intended to represent a component of the actual physical process of groundwater discharge (again, recall that stocks can be influenced only through their flows).

Melting of ice occurs according to the following equation,

$$M = M_0 \cdot {}^{IS}/_{IS_0} \cdot T_{feedback}^2 \tag{2.99}$$

where M_0 is the initial rate of ice melt, given in Table 2.7, IS_0 is the initial water content of ice sheets and glaciers, given in Table 2.5, and the $T_{feedback}$ is explained in the intersectoral feedbacks section, below. Note that the exponent on $T_{feedback}$ means that melting accelerates with changing temperature.

2.1.7.2 Water Demand Sector

Anthropogenic water withdrawals and consumption depend on overall surface water availability. The first requirement in computing the anthropogenic water use, is to determine a stable, or steady-state, runoff value, which occurs at some fraction of the total average runoff. Shiklomanov (2000: 18) sets this steady-state value at 37% of the total volume, while Simonovic (2002) and Alcamo et al. (2003a) use similar values of 33% and 32%, respectively. In this model, the available surface water is set to 37% of the total runoff, giving a base value of roughly 16000 $km^3\ yr^{-1}$, as in Shiklomanov (2000).

The available surface water can be allocated to two forms of human water use: water withdrawals and water consumption. These two terms require definitions because of differences in terminology from one study to another. According to Gleick (2000b: 41), the term 'withdrawal' refers to water removed from a source and used for human needs. Some of this

water may be returned to the original source with changes in the quantity and quality of the water. 'Water consumption' on the other hand refers to water withdrawn from a source and made unusable for reuse in the same basin, through evaporation, seepage to a saline sink, or through contamination (Gleick, 2000b: 41). In other words, water withdrawal is the sum of water consumption and returnable water. Note that the water returned after use to the surface flows, or the returnable water, may cause surface water to become polluted, which has important effect on the availability of surface water (Shiklomanov, 2000; Simonovic, 2002).

Both water withdrawals and water consumption have three components – domestic, industrial, and agricultural – as in other water models, such as those developed by Alcamo et al. (2003a), Simonovic (2002), and Vörösmarty et al. (2000). Each of these components has different drivers, which are related to the quantitative elements of anthropogenic water demand.

In this ANEMI model water use for domestic sector is based on per capita water requirement (Figure 2.19). Again per capita water consumption is not a fixed value, rather it depends on standard of living as well as technological improvement. Technological improvement covers the area of efficiency of municipal water supply as well as water consumption by the daily use commodities. Alcamo et al. (2003a) introduced the term "structural change", which combines standard of living and municipal water system efficiency. However, in the global version of the ANEMI model version 2, an aggregate value of water system efficiency and standard of living on a global scale is used.

The industrial sector is more efficiency driven compared to the previous one. The drivers include: 1) ongoing changes in the approach to cooling power generation plants, in an effect called structural change, and 2) changes in water use efficiency per unit of energy required for industrial production via technological change (Alcamo et al., 2003a). Industrial water demand is modelled on an energy-intensity basis (m^3 water MWh_{energy}^{-1}), which provides a connection to

a simple power generation sector in the model, while the level of structural change is driven by the economic sector (Davies and Simonovic., 2008). In terms of the first industrial sector driver, water use depends on the transition from once-through flow to circulating water supply systems for power generation, and on the development of dry technologies in the manufacturing industries (Shiklomanov, 2000). The most important result of a switch from once-through flow to circulating water systems for industrial cooling is that water withdrawals decrease strongly, while water consumption levels increase. Technological change, the second driver, “almost always leads to improvements in the efficiency of water use and the decrease in water intensity” (Alcamo et al., 2003a: 322), unlike structural changes which can either increase or decrease water intensity.

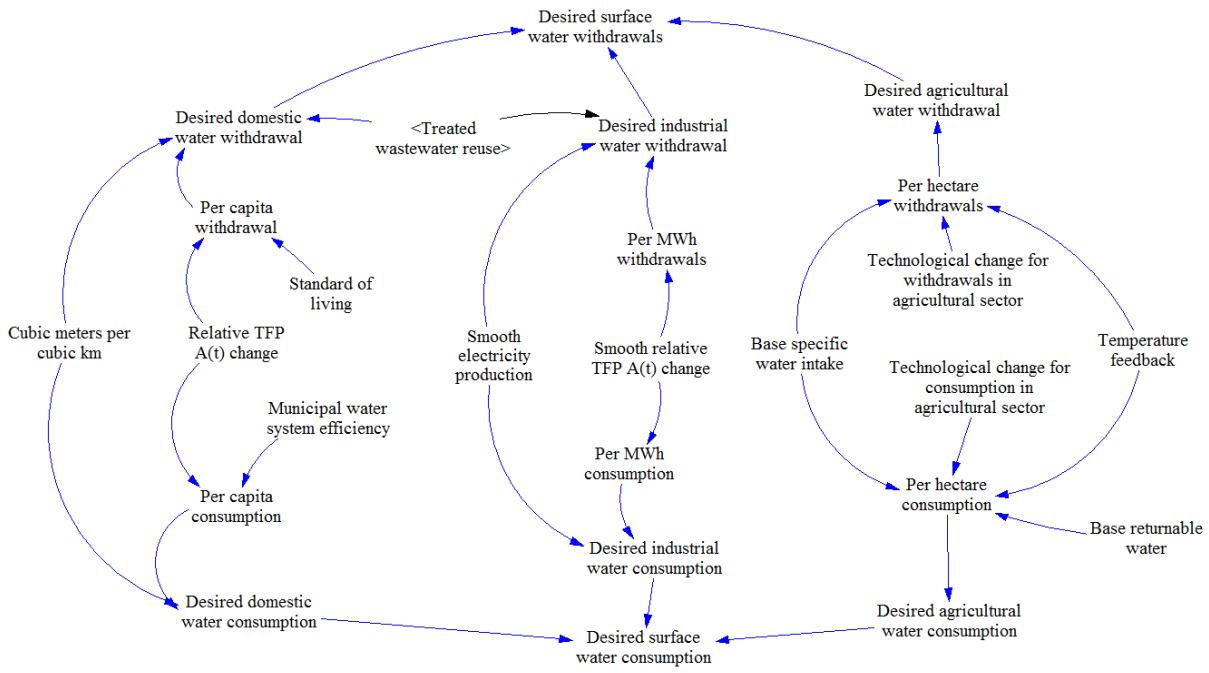

Figure 2.19: Model structure of the ANEMI water demand sector

Agriculture sector continues to demand the major share of water supply throughout the world. Around 70% of water is consumed for agricultural purpose. The fresh water used for agriculture

sector is becoming increasingly scarce, because of increasing population and climate change. Although water-stress seems somewhat localized problem, the impact of agricultural water consumption is not, as its far reaching and global in nature. In this model the main drivers of water use are total irrigated area, change in temperature and technological change. The irrigated area expanded rapidly between 1950s and 1970s in both, developed and developing countries. After 1970s the expansion slowed down, because of very high cost of irrigation system construction, soil salinization, depletion of water resources, and environmental protection problems (Davies and Simonovic., 2008). According to Postel (1999: 60), "irrigation has simply begun to reach diminishing returns. In most areas, the best and easiest sites are already developed." Anthropogenic climate change does not only affect available water resources but also water demand. Using a new global irrigation model, with a spatial resolution of 0.5^0 by 0.5^0, the first global analysis of the impact of climate change and climate variability on irrigation water requirements was done by Döll (2002). This work shows that the computed long-term average irrigation requirements might change under the climatic conditions of the 2020s and the 2070s, and relate these changes to the variations in irrigation requirements caused by long-term and interannual climate variability in the 20th century. Döll study shows clearly that there is every possibility of increased irrigation water requirements with the projected climate change scenarios. The last agricultural driver, technological change, affects the specific water intake value, or base irrigation water requirement per hectare of irrigated land (Shiklomanov, 2000), used in the model. To model the effects of technological change, it is important to recognize that the overall efficiency of irrigation worldwide may be as low as 40% presently, and that certain advanced irrigation techniques can increase efficiency quite significantly (Gleick, 2000a).

Causal Structure of the ANEMI Water Demand Sector

It's already mentioned that the surface water use can be classified as consumption and withdrawal. After Alcamo et al. (2003a), Simonovic (2002), and Vörösmarty et al. (2000), both water withdrawals and water consumption are classified in to three components based on the usages – domestic, industrial, and agricultural. Both, domestic water withdrawals and

consumption are based on the technological efficiency, GDP, population and etc. (Figure 2.20). In case of industrial water, energy production is playing a major role by dominating the 'industrial structural water intensity'. However, the agricultural water withdrawal and consumption are bit different.

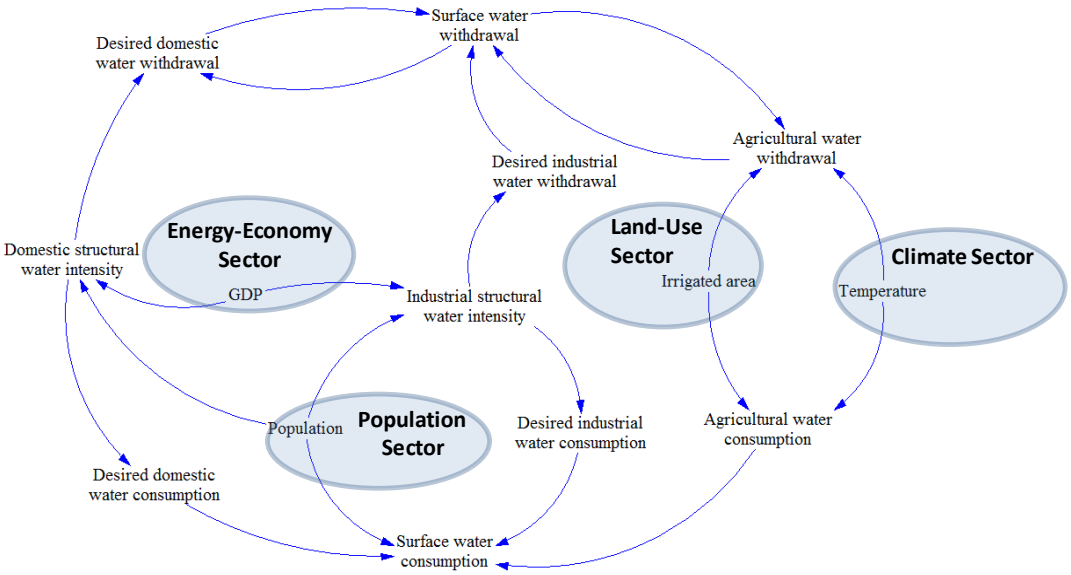

Figure 2.20: Causal loop diagram of the ANEMI model water demand sector

Mathematical Description of the Water Demand Sector of ANEMI Model

Desired surface water withdrawal (W_w) is the total withdrawal by all three types of water usage. In this case, desired domestic, industrial and agricultural water withdrawal are denoted by W_{dw}, W_{iw}, and W_{aw} respectively.

$$W_w = W_{dw} + W_{iw} + W_{aw} \tag{2.100}$$

The desired surface water consumption is calculated in the same fashion as Equation (2.100).

$$W_c = W_{dc} + W_{ic} + W_{ac} \tag{2.101}$$

where W_{dc} is desired domestic water consumption, W_{ic} is industrial water consumption, and W_{ac} is agricultural water consumption.

Domestic water withdrawals and consumption are both dependent on the population size (P_{total}) and its water requirement. However, the amount of desired industrial water withdrawal is reduced by the reuse of treated water (W_{dtwr}) and desalinated water (W_{ddsw}).

$$W_{dw} = P_{total} \cdot W_{pcw} - W_{dtwr} - W_{ddsw} \tag{2.102}$$

$$W_{dc} = P_{total} \cdot W_{pcc} \tag{2.103}$$

where W_{pcw} and W_{pcc} represents the per capita water withdrawal and consumption respectively.

Desired industrial water withdrawal and consumption are basically dependent on the industrial structural water intensity (ISWI), technological change and a function of electricity production (E_p) . However, for the calculation of 'industrial water withdrawal', treated industrial water for reuse (W_{itwr}) needs to be subtracted.

$$W_{iw} = f(E_p) \cdot ISWI \cdot TFP - W_{itwr} \tag{2.104}$$

$$W_{ic} = f(E_p) \cdot ISWI \cdot TFP \quad (2.105)$$

Desired agricultural water withdrawal and consumption are calculated based on the irrigated land (A_{tirr}), per hectare water withdrawal (W_{phw}) and consumption (W_{phc}). In case of agricultural activities, a significant portion of water is coming from the treated wastewater (W_{atwr}), as well as from ground water withdrawal (W_{wgw}).

$$W_{aw} = A_{tirr} \cdot W_{phw} - W_{atwr} - W_{wgw} \quad (2.106)$$

$$W_{ac} = A_{tirr} \cdot W_{phc} \quad (2.107)$$

where desired agricultural water withdrawal and consumption are denoted by W_{aw}, and W_{ac} respectively.

2.1.7.3 Water Quality Sector

In the ANEMI model version 2 surface water is mainly considered, in modeling water quality and subsequently water availability. While dealing with water pollution sources; domestic, industrial and agriculture use are counted as the main sources of wastewater (**Error! Reference source not found.**).

Shiklomanov (2000) stated that every cubic meter of contaminated wastewater discharged into the water bodies and streams renders eight to ten cubic meters of clean water unsuitable for use. Falkenmark (2005), Miller (2006), and Gleick (2000a) also recognized the importance of inclusion of polluted water while accessing the availability of surface water. Simonovic (2002:

263), who includes wastewater effects in his model, states that “the main conclusion of [his] research is that water pollution is the most important future water issue on the global scale.”

To include the effects of wastewater on surface water availability, it is important to separate the water use types (domestic, industrial, and agricultural), since each has different characteristics (Davies and Simonovic, 2008). In the domestic sector, all returnable water require treatment (Gleick, 2000b), while in the industrial sector, only the wastewater from manufacturing processes requires treatment, since thermal power plants do not generate chemical pollution (Vassolo and Döll, 2005). In the agricultural sector, returnable water comes from broadly distributed fields and cannot be treated, despite the presence of fertilizers and toxic chemicals (Postel, 1999).

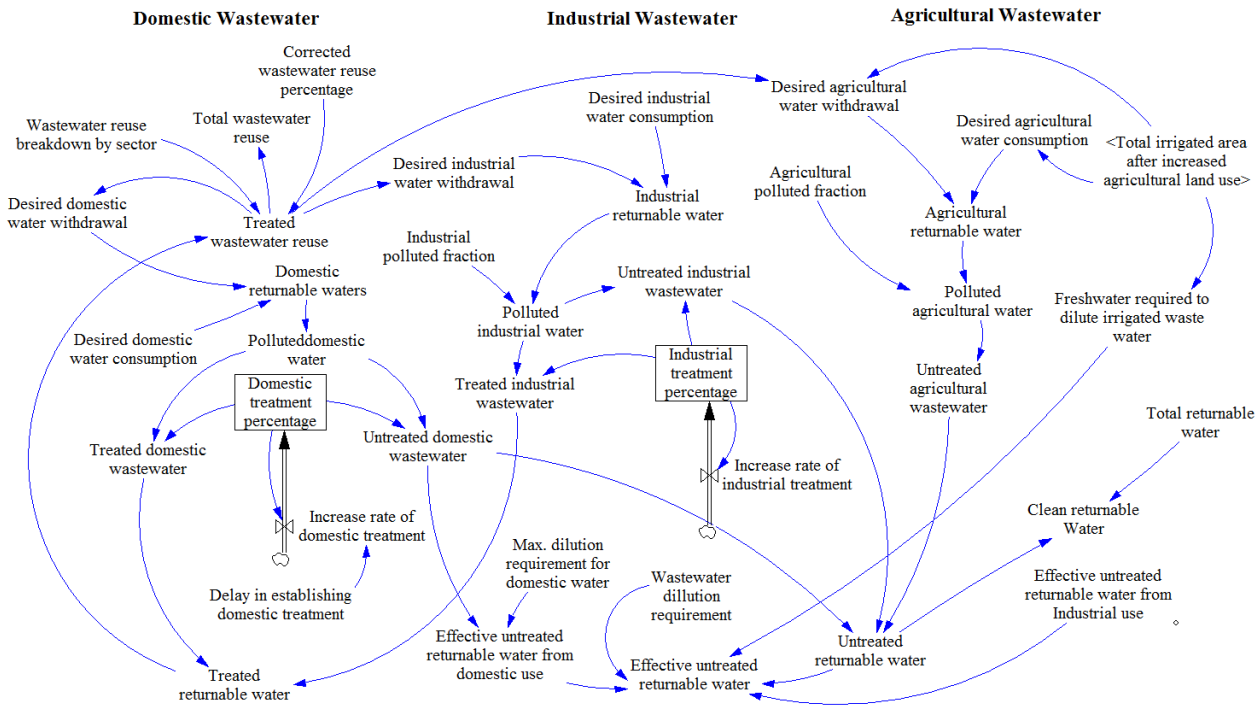

Figure 2.21: Model structure of the ANEMI water quality sector

Human withdrawal of water from the natural resources along with pollution and dilution requirements makes fresh water scarce in many places around the world. Water scarcity is often measured using an indicator called 'water-stress', which "is a measure of the degree of pressure put on water resources by users of the resources, including municipalities, industries, power plants and agricultural users" (Alcamo and Henrichs, 2002: 353). The most commonly used indicator of water-stress is the annual withdrawals-to-availability (wta) ratio, although per capita measures are also available (Arnell, 1999b). Alcamo and Henrichs (2002) write that 'wta' values of 0.2 indicate 'mid-stress' and that values of 0.4 and higher indicate 'severe stress', and Vörösmarty et al. (2000) use a similar scale. Indicator values of 0.2 or higher suggest that water-stress is likely to limit development (Arnell, 1999b). The concept of water scarcity is most meaningful at the watershed or sub-watershed level. Identifying water-stressed nations may not be overly meaningful (Davies and Simonovic, 2008). In this study, the measurement of water-stress is on global scale because each connected sector is aggregated separately in a single global value. If the model shows water scarcity at a global scale, it doesn't necessarily mean that every part of the globe is under water-stress, which is one of the limitations of this global version of ANEMI model. However, the individual sector based fresh water requirement to dilute polluted water to an acceptable level makes the model unique.

As per the literature (Gleick, 2000a; Gleick, 2000b; Simonovic, 2002), water reuse offers means to reduce the water-stress in many of regions of the world, such as the United States, Southern Africa, Israel, and the Middle East. The ANEMI model version 2 has adapted such mechanism into its modeling structure. With increasing water-stress indicator, the level of wastewater treatment is unlikely to increase for low stress condition (less than 0.4). For moderate to high water-stress condition (values above 0.4), the model will certainly trigger the rate of wastewater treatment and reuse, with some delay. Therefore, the treated wastewater reuse will increase over time and according to Gleick (2000b), irrigation sector will receive most of the treated water followed by industrial and domestic uses. Unfortunately this model feature can't be tested fully because of water reuse data unavailability.

In the ANEMI version 2 model, the amount of treated wastewater reuse increases over time, with the rate of increase dependent on (a) the level of global water-stress, (b) the parameter that represents a real-world infrastructure, and (c)the decision-based delay. The effect of water reuse is to reduce the desired surface water withdrawal volume from each water use sector by the volume of treated wastewater used. According to Gleick (2000b), irrigation generally receives the most treated wastewater for reuse, followed by industrial and domestic uses. Unfortunately, wastewater reuse figures are generally anecdotal, so it is difficult to determine actual usage, particularly at a global level – the values in Table 2.8 are assumed to be representative, at present.

Table 2.8: Treated wastewater resue allocations to water use sectors

Parameter Name	**Sector**			**Source**
	Domestic	Industrial	Agricultural	
Treated Wastewater Reuse	10%	30%	60%	Gleick (2000b)

Causal Structure of the ANEMI Water Quality Sector

Water-stress measures the level of pressure on water resources. In other words, it expresses how much water is left for the ecosystem health. It accounts for the water withdrawal as well as return of unused water to the water resources (Figure 2.22). It also consideres the amount of fresh water required to dilute the wastewater, so that the discharged water quality can be within the acceptable range.

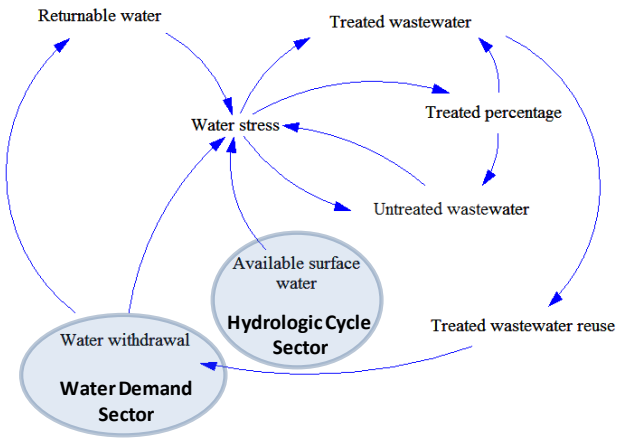

Figure 2.22: Causal loop diagram of the ANEMI model water quality sector

Mathematical Description of the Water Quality Sector of ANEMI Model

According to the usual ratio, water-stress equals the total withdrawal over the surface water availability, or,

$$wta = {W_w}/{(SF + GD)} \tag{2.108}$$

where W_w is the actual surface water withdrawal and *(SF+GD)* is the total surface runoff available for human use; however, Hoekstra et al. (1997) argue that this total runoff approach leads to overestimation of surface water availability. They recommend instead that water availability be considered as a portion of the total runoff.

In this model, water-stress is altered in two ways to take water pollution into account by using effective, rather than actual, withdrawal, as explained above and a reduction fraction of the total runoff, called A_S. This modification gives water-stress the following form,

$$wta = {}^{W_{SW}}/_{A_S} \tag{2.109}$$

where wta is now the effective surface water withdrawal, W_{SW}, divided by the available runoff volume, A_S. The result is a much higher value of water-stress than is calculated in the general fashion.

Incorporation of the Green Water Consumption

Green water consumption in global agriculture sector is incorporated to reflect the water quality effects on water-stress for rainfed cropland runoff. The ANEMI model computes the volume of runoff from rainfed cropland and pasture as an area-weighted fraction of the total runoff from the land surface. Later, fresh water requirement to dilute agrochemicals (used on the rainfed cropland) are computed by multiplying the "rainfed cropland runoff" with the "green water" dilution multiplier.

In some regions, food production almost entirely depends on the green water (>95% in sub-Saharan Africa). Green water is also important for irrigated land, as blue water is supplied there only to the amount that precipitation water is not sufficient for ensuring optimal crop growth. Hence, the global agricultural water consumption is much higher than suggested by figures that refer to blue water only. The outstanding importance of the green water is demonstrated by Rost et al (2008). Their work strengthens the need for including green water flows in the assessments of global water resources and water scarcity. The green water can be broadly classified into green crop water and green pasture water. Green crop water is basically the overland flow/runoff that is coming from the agricultural areas which are not under irrigation (rain feed agricultural area) and the green pasture water is the flow from the pasture land.

In the simple way the rainfed crop land (A_{RCA}) can be computed by deducting the irrigated area (A_{tirr}) from the total agricultural land (A_{arable}) as,

$$A_{RCA} = A_{arable} - A_{tirr} \tag{2.110}$$

while for computing the rainfed cropland runoff, area-weighted method is chosen considering the equal distribution of runoff over the total biome area. Therefore, the rainfed cropland runoff (Q_{RCR}) is

$$Q_{RCR} = Q_S \cdot \left(\frac{A_{RCA}}{A_{tbio}}\right) \tag{2.111}$$

where Q_S is the total renewable flow, and A_{tbio} is the total biome area.

The green crop water dilution requirement is the amount of fresh water required to dilute the polluted crop water. On the basis of the study done by Chapagain et al (2006), and Dabrowski et al. (2009), the dilution requirement of the green crop water is assumed to be 1:1. So, the green crop water dilution requirement (Q_{gcwdr}) can be formulated as follows,

$$Q_{gcwdr} = Q_{RCR} \cdot F_{gcwd} \tag{2.112}$$

Since, as mentioned earlier, the green crop water dilution requirement factor (F_{gcwd}) is considered as 1, the above equation can be rewritten as

$$Q_{gcwdr} = Q_{RCR} \tag{2.113}$$

However, the computation of the green water from the pasture land is not as straightforward as for rainfed cropland, because of the complexity in determining the total pasture land. In the ANEMI model version 2 the pasture land is calculated based on the requirements for increased animal production as a portion of the food supply for growing population. Therefore the pasture land productivity is a function of increase in human food production (P_{ipfood}) and Pasture area (A_{Pa}) calculation takes the following form

$$A_{Pa} = \left(f(P_{ipfood})\right).dt \Big/ Y_{Apa} \tag{2.114}$$

where Y_{Apa} is the average yield from pasture land.

Runoff over the pasture land is computed in the similar fashion as crop land. So the simplified form of the pasture land runoff (Q_{paR}) calculation formula is

$$Q_{paR} = Q_S \cdot \left(\frac{A_{pa}}{A_{tbio}}\right) \tag{2.115}$$

where Q_S is the total renewable flow, and A_{tbio} is the total biome area.

The green pasture water is relatively less polluted than the runoff from the crop land. In this study it's assumed to be 1/10 of the crop land. The green pasture water dilution requirement (Q_{gpadr}) can be then written as

$$Q_{gpadr} = Q_{PaR} \cdot F_{gpad} \quad (2.116)$$

As the green crop water dilution requirement is only 10% of the (F_{gcwd}) polluted water, so the dilution requirement (F_{gpad}) will be 0.1 and the simplified form of the above equation will be

$$Q_{gcwdr} = 0.1 Q_{RCR.} \quad (2.117)$$

2.1.8 Sea-Level Rise

Another important water-related sector is incorporated in the ANEMI model version 2 dealing with global and regional water resources - the sea-level rise. It is introduced into the ANEMI model to understand the feedback relationships between climate, water, and land-use sectors.

Processes in several nonlinearly coupled components of the Earth system contribute to sea-level change, and understanding these processes is therefore of high importance. The climate change on decadal and longer time scales, alters the volume of water in the global ocean by: (i) thermal expansion, and (ii) the exchange of water between other reservoirs (glaciers and ice caps, ice sheets and other land water reservoirs) and oceans (IPCC, 2007c). Vertical land movements such as glacial isostatic adjustment, tectonics, subsidence and sedimentation, influence local sea-level but do not alter the ocean water volume.

Global sea-level rose by about 120m during the several millennia of the last ice age (approximately 21,000 years ago), and stabilised between 3000 and 2000 years ago (IPCC, 2007c). Different indicators such as: marine deposits and lower boundary of mangrove growth, show that the global sea-level did not change significantly from then until the late 19th century. Estimates for the 20th century showed that global average sea-level rose at a rate of about 1.7 mm/yr. It is believed that on average, over the period from 1961 to 2003, thermal expansion

contributed about half of the observed sea-level rise, while melting of the land ice accounted for less than half, although there is some uncertainty in these estimates.

Understanding global sea-level change is not an easy task, rather a difficult scientific problem. It includes complex mechanisms and large number of feedback relationships. Significant uncertainties are still present, even in the projection of thermal expansion. In such a situation, semi-empirical model can provide a pragmatic alternative to estimate the sea-level response.

In the ANEMI model version 2, global average near surface air temperature is considered as the driver for the sea-level change. As per Rahmstorf (2007), sea-level is rising as the ocean takes up heat and ice starts to melt until (asymptotically) a new equilibrium sea-level is reached. Paleoclimatic data suggest that changes in the final equilibrium level may be very large; sea-level at the last glacial maximum, about 20000 years ago, was 120 m lower than the current level, where global mean temperature was 4^0 to 7^0 C lower. Three million years ago, during Pliocene, the average climate was about 2^0 to 3^0 C warmer and sea-level was 25 to 35 m higher than today's value. These data suggest changes in sea-level on the order of 10 to 30 m per ^{0}C.

The initial rate of rise is mainly to be proportional to the temperature increase,

$$\frac{dH}{dt} = a\,(T - T_0) \tag{2.118}$$

where *H* is the global mean sea-level, *t* is time, a is the proportionality constant, *T* is the global mean temperature, and T_0 is the previous equilibrium temperature value. The equilibration time scale is expected to be in the order of millennia. As long as the linear approximation holds, the sea-level rise from the previous equilibrium state can be computed by the following equation:

$$H(t) = a \int_{t_0}^{t} (T(t') - T_0)dt \tag{2.119}$$

where t' is the time variable.

Rahmstorf (2007) established a highly significant correlation of global temperature and sea-level rise (r=0.88, P=1.6 x 10^{-8}) with a slope of a = 3.4 mm/year per ^{o}C. The baseline temperature T_0, at which sea-level rise is zero, is 0.5 ^{0}C below the mean temperature of the period 1951-1980.

Till now, only a few research groups worked on the impact analysis of sea-level rise at a global scale utilizing satellite and remote sensing data in GIS environment. Nicholls et al. (1999), Nicholls (2002 and 2004), and Nicholls and Tol (2006) examined the potential impacts of global sea-level rise on coastal flooding. Their analyses are at the scale of coastal countries and are limited by the assumptions that the coastal country polygons have a constant slope and that the population distribution within the polygons is uniform. On the other hand, Dasgupta et al. (2009) considered only 84 developing countries in their impact analyses, leaving developed countries out of calculation. After a while, Xingong et al (2009) published their research paper on the sea-level rise on global scale where they used GIS methods to assess and visualize the global impacts of potential inundation using the best available global datasets.

Inundated Area by the Sea-Level Rise

Sea-level rise (SLR) due to climate change is a serious threat to the low lying countries with densely populated coastal regions that are also used for significant level of economic activity. Geographic Information System (GIS) software is used to overlay the best available, spatially disaggregated global population and land use, with the inundation zones corresponding to projected for 1- 6 m sea-level rise. The inundation data sets are collected from the Center for Remote Sensing of Ice Sheets (CReSIS), a Science and Technology Center established by the National Science Foundation (NSF) in 2005 (https://www.cresis.ku.edu/, last accessed August 2011).

CReSIS used the Global Land One-km Base Elevation (GLOBE) digital elevation model (DEM), a raster elevation dataset covering the entire world to calculate the inundation area. Cells in GLOBE have a spatial resolution of 30 arc seconds of latitude and longitude (approximately one kilometre at the equator), with each land cell in the grid assigned an elevation value (meters) in whole number increments. Potentially inundated areas are computed based on elevation and proximity to the current ocean shoreline. In simple form, to determine an inundation area for a sea-level increase of one meter above the current sea-level, all cells in the DEM that are adjacent to the ocean and that have a value less than or equal to one are selected and converted to water (i.e., they are inundated in the resulting output).

Impact on Agricultural Land

Agricultural area coverage data is collected from the International Centre for Tropical Agriculture (CIAT) and overlaid CReSIS based inundation map. The data are in ARC GRID format, in decimal degrees and datum WGS84 (World Geodetic System). They are derived from the NASA SRTM data (http://www2.jpl.nasa.gov/srtm/, last accessed August 2011). International Centre for Tropical Agriculture (CIAT) has processed this data to provide seamless continuous topographical surfaces. Areas with regions with no data in the original SRTM data have been filled in using interpolation methods.

There is a widespread perception that there is very little new land to bring under agriculture production. This perception may be well grounded for specific land-scarce locations such as Japan, South Asia and the Near East/North Africa. However, this perception may be wrong for other parts of the world. There are large tracts of land with varying degrees of agricultural potential in several countries, most of them in Sub-Saharan Africa and Latin America, and some in East Asia. In reality, expansion of agricultural land takes place all the time in countries with growing needs for food production. It is also evident that most of the low laying coastal areas

with fertile land are already used for agricultural activities. Thus, the rate of increase in agricultural area is very small, even though the global expansion may not be insignificant. This restricted the ANEMI model version 2 reliance on forecasted global average agricultural land expansion rate. The modeling process involves selection of year 1990 as the base year for agricultural land estimate, and after that, the expansion of agricultural land in the low lying coastal belt is considered negligent.

Impact on Population

Using an innovative approach with Geographic Information System and remote sensing data, the Oak Ridge National Laboratory (ORNL) produced LandScan population distribution database of the global population distribution (http://www.ornl.gov/sci/landscan/, last accessed August 2011). The model uses annual mid-year sub-national population estimates from the Geographic Studies Branch, US Bureau of Census to allocate population counts within administrative units. The LandScan model uses spatial data and imagery analysis technologies and a multi-variable dasymetric modeling approach to disaggregate census counts within an administrative boundary. Since no single population distribution model can account for the differences in spatial data availability, quality, scale, and accuracy as well as the differences in cultural settlement practices, LandScan population distribution models are tailored to match the data conditions and geographic nature of each individual country and region.

The binary raster format dataset is used for this analysis, which consists of 20,880 rows and 43,200 columns covering North 84 degrees to South 90 degrees and West 180 degrees to East 180 degrees. The values of the cells are integer population counts representing an average population distribution. The dataset has a spatial resolution of 30 arc-seconds and is output in a geographical coordinate system - World Geodetic System (WGS) 84 datum. The 30 arc-second cell, or 0.008333333 decimal degrees, represent approximately 1 km^2 near the equator. Since the data is in a spherical coordinate system, cell width decreases in a relationship that varies with the cosine of the latitude of the cell. Thus a cell at 60 degrees latitude would have a width

that is half that of a cell at the equator (cos60 = 0.5). The height of the cells does not vary. The values of the cells are integer population counts, not population density, since the cells vary in size.

2.2 Intersectoral Feedbacks

In the past years water as well as energy resources management received increased attention due to their role in socio-economic development, energy security and fight against global warming. It became clear, though, that water as well as energy resources cannot be evaluated independently of the rest of the economic and social processes, and therefore understanding of intersectoral feedback effects in the ANEMI model is important. Integrated Assessment Models (IAMs), have recently been employed in order to study the effects of climate change policy options. Such modeling framework unveils direct and indirect feedback effects of certain policy choices across various model sectors. ANEMI model version 2 is thus well suited for the study of complex society-biosphere-climate-energy-economy system. The model contains many closed-loop feedback relationships among nine model sectors. All of the major elements of the system are endogenous or included explicitly, so that the dynamic behaviour of the model arises from the system structure rather than input data.

In **Error! Reference source not found.**, each arrow indicates the connection between the two connecting model sectors and title associated with the arrow identifies the element/elements by which those sectors are connected. The positive and negative polarity associated with each arrow specifies the direction of change in two model sectors connected by the arrow. Here, positive sign represents change of connected variables in the same direction (increase/decrease in one variable causes an increase/decrease in the other). In case of negative sign, the change occurs in the opposite directions (increase in one variable causes a decrease in the other).

In a brief descriptive way the connections between different sectors of ANEMI model (**Error! Reference source not found.**) are:

- The *carbon* and *climate* sectors through atmospheric CO_2 concentrations;
- The *carbon* and *food production* sectors through emission index;
- The *carbon* and *population* sectors through population index;
- The *climate* and *hydrologic cycle* sectors through surface temperature change;
- The *climate* and energy-*economy* sectors through surface temperature change;
- The *climate* and *population* sectors through surface temperature change;
- The *hydrologic cycle* and *water demand* sectors through surface water availability;
- The *hydrologic cycle* and *population* sectors through water-stress;
- The *water demand* and *hydrologic cycle* sectors through water consumption;
- The *water demand* and *water quality* sectors through wastewater treatment;
- The *water demand* and *food production* sectors through water-stress;
- The *water quality and water demand* sectors through wastewater reuse;
- The *population* and *water demand* sectors through total water demand;
- The *population* and *land-use* sectors through forest and grassland clearing and burning;
- The *population* and energy-*economy* sectors through consumption per capita and labour;
- The energy-*economy* and *water demand* sectors through economic output (GDP), water use efficiency and electricity production;
- The energy-*economy* and *population* sectors through GDP allocation for fertility control;
- The energy-*economy* and *food production* sectors through GDP allocation for agriculture;
- The *energy-economy* and *carbon* sectors through industrial emissions;
- The *land-use* and *carbon* sectors through land-use emissions;
- The *land-use* and *food production* sectors through arable land; and,
- The *food production* and *population* sectors through per capita food availability.

The following two sub-sections are divided based on the feedback descriptions of water and non-water sectors – since the water demand, water quality, and hydrologic cycle (water quantity) sectors are interdependent and essentially inseparable.

2.2.1 Feedbacks within the ANEMI Model Water Sectors

The hydrologic cycle, water demand, and water quality sectors are very tightly linked with each other through total available water, water consumption and withdrawal, polluted waste water and water-stress, and waste water treatment and reuse. Thus they form a closed loop system with following feedback relations:

- High intensity of water use requires high amount of water withdrawal from the available water sources;
- Increased evaporation reduces the amount of available water from soil and open water body;
- Decrease of snowmelt can lead to less stream flow and therefore lower amount of available water;
- Decrease in the amount of available water and high water withdrawals lead to higher water-stress;
- High water-stress leads to other alternative choices including: larger groundwater withdrawals, introduction of desalination, and wastewater treatment and reuse.

The tight structure of water sectors, compared to other sectors of the model, requires the introduction of more feedback relationships as shown in Figure 2.23. The major links of each sector are discussed further.

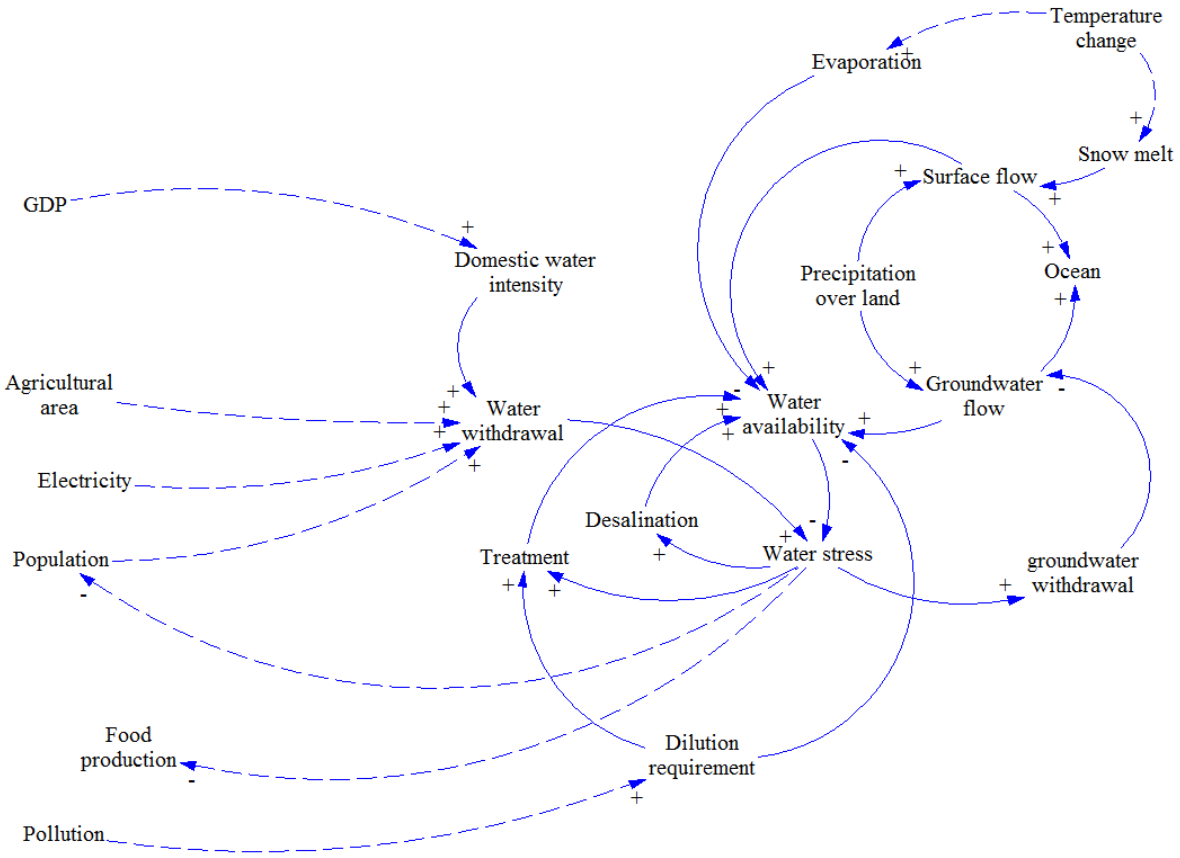

Figure 2.23: Feedback loops within ANEMI model water sectors

The water-stress is a measure of water scarcity, and is calculated as the ratio between the effective withdrawal (including effective blue water withdrawal and withdrawals for dilution requirement) and the total renewable flow.

$$wta = {}^{W_{SW}}/_{Q_S} \tag{2.120}$$

where W_{SW} represents the total water withdrawal for domestic, industrial and agricultural use along with the water required for dilution purpose. Q_S is the total renewable flow for human

use, measured in $km^3\ yr^{-1}$, which is the sum of the global annual surface flow and groundwater discharge.

In the ANEMI model version 2, non-renewable or fossil ground water extraction is treated as ground water withdrawal. When the water demand exceeds the available renewable surface water resources an additional 8.4 $km^3\ yr^{-1}$ can be taken from the non-renewable groundwater resources (Simonovic, 2002). Therefore, the non-renewable water withdrawal is expressed as:

$$\frac{dGW_{fraction}}{dt} = \begin{cases} if\left(GW_{fraction} < 1\right), \\ \left(wta\ .\ GW_{fraction}\right)\Big/_{t_{pump}} \\ else\left(GW_{fraction} = 1\right); \end{cases} \tag{2.121}$$

where $GW_{fraction}$ is the current fraction (0.0 to 1.0) of the global maximum of groundwater withdrawal and t_{pump} is the delay in introducing additional groundwater pumping capacity, set to 10 yr.

Even though, the above expression is very simple, it changes the ground water extraction amount exponentially. The upper limit of the allowable non-renewable groundwater will restrict further fossil ground water withdrawal irrespective of the water-stress. The annual extraction volume of non-renewable water is the product of current fraction of the global maximum of groundwater withdrawal and maximum allowable withdrawal volume.

$$G_w = GW_{fraction}\ .\ G_{w,max} \tag{2.122}$$

where G_w is the annual volume of groundwater extraction and $G_{w,max}$ is the capped-maximum value.

Desalination in the water sectors is modeled in a similar way as groundwater withdrawal, which means that with the increase of the water-stress, a certain percent of water will be desalinated (Davies, 2007; Davies and Simonovic, 2008).

The reuse of treated wastewater is never been a first choice. With the increased water-stress level, people are forced to reuse treated wastewater. The reuse trend is exponential:

$$\frac{d\tau_{ww\ reuse\%}}{dt} = if(\tau_{ww\ reuse\%} < 100),$$
$$(wta.\tau_{ww\ reuse\%})/t_{reuse} \quad (2.123)$$
$$else(\tau_{ww\ reuse\%} = 100)$$

where $\tau_{ww\ reuse\%}$ represents the global percentage of treated wastewater reuse, wta water-stress, and t_{reuse} is the time required to plan and institute treated wastewater reuse programs.

Treated wastewater is then allocated to the domestic, industrial, or agricultural sector for reuse. The percent allocation to each sector is set to 10%, 30% and 60% respectively for the domestic, industrial and agricultural sectors, based on anecdotal information from the literature (Davies and Simonovic, 2008).

$$Q_{ww\ reuse}\lfloor sector\rfloor = \left({}^{\tau_{ww\ reuse\%}}/_{100}\right).\left(\tau_{ww\ \%\ by\ sector}\lfloor sector\rfloor/_{100}\right).Q_{treated\ ww} \quad (2.124)$$

where $Q_{ww\ reuse}\lfloor sector\rfloor$ is the amount of treated wastewater allocated to each sector, the '$\lfloor sector\rfloor$' term counts a three-member array of domestic, industrial and agricultural uses, $\tau_{ww\ reuse\%}$ is reuse in percent, and $Q_{treated\ ww}$ is the amount of treated wastewater.

From the above equation it is found that there is a scope for re-using wastewater for various purposes, which could potentially reduce the water withdrawal and ultimately reduce the excess pressure on the global water resources. Therefore, the modified/ultimate withdrawal (W_i) would be,

$$W_i = W_{i,\ desired} - Q_{ww\ reuse,\ i} \quad (2.125)$$

While calculating the dilution requirement to bring wastewater in a acceptable range before disposing it into water body, three main parameters are considered: Nitrogen (total N), Phosphorous (total P), and 5-day Biochemical Oxygen Demand (BOD_5). The ANEMI model version 2 is not structured to produce individual components of wastewater quality. Rather, it provides the total volume of wastewater. Therefore, very standard values are adopted from Metcalf and Eddy Inc. (2003, pp186) for domestic and industrial waste water. The model is calculating dilution requirement for each type of water use and then considers the maximum value for further calculation:

$$MAX\left(\frac{C_{typic\,[sector]}}{C_{allow\,[sector]}}\right) . Q_{ww[sector]} = Q_{dilution[sector]} \quad (2.126)$$

where $C_{typic[sector]}$ and $C_{allow[sector]}$ staend for the typical concentration of pollutants from the different sectors and allowable concentration, respectively. The total amount of fresh water required $Q_{dilution[sector]}$ to dilute the $Q_{ww[sector]}$ amount of wastewater from different sectors.

In case of computing dilution requirement for agricultural sector, a different method is selected (Dabrowski et al., 2009). Two water quality variables are considered in case of dilution requirement for the agricultural sector: nitrogen and phosphorus. Estimates of the total amount of fertilizer (as mass of total P or N) applied and loss of chemicals (in tonnes) from each crop area are obtained from Dabrowski et al (2009). Nitrogen and phosphorus losses from agriculture were assumed to be in the form of soluble nitrate (NO_3) and phosphate (PO_4), respectively.

Agricultural water quality is based on the principal of allocatable water quality (A_{wq}):

$$A_{wq} = Target_i - Background_i \quad (2.127)$$

where $Target_i$ is the maximum allowable concentration for the water quality variable (i), and $Background_i$ is the background concentration of that variable in the source water. For the simplicity, prescribed values for $Target_i$ (3.38 mg/l and 0.07 mg/l for nitrogen and phosphorus respectively), and $Background_i$ (0.62 mg/l and 0.06 mg/l for nitrogen and phosphorus respectively) are taken from Dabrowski et al (2009).

The amount of water required (VW_{qual}) to dilute the estimated quantities of nutrients down to the maximum allocatable water quality concentration is calculated according to the following equation:

$$VW_{qual} = \left(\frac{Loss_i \; X \; 10^6}{A_{wq}}\right) \tag{2.128}$$

where $Loss_i$ is the total amount of chemical (i) lost (tonnes) to surface water per year.

While computing the dilution requirement for the agricultural sector, three assumptions are considered: (i) water quality guideline established for South Africa's water resources is used for the whole world; (ii) average fertilizer application rate (computed for maize, wheat, sugarcane and citrus) is used for all types of crops; and (iii) only irrigated agricultural areas are taken into count, while calculating dilution requirement. These assumptions are introduced due to the unavailability of information related to total fertilizer use in agriculture.

2.2.2 Feedbacks in the ANEMI Model Non-Water Sectors

The carbon sector has two major feedbacks, which are producing radiative forcing that leads to increase in temperature. In climate sector atmospheric CO_2 is translated in the radiative forcing with the forcing equation. The other sources of radiative forcing are computed from other gases: methane, nitrous oxide, chlorofluorocarbons and other Montreal protocol gases. All the forcings are then added together to feed into the climate sector as an input variable.

$$F_{total} = F_{co_2} + F_{other} \tag{2.129}$$

$$F_{co_2} = S.\ \frac{\ln\left(C_A/C_{A0}\right)}{\ln(2)} \tag{2.130}$$

$$F_{other} = F_{cfc} + F_{CH4} + F_{N_2O} + F_{MP} \tag{2.131}$$

where F_{total} is for total forcing in W m^{-2}, F_{CO_2}, F_{cfc}, F_{N_2O} stands for radiative forcing from carbon-dioxide, chlorofluorocarbon and nitrous oxide respectively. F_{MP} represents Montreal Protocol and other gases, while C_A and C_{A0} denote the current and initial atmospheric carbon dioxide concentrations respectively.

Climate sector plays a very important role in the ANEMI model, where its product, temperature change, impacts almost all the sectors of the model. The population, food production, hydrologic cycle, land-use, water demand, and water quality sectors are connected with the climate sector through the global temperature. In many cases the temperature rise may have more negative than positive effects. Increased temperature could boost the evaporation from a water body and increase the water-stress by lowering the stock of available water. However, there is a chance that some countries of the northern hemisphere, like Canada could be able to expand its agricultural area further north, if the temperature change takes place. On the other hand, the increase in temperature could potentially increase the irrigation demand, which may act as a constraint for agricultural land expansion.

For estimating the impact in the energy-economic sector based on current trend of climate change, the climate damage function is introduced, assuming a relationship between economic damage and the extent of warming. According to Nordhaus and Boyer (2000), the specific

relationship between global temperature increase and income loss is expressed by damage function in quadratic form:

$$D_t = \theta_1 . \Delta T_t + \theta_2 . \Delta T_t^2 \quad (2.132)$$

where D_t is the damage from climate change, as a fraction of output and ΔT_t atmospheric temperature increase (in degree Celsius) over year 1900 level, and $\theta_1 \& \theta_2$ are parameters of the damage function.

Increase in temperature is affecting the global hydrologic cycle by changing the intensity of evaporation, precipitation pattern, starting day of snow melt, and etc. The simplest way of introducing the effect of temperature change in the hydrologic cycle is by defining a fixed temperature multiplier. In many cases, this linear relationship may not be valid because of nonlinear feedback effects. Current understanding of Arctic ice melt is an interesting example. Light covered surfaces such as ice and snow reflect the incoming solar radiation back into outer space, while dark covered surfaces such as oceans and land absorb the incoming radiation, which increases the temperature and contributes to further warming. The higher global temperature triggers the melting of Arctic sea-ice and as the sea-ice melts there is less ice to reflect the incoming solar radiation and more open ocean to absorb the solar energy. This absorbed energy triggers a positive feedback that warms the ocean further causing more ice to melt faster. Huntington (2006) stated that global precipitation is energy rather than moisture limited, and so precipitation is expected to rise by 3.4% per 1℃ surface temperature increase. This leads to the following functional relationship:

$$P_{mult} = P_{mult,\ base} . \Delta T_s \quad (2.133)$$

$$T_{feedback} = 1 + \left({}^{P_{mult}}/_{100} \right) \quad (2.134)$$

where $T_{feedback}$ is the temperature multiplier, which takes its value from P_{mult}, the precipitation multiplier ΔT_s is measured in Kelvin, which denotes the change in surface temperature; $P_{mult,\ base}$ is a fixed value of 3.4% K^{-1}.

This simple relationship is used to establish feedback link between climate, water use, water demand, and evaporation calculation. To model the effects of climate change on irrigation water requirements, the "per hectare water withdrawals" and "per hectare water consumption" are multiplied by the same 'temperature multiplier'. Carbon sector of the ANEMI model version 2 is taking care of the total carbon balance at global scale, even though a significant portion of carbon is produced in another sector (energy-economy sector).

Population sector is linked to the land-use sector, based on the approach of Goudriaan and Ketner (1984). Significant land conversion, or change of land-use, is driven by expansion of human population. Therefore, yearly conversion from one biome type to another follows the rate of population growth. Clearing and burning, a conventional way of converting forest area into agricultural land is also linked to population. It follows the same trend but as a square-root of the population growth (Goudriaan and Ketner, 1984).

In the ANEMI model version 2, the land-use sector is represented by a 6x6 transfer matrix, TM_{ij}, row = *i* and column = *j* subscripts, where column headings j mean 'from biome type' and row headings *i* mean 'to biome type'. Thus, in case of Table 2.5, TM_{31} means a change in land-use from tropical forest to grassland. Transfer matrix entries, of which there are 6 x 6 = 36, can be either zero (24 in total) or non-zero (12 in total) and are measured in biome area use or transfer

of Mha yr^{-1}. To determine changes in the land area of a biome, there are two equations; one is applicable to diagonal components and other is valid for the rest of the transfer matrix elements. For all *i= j* (the diagonal members for cultivation and burning within the tropical biome):

$$\frac{dTM_{ij}}{dt} = r^{1/2}.TM_{ii} \quad (2.135)$$

while for i≠ j (which represents a change of biome area from type j to type i):

$$\frac{dTM_{ij}}{dt} = r.TM_{ii} \quad (2.136)$$

where $\frac{dTM_{ii}}{dt}$ and $\frac{dTM_{ij}}{dt}$ represent the change in the annual cultivation and burning within a biome and change in biome area, respectively, while r is the annual population growth rate. The logical form of the above equation can be represented as:

$$\frac{dTM_{ij}}{dt} = for\ all\ (i,j) \quad (2.137)$$

$$if\ (i = j),$$

$$r^{1/2}.TM_{ij},$$

$$else\ (r \cdot TM_{ij})$$

The *'for'* condition requires the above equation to run thirty-six times, once for each separate combination of i and j, since $i \times j = 36$. Land-use via shifting cultivation and burning produces a large portion of biomass and litter, which are directly released into the atmosphere.

Emission from the energy-economy sector is directly imported and added to the carbon sector. Carbon emissions from each type of energy source are calculated based on energy consumption and carbon content. The following equation is computing the CO_2 emission in 10^6 tons C.

$$CO_{2i} = P_i \,.\, FO_i . C_i \qquad (2.138)$$

where P_i = annual production in 10^6 tons of fossil fuel equivalent ($\pm$ approx. 11.2%), FO_i stands for effective fraction oxidized in the year of production and C_i for carbon content in tons C per ton coal equivalent/ tons C per thousand 10^{12} joules . The conversion factor used for 1 ppmv of atmosphere CO_2 = 2.13 Gt C.

All the three water related sectors are linked with both, food production and population sector, through the 'water-stress' variable. Water link to social development is captured by the water impacts on health. Without safe drinking water, humans cannot survive. Water transmitted diseases are amongst the most common causes of illness and death, and the majority of people affected by them are living in developing countries. With the increase in population, it is required to find a way to add a huge amount of water to the global water supply in each year. In addition, some areas are expected to get the lower amount of rainfall due to climate change and therefore these areas will face an alarming level of 'water-stress'. Human life expectancy is therefore expressed as an inverse function of 'water-stress' level.

Agricultural sector fully depends on water supply in many regions of the world. While irrigation is continuing to play a crucial role in agricultural, the global amount of available water becomes

a limit. The limitation in water availability is serving as one of the constraints for increase of the agricultural land. The agricultural sector is inversely related to water-stress.

2.2.3 Summary

In this section of the report the feedbacks are differentiated as: intersectoral feedbacks within the water sectors; and intersectoral feedbacks with rest of the sectors. This section is intended to help the reader in tracing the effects of change in a variable in one sector and subsequent reaction/changes occurring in other sectors.

Error! Reference source not found. and Figure 2.23 facilitates the understanding of the basic structure of the model and can guide the reader through the identification of feedback polarity, as well as the polarity of feedback loops that are connecting different sectors of the model.

2.3 Global Model Performance

Traditional model calibration is a process, which consists of changing values of model input parameters to match the observed behaviour within some acceptable criteria. However, calibration in the context of global change research faces a key limitation: there is only one Earth, and therefore only one set of globally-aggregated data available. Model calibration therefore proceeded in several steps here: 1) parameters were adjusted in individual sectors first, 2) the individually-calibrated sectors were checked against historical data and against data from other models, and 3) the sectors were integrated and model output was again tested against other sources. Since many of the model sectors are based on previous modelling work, they use the same parameter values as other models. Furthermore, where parameters were based on well-established, quantifiable, and measurable characteristics, the values obtained here were checked against real-world data. However, when the parameters had no strong

physical basis, the effects of parameter variations on whole-model behaviour were checked through sensitivity analysis.

Validating the models requires comparing variable estimated by the model to historical data. Model verification can be defined as the process of determining, is the logic that describes the underlying mechanics of the model, as specified by the modeller, faithfully capturing /representing the near world situation. Therefore, model validation is considered to be the process of determining to what extent the model's underlying fundamental rules and relationships are able to adequately capture the targeted emergent behaviour, as specified within the relevant theory and as demonstrated by field data.

Model performance and calibration/validation are evaluated through qualitative and quantitative measures, involving graphical comparisons and statistical tests. For the ANEMI model version 2, a satisfactory number of comparisons are performed on yearly basis, based on the data availability. Simulated values in Table 2.9 to Table **2.20** provide information on model performance.

The individual sectors are first developed and calibrated before combining all the sectors together. Once the individual sectors demonstrated satisfactory performance with reasonable parameter values, the next step of integration took place. During the isolated runs the intersectoral feedbacks are not activated, rather they are in predefined path/value. With the establishment of the feedback relationships, model showed a deviation from the performance obtained through the simulation of individual sectors, requiring further adjustments of model parameters. It is worthwhile to mention that this society-biosphere-climate-energy-economy system model is not meant to predict the future, rather it aims to help understanding the system behaviour and to understand the behavioural consequences of various policy options.

This section demonstrates the performance of a feedback based fully integrated society-biosphere-climate-economy-energy system through analyses of the model's base run. The individual sectors of the fully integrated version of the ANEMI model is tested against measurements and literature data from 1980 to 2010 (Table 2.9 to Table 2.20). Even with a small number of exogenous inputs (mainly future fossil fuel discovery) this comprehensive feedback based integrated modeling system proves its superiority by producing a very close agreement with the real world data.

2.3.1 Water Use

Water use has been growing rapidly in the last hundred years due to increasing water demand and population growth. Such enormous change (nearly 5 times) is mainly caused by a significant increase of water use in agricultural sector. In the ANEMI model version 2, water consumption and withdrawal are calculated for three individual groups (domestic, industry and agriculture). The model results are compared to IHP (2000) data, projections by Simonovic (2002), Alcamo et al (2003b), and Cosgrove and Rijsberman (2000). The calibrated ANEMI model version 2 shows a good agreement with the historical data (Table 2.9) and projections available in the literature (Table 2.10).

Table 2.9: Assessed global water withdrawals and consumption (in km3/yr)

Year	1980	1990	1995
IHP(2000)			
Domestic Withdrawals	219	305	344
Domestic Consumption	38.3	45.0	49.8
Industrial Withdrawal	713	735	752
Industrial Consumption	70.9	78.8	82.6
Agricultural Withdrawal	2112	2425	2504
Agricultural Consumption	1445	1691	1753
Simulated Value			
Domestic Withdrawals	210	315	349
Domestic Consumption	39	48	53
Industrial Withdrawal	560	570	615
Industrial Consumption	57	62	70
Agricultural Withdrawal	2100	2600	2800
Agricultural Consumption	1440	1880	1980

Table 2.10: Projected global water withdrawals and consumption (in km3/yr)

Year	2000	2010	2025
IHP(2000)			
Domestic Withdrawals	384	472	607
Domestic Consumption	52.8	60.8	74.1
Industrial Withdrawal	776	908	1170
Industrial Consumption	84	120	167
Agricultural Withdrawal	2605	2817	3189
Agricultural Consumption	1834	1987	2252
Simonovic (2002)			
Domestic Withdrawals	-	-	723
Industrial Withdrawals	-	-	520
Agricultural Withdrawals	-	-	3554
Cosgrove and Rijsberman(2000)			
Domestic Withdrawals	-	-	900
Domestic Consumption	-	-	100
Industrial Withdrawal	-	-	900
Industrial Consumption	-	-	120
Agricultural Withdrawal	-	-	2300
Agricultural Consumption	-	-	1700
Simulated Values			
Domestic Withdrawals	413	572	752
Domestic Consumption	62	80	93
Industrial Withdrawal	690	880	987
Industrial Consumption	80	90	105
Agricultural Withdrawal	2900	3100	3300
Agricultural Consumption	2070	2210	2350

2.3.2 Sea-Level Rise

Inundated Area by Sea-Level Rise

For the global inundated land area calculation, Xingong et al (2009) used the GLOBE dataset because of its improved version of the GTOPO30 data, which is compiled from the best global and regional raster and vector elevation datasets available at the time of compilation (Hastings and Dunbar, 1998). On the other hand, Dasgupta et al (2009) used WVS (World Vector Shoreline) dataset of NASA (http://gcmd.nasa.gov/records/GCMD_WVS_DMA_NIMA.html, last accessed Aug, 2011). ANEMI model version 2 is using a lookup table, is produced from Xingong et al (2009) to calculate total inundated area from different level of sea-level rise. Utilizing the lookup table ANEMI model show that 1,098,000 Km^2 area will be inundated at the end of 21^{st} century when the sea-level rises to 1.15 meter, and by 2092-93 sea-level may rise by one meter.

Sea Level Rise Impact on Agricultural Land

The ANEMI model version 2 requires percentage value of impacted agricultural land for calculation of the impact of sea level rise on the agricultural land, which is extracted from Xingong et al (2009). Simulated results show that the total impacted agricultural area would be 46,095 Km^2 at the end of 21^{st} century.

Sea Level Rise Impact on Population

In the ANEMI model version 2, the computation of the affected population is done exogenously because of insufficient data and global nature of the population structure in the model (no spatial distribution along the coast lines). To overcome this constraint, a combined approach is carried out where an average percentage of impacted population is computed from Dasgupta et al (2009) and Xingong et al (2009). This process is carried out for each level of sea-level rise. The computed value of 171 million impacted people is obtained for 1-meter sea-level rise.

Nicholls (2002) estimated that the number of people exposed to flooding by storm surges in 2100 would range between 503 and 755 million people at 96 cm sea-level rise. The ANEMI model is only considering the sea-level rise as a consequence of ocean thermal expansion and ice melt, but not the storm surges.

2.3.3 Global Population

The United Nations (UN) Population Division provides population data over the period of 1950 to 2050 out of which projected data started from 2005. The UN Population Division is under the United Nations Department of Economic and Social Affairs (UNESA), which is responsible for monitoring and appraisal of the broad range of areas in the field of population. International Institute for Applied Systems Analysis (IIASA) also provides 100 year population projection, last time revised in 2007. This is an international research organization that conducts policy-oriented research into problems that are too large or too complex to be solved by a single country or academic discipline. Scenarios used for global change, such as Nakicenovic and Swart (hereafter, IPCC 2000), Alcamo et al (1996) and RCPs (Moss et al, 2008) provide figures of population growth into the future. Nordhaus (2007) used the DICE model to simulate the future population which is a well-accepted result by the integrated assessment modeling communities.

It is observed from the historical global population comparison (Table 2.11) that the global version 2 of the ANEMI model is capable of generating an acceptable trend in population close to historical data (UNESA, 2006). The simulated population value from the version 1 of the model (Davies and Simonovc, 2008) is also included for comparison.

Compare of simulated future population values is performed using data from various sources various projection scenarios (Table 2.12, and Figure 2.24). In a few cases, the global population

starts to decline after 2075 but in most of the projections the population growth rate declines but not the total population. The simulated result from the ANEMI model is showing the same tendency of lower population growth rate.

Table 2.11: Comparison of historical global population (in billions)

Year	1980	1985	1990	1995	2000	2005
UNESA (2006)	4.45	4.86	5.30	5.72	6.12	6.51
Davies and Simonovic (2008)	4.51	4.91	5.31	5.7	6.09	6.47
ANEMI simulated population	4.44	4.75	5.13	5.52	5.91	6.32

Table 2.12: Comparison of future global population (in billions)

Year	2010	2025	2050	2075	2100
UNESA (2006)	6.91	8.01	9.15		
IPCC (2000) Scenario A1B	-	7.66	8.70	-	7.10
IPCC (2000) Scenario A2	-	8.81	11.3	-	15.10
IPCC (2000) Scenario B1	-	7.82	8.70	-	7.00
RCP8.5 (Riahi et al,2007)	7.0	8.30	10.2	11.80	12.02
RCP6 (Fujino et al, 2006; and Hijioka et al, 2008)	7.0	7.95	9.04	9.095	9.09
RCP4.5 (Clarke et al, 2007; Smith et al, 2006; and Wise et al, 2009)	7.0	7.95	9.01	9.030	9.025
RCP3-PD (van Vuuren et al, 2006; 2007)	7.0	7.95	8.095	9.00	8.060
Alcamo et al (1996), Base A	7.11	-	10.10	-	11.50
Alcamo et al (1996), Base B	6.70	-	7.84	-	6.43
Fiddaman (1997)	7.23	8.41	9.98	11.10	11.80
Nordhaus and Boyer (2000)	6.88	7.96	9.29	10.20	10.70
DICE_2007 (Nordhaus, 2007)	6.93	8.02	8.55	8.67	8.69
Davies and Simonovic (2008)	6.84	7.87	9.36	10.60	11.70
IIASA (low)	6.74	7.44	7.78	7.15	6.16
IIASA (medium)	6.82	7.79	8.75	8.87	8.39
IIASA (high)	6.88	8.16	9.90	10.80	11.05
ANEMI simulated population	6.77	7.98	9.32	9.97	10.53

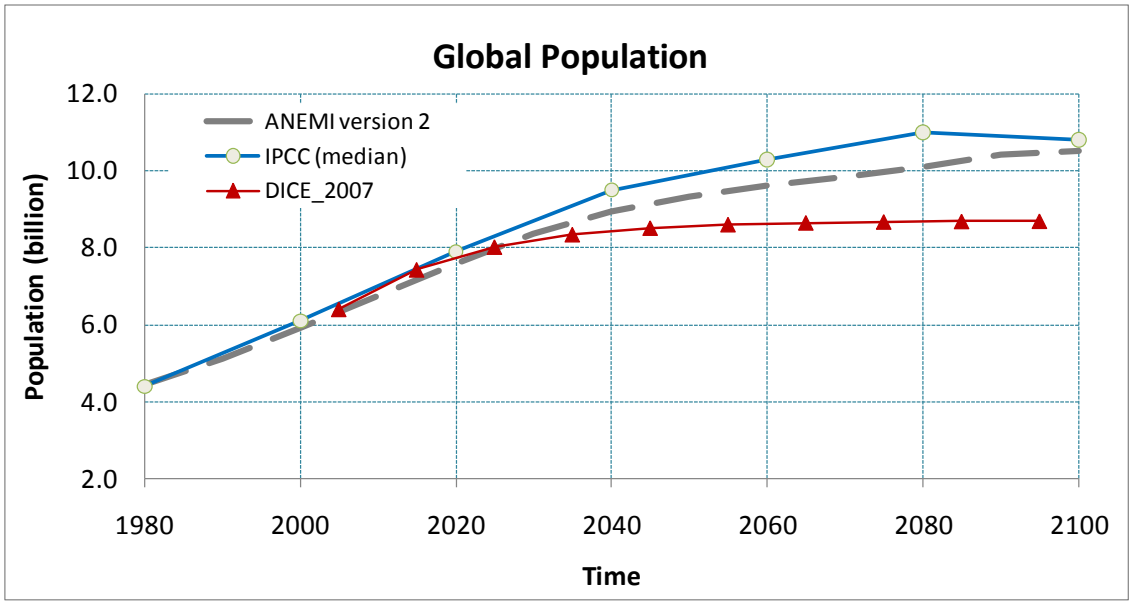

Figure 2.24: Comparison of global population projection

2.3.4 CO_2 Emissions from Energy Production

The two main sources of CO_2 emissions are: energy production, and land-use change (which affects the radiative forcing). The emissions from the fossil fuel burning represent the most significant contribution. Therefore, the extent of future climate change is heavily dependent on the fossil fuel burning rate for energy (both heat and electric energy) production. The ANEMI model version 2 is extremely sensitive to fossil fuel price and follows market clearing mechanism (a simplifying assumption made by the new classical school of economics that markets always go where the quantity supplied equals the quantity demanded; or the process of getting there via price adjustment). The IPCC (2000) and Marland et al (2008) data show a good match with the ANEMI simulated results with some level of overestimation from 1980 to 2000 (Table 2.13, and Figure 2.25).

Table 2.13: Comparison of historical industrial emissions (in Gt C/yr)

Year	1980	1985	1990	1995	2000	2005
IPCC (2000) Scenario A1B	-	-	6.0	-	-	-
IPCC (2000) Scenario A2	-	-	6.0	-	-	-
IPCC (2000) Scenario B1	-	-	6.0	-	-	-
Marland et al (2008)	5.35	5.44	6.16	6.4	6.75	7.99
Davies and Simonovic (2008)	5.11	-	5.96	6.32	6.77	-
ANEMI simulated emissions	5.38	5.78	6.21	6.68	7.21	7.86

In case of simulated future emissions, the model behaves in a logical fashion till 2050 and the results are compliant with most of the projections from IPCC (2000), Alcamo et al (1996) Nordhaus and Boyer (2000), Goudriaan and Ketner (1984) and RCPs (Moss et al, 2008). While, after 2050 the emission production from the energy sector starts to decline and emissions follow a very different path than other projections available in the literature. Whereas, 2007 version of DICE model (Nordhaus, 2007) showed, incremental rates of emission till the end of this century (Figure 2.25). By the end of this century the ANEMI version 2 simulation results are showing almost zero emissions (Table 2.14). Such behaviour is not unexpected, since the in-depth investigation reviles that the world would be out of available known fossil fuel reserves by 2100, if the present extraction trend continues. Therefore, the industrial emissions approach zero value. It is assumed that the nuclear, hydro and alternative energy sources will take care of the future energy demand leaving almost zero fossil fuel energy based emissions to the atmosphere.

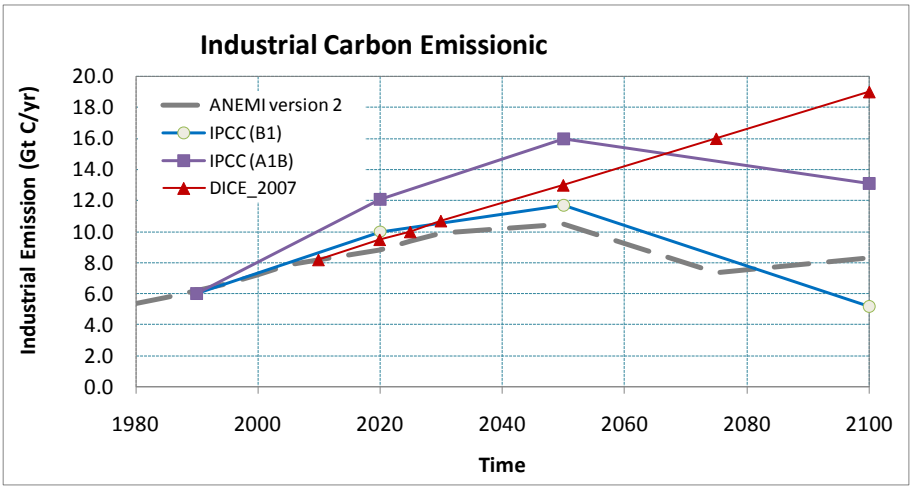

Figure 2.25: Comparison of industrial carbon emission

Table 2.14: Simulated industrial emissions (in Gt C/yr)

Year	2010	2020	2025	2030	2050	2075	2100
IPCC (2000) Scenario A1B	-	12.1	-	-	16.0	-	13.1
IPCC (2000) Scenario A2	-	11.0	-	-	16.5	-	28.9
IPCC (2000) Scenario B1	-	10	-	-	11.7	-	5.2
RCP8.5 (Riahi et al,2007)	8.926	11.538	-	13.839	20.205	26.684	28.740
RCP6 (Fujino et al, 2006; and Hijioka et al, 2008)	8.512	8.95	-	9.995	13.044	16.894	13.753
RCP4.5 (Clarke et al, 2007; Smith et al, 2006; and Wise et al, 2009)	8.607	9.872	-	10.953	11.031	5.65	4.203
RCP3-PD (van Vuuren et al, 2006; 2007)	8.821	9.288	-	7.157	3.186		
Alcamo et al (1996), Base A	11	13	-	14	15.5	18.0	22.0
Alcamo et al (1996), Base B	8	10	-	9.5	9.0	8.0	8.0
Goudriaan and Ketner (1984), Low Emission	-	-	-	8.9	-	-	-
Goudriaan and Ketner (1984), High Emission	-	-	-	16.2	-	-	-
DICE _2007 (Nordhaus, 2007)	8.2	9.5	10.0	10.7	13.0	16.0	19.0
Davies and Simonovic (2008)	7.54	8.19	-	8.82	10.11	11.93	13.98
ANEMI simulated emissions	8.18	8.82	9.4	9.92	10.49	7.35	8.3

2.3.5 Gross Domestic Product (GDP)

The gross domestic product (GDP) is the most commonly used indicator to express the economic wealth of a region at a global or regional scale. Total dollar value of all goods and services of a specific time can be represented by GDP. Therefore, the monetary value of all the finished goods and services produced within a country's borders in a specific time period, though GDP is usually calculated on an annual basis. It includes all of private and public consumption, government outlays, investments and exports less imports that occur within a defined territory. Nordhaus (2007) used the DICE model to simulate the future GDP which is a well-accepted result by the global communities. The simulated GDP from the ANEMI model version 2 shows a very close match **Error! Reference source not found.**Figure 2.26) with the Nordhaus (2007), which proves its satisfactory representation of the global energy-economy sector.

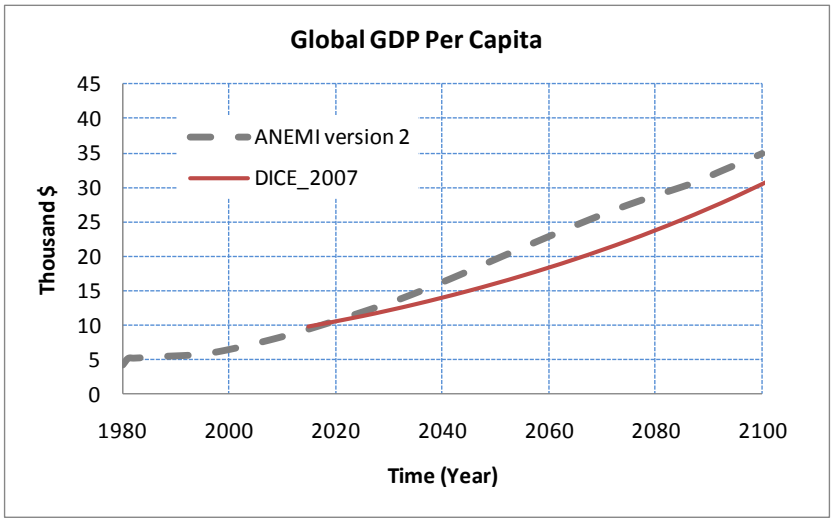

Figure 2.26: Comparison of GDP per capita

2.3.6 Physical Characteristics of the Earth System

The physical characteristics of the Earth system include atmosphere, biosphere, hydrosphere, and geosphere. The following is the detailed analyses of the ANEMI model version 2 surface temperature, atmospheric CO_2 concentration, and net primary productivity (NPP) results.

Surface Temperature

The global mean surface temperature increased by around 1 ^{0}F (0.55556 ^{0}C) since 1880, which is established by the measurements from land stations and ocean vessels. These measurements also indicate a near level trend in temperatures from 1880 to about 1910, a rise to 1945, a slight decline to about 1975, and a rise to the present (NRC, 2006). Based on the observations of increases in global average air and ocean temperatures, widespread melting of snow and ice, and rising global average sea-level, the Intergovernmental Panel on Climate Change (IPCC) stated that warming of the climate system is now "unequivocal," (IPCC, 2007a). The IPCC also concluded that most of the observed warming in global average surface

temperature that has occurred since the mid-20th century is very likely a result of human activities.

Vinnikov et al (2006) analyzed the satellite data and concluded that the global surface temperatures changed by 0.2°C per decade between 1978 and 2004. This value is also consistent with the studies by Brohan et al (2006) and Smith and Reynolds (2005). They calculated temperature anomalies based on the deviation, in degree Celsius, from a long-term 1961-1990 temperature average. Nordhaus and Boyer (2000) calculated their temperature anomaly based on the pre-industrial average surface temperature, so that their starting, 1995 value for the temperature anomaly is 0.43°C. Davies and Simonovic (2008) corrected that by subtracting 0.15°C from their calculated values, since 1960 was roughly 0.15°C warmer than 1900. . Davies and Simonovic (2008) also used the ANEMI model version 1 results to calculate the temperature anomaly based on the difference between simulated values for the years in question (1960, 1970, and so on) from the simulated 1961-1990 average surface temperature.

The basic Goddard Institute for Space Studies (GISS) temperature analysis scheme is defined in the late 1970s by James Hansen. Prior temperature analyses covered only 20-90°N latitudes. The first published result (Hansen et al. 1981) of NASA (National Aeronautics and Space Administration) showed that, contrary to impressions from northern latitudes, global cooling after 1940 was small, and there was a net global warming of about 0.4°C between the 1880s and 1970s. Some improvements in the analysis were made several years ago (Hansen et al 1999; 2001), including use of satellite-observed night lights to determine which stations in the United States are located in urban and pre-urban areas, the long-term trends of those stations are being adjusted to agree with the long-term trends of nearby rural stations. In the ANEMI model version 2, the average temperature (14.0066 ^{0}C) is calculated based on the NASA data (from 1961 to 1990), as the model simulation starts from 1980 (http://data.giss.nasa.gov/gistemp/, last accessed Aug, 2011). The anomaly for this model is of course higher than the values provided by Davies and Simonovic (2008), as radiative forcing

from the other gases except CO_2 were not considered by the ANEMI version 1 model (Table 2.15).

Table 2.15: Global surface temperature change (in ^{o}C)

Year	1980	1985	1990	1995	2000	2005
Brohan et al (2006)	0.05	-	0.15	0.25	0.35	0.45
Smith and Reynolds (2005)	0.10	-	0.18	0.25	0.38	0.45
Nordhause and Boyer (2000)	-	-	-	0.28	-	0.34
NASA	0.17	0.04	0.36	0.36	0.32	0.61
Davies and Simonovic (2008)	.01	-	.07	.11	.14	.19
ANEMI simulated values	-0.01	0.10	0.21	0.33	0.44	0.56

IPCC models estimated that the Earth will warm between two and six degree Celsius over the next century, depending on how fast carbon dioxide emission increases. Scenarios which assume that people will burn more and more fossil fuel provide the estimates at the upper end of the temperature range, while scenarios that assume that greenhouse gas emissions will grow slowly gave lower temperature predictions. Based on the Fourth Assessment Report of the IPCC, Meehl et al. (2007) produced an 'average climate period' of 1980-1999 and presented 20 year averages of surface temperature anomalies over three periods of 20st century: 2011-2030, 2046-2065, and 2080-2099, which are used to verify the performance ANEMI model version 2. The future anomaly values calculated by the ANEMI model version 2 are again at the upper bound of the published values (Table 2.16). Such behaviour is not unusual, because of the higher fossil fuel based energy consumption till mid of the 21st century.

Table 2.16: Future global surface temperature change (in ^{o}C)

Year	2011 – 2030	2046 – 2065	2080 - 2099
Meehl et al (2007), SRES A2	0.64	1.65	3.13
Meehl et al (2007), SRES A1B	0.69	1.75	2.65
Meehl et a. (2007), SRES B1	0.66	1.29	1.79
Alcamo et al (1996), Base A	0.80	1.60	2.60
Alcamo et al (1996), Base B	0.50	1.10	1.45
Nordhaus and Boyer (2000)	0.34	1.05	1.76
Davies and Simonovic (2008)	0.27	0.70	1.28
ANEMI simulated anomaly	0.85	1.7	2.5

Atmospheric Carbon Dioxide Concentration

Carbon dioxide (CO_2) is emitted into atmosphere naturally through the carbon cycle and through human activities, like the burning of fossil fuels. Natural CO_2 is circulating within the carbon cycle where billions of tons of atmospheric CO_2 being absorbed from the atmosphere by oceans and forests, and discharged back into the atmosphere through natural processes. Under the balanced conditions, the total carbon dioxide emissions and removals from the entire carbon cycle remains roughly equal. Ice core analyses data revel that during the past 1000 years, until about the year 1800, atmospheric CO_2 was fairly stable at levels between 270 and 290 ppm. The 1994 value of 358 ppm is higher than any CO_2 level observed over the past 220,000 years (Schimel et al, 1994).

Carbon dioxide and its concentration in the atmosphere is the core of climate change theory and policy, because of its large share in radiative forcing. The scientific consensus is that we must limit the release of carbon dioxide and similar greenhouse gases if we are going to reduce the antropogenic impacts on the climate. It's not true that human activities are the only sources of atmospheric CO_2 concentration. Even though, compared to the natural sources, human contribution is not the only factor, it is more than enough to hamper the delicate balance. The rise of atmospheric CO_2 closely parallels the emissions history from fossil fuels and land use changes (Schimel et al, 1994). The average annual increase in CO_2 went up from, about 0.9 ppm/year during the 1960s to about 1.5 ppm/year during the 1980s.

The computed CO_2 concentration can be verified with the observed and projected CO_2 concentrations reported in the literature. Mauna Loa Observatory (MLO) is a premier atmospheric research facility that has been continuously monitoring and collecting data related to atmospheric change since the 1950's (http://www.esrl.noaa.gov/gmd/obop/mlo/livedata/livedata.html, last accessed Aug, 2011). The undisturbed air, remote location, and minimal influences of vegetation and human activity at MLO are ideal for monitoring constituents in the atmosphere that can cause climate change.

Other model results from the literature which are considered for the comparison are: Alcamo et al (1994), Nordhaus and Boyer (2000), Goudriaan and Ketner (1984) and Davies and Simonovic (2008). The ANEMI model version 2 generated CO_2 concentrations produces a comparable result to the available observations and published values in the literature (Table 2.17).

Table 2.17: Global atmospheric CO_2 concentration (ppm)

Year	1980	1990	1995	2000	2004
Alcamo et al (1994)	340	358	-	-	-
Goudriaan and Ketner (1984)	340	-	-	-	-
Mauna Loa observations	339	354	361	369	377
Nordhaus and Boyer (2000)	-		349	-	369
Davies and Simonovic (2008)	322	337	345	354	361
ANEMI simulated value	339	358	367	376	383

The atmospheric concentration of carbon dioxide in 2005 exceeds by far the natural range over the last 650,000 years (180 to 300 ppm) as determined from the ice cores (IPCC, 2007a). As fossil fuel is the main source of CO_2 emissions, it is expected that future CO_2 emission levels will depend primarily on the total energy consumption and the structure of energy supply. In the ANEMI model version 2, the total energy consumption is driven by population size, technological development, environmental concerns, and other factors. The composition of energy supply is determined by the fossil fuel reserves, price and efficiency. Emissions from gas flaring, cement production are much lower in comparison with energy-related emissions. In 1990, the global emissions from cement made up about 2.5% of the total global CO_2 emissions (Houghton et al, 1995).

SRES scenarios cover a wide range of annual emissions, and the uncertainties in future emission levels increase with time. Up to about the 2040s and the 2050s, emissions tend to rise in all scenarios, but at different rate. By 2050, the emissions range covered by the 40 SRES scenarios from 9 to 27 Gt C, with the mean and median values equal to about 15 Gt C. The range between the 25th and 75th percentiles of emissions (the "central tendencies") extends from 12 to 18 GtC (i.e. from twice to three times that of 1990). Beyond 2050, the uncertainties in energy and

industrial CO_2 emissions continue to increase. By 2100, the range of emissions across the 40 SRES scenarios is between 3 and 37 GtC, which reflects either a decrease to half of the 1990 levels or an increase by a factor of six. Emissions between the 25th and 75th percentiles range from 9 to 24 GtC, while the range of the four marker scenarios is even wider, 5 to 29 GtC. The 2100 median and mean of all 40 scenarios are 15.5 and 17 GtC, respectively (IPCC, 2000).

The following projected CO_2 values (in ppm) from the literature: IMAGE 2.1 simulations (Alcamo et al, 1996), a coupled climate-carbon model called IPSL (Berthelot et al, 2002), A2 scenario (IPCC, 2000), STERN review (Stern, 2007), and Goudriaan and Ketner (1984) are introduced for the ANEMI model verification purposes. Other model results from Davies and Simonovic (2008), and Nordhaus and Boyer (2000) are also included in the following table (Table 2.18). Davies and Simonovic (2008) converted the value of Berthelot et al (2002) to be in the same units, assuming a base atmospheric CO_2 content in 1860 of 595 Gt C (283 ppm).

Table 2.18: Future global atmospheric CO_2 concentration (ppm)

Year	2010	2020	2030	2050	2075	2100
IPCC (2000) Scenario A1	-	-	-		-	-
IPCC (2000) Scenario A2	-	-	-		-	-
IPCC (2000) Scenario B2	-	-	-		-	-
RCP3-PD (van Vuuren et al, 2006; 2007)	389.29	412.07	430.78	442.70	434.55	420.90
RCP4.5 (Clarke et al, 2007; Smith et al, 2006; and Wise et al, 2009)	389.13	411.13	435.05	486.54	527.72	538.35
RCP6 (Fujino et al, 2006; and Hijioka et al, 2008)	389.07	409.36	428.88	477.67	572.04	669.72
RCP8.5 (Riahi et al,2007)	389.32	415.78	448.84	540.54	717.63	935.87
Alcamo et al (1996), Base A	400	425	460	510	610	745
Alcamo et al (1996), Base B	390	410	420	450	480	515
Goudriaan and Ketner (1984), Low Emission	-	-	431	-	-	-
Goudriaan and Ketner (1984), High Emission	-	-	482	-	-	-
Berthelot et al (2002), Coupled	383	414	445	502	616	782
Berthelot et al (2002), Fertilization	373	397	426	485	573	700
Nordhaus and Boyer (2000)	-	-			502	
Davies and Simonovic (2008)	373	393	415	462	534	624
ANEMI simulated value	395	417	445	502	553	575

From Tables 2.15 to 2.18 and Figure 2.27, it can be concluded that the ANEMI model version 2 shows a reasonable match with the observed values as well as with other values from the literature.

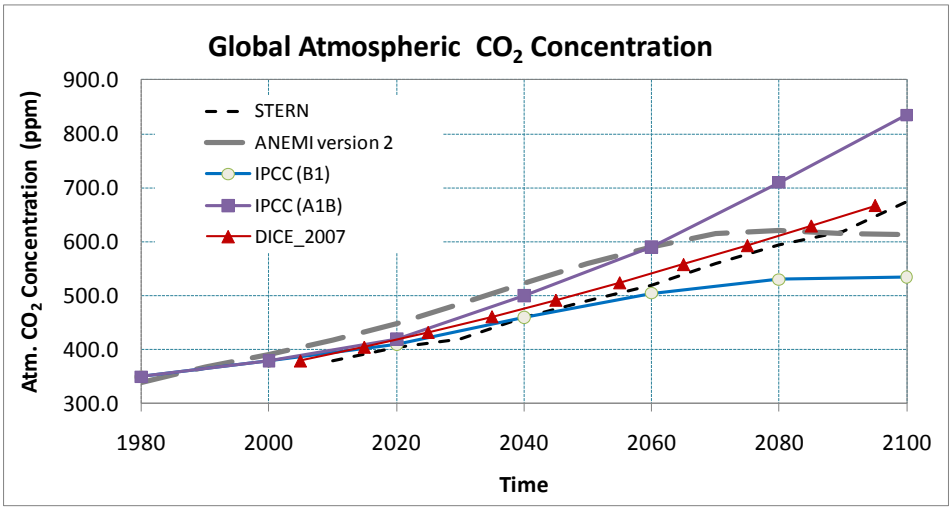

Figure 2.27: Comparison of Atmospheric CO_2 concentration

Net Primary Productivity

Net Primary Productivity (NPP) is an essential component of the global carbon budget, which is used as an indicator of the ecosystem function. NPP is the rate at which vegetation fixes CO_2 from the atmosphere (gross primary productivity, GPP) minus the rate at which the vegetation returns CO_2 to the atmosphere through plant respiration. Only a small part of the carbon fixed through NPP is retained for a significant time, and NPP is only one component of the full carbon cycle of terrestrial ecosystems (IGBP, 1998). The total NPP is influenced by various climatic factors such as: atmospheric CO_2 concentration, rainfall, cloud cover, and the temperature. Approximately, a seventh of total atmospheric carbon dioxide is passed into vegetation annually.

There are many ways to estimate terrestrial NPP from field data that depend on the type of plants and available measurements. However, due to measurement complexity it is not possible to get an accurate value of global NPP. IPCC is using NPP value from a study that was

done in 1979 (Atjay et al, 1979). Dynamic Global Vegetation Models (DGVM) are mostly used in computing the global NPP value. Cramer et al (1999) experimented with sixteen different DGVMs using long-term average monthly climate values and base atmospheric CO_2 concentrations. Average NPP value of 54.9 Pg C per year was calculated, assuming base global atmospheric CO_2 concentration of 340-360 ppm. In continuation of that study Cramer et al (2001), utilized six DGVMs based on IPCC IS92a emission scenarios to derive NPP values, which were between 45 and 60 Pg C per year. Some other published NPP values are available from Berthelot et al (2002), Cox et al (2000), Goldewijk et al (1994), Cramer et al (2001), Goudriaan and Ketner (1984), and so on. Simulated result of the ANEMI model version 2 show satisfactory agreement with the other literature values, even though they are following the lower bound of the various study results (Table 2.19).

Table 2.19: Historical net primary productivity (NPP), 1980-2005

Year	1980	1990	1995	2000	2005
Berthelot et al (2002), Coupled	63	65	66	67.5	67.5
Berthelot et al (2002), Fertiliz	63	65	66	67.5	68
Cramer et al (2001), CO_2+ΔT	-	-	-	61	-
Goudriaan and Ketner (1984)	61.9		-	-	-
Goldewijk et al(1994)		60.6	-		
Davies and Simonovic (2008)	58.1	59.0	59.4	59.5	60.3
ANEMI simulated value	60.0	61.6	62.2	62.7	63.3

It is clear that NPP is not dependent only on a single parameter, rather it depends on human consumption, related environmental impacts, policy options, degree of deforestation and so on. The following two major sources of uncertainty exist in projecting NPP under climate change: (a) uncertainty with respect to the description of dependence of NPP on climate; and (b) uncertainty with respect to climate predictions.

A summarized NNP values produced by the previously research are stated in the Table 2.20. Comparison with Nordhaus and Boyer (2000) and Fiddaman (1997) are not possible because of differences in representation of the carbon cycle (Nordhaus and Boyer, 2000), or no explicitly presentation of NPP values (Fiddaman, 1997).

Table 2.20: Future net primary productivity (NPP)

Year	2010	2025	2030	2050	2075	2100
Berthelot et al (2002), Coupled	68	70	71	74	78	82
Berthelot et al (2002), Fertiliz	68	72	73	79	85	94
Cramer et al (2001), CO_2+ΔT	-	-	-	75	-	84
Goudriaan and Ketner (1984)	-	-	65.3	-	-	-
Goldewijk et al (1994)	-	-	-	82.5	-	-
Davies and Simonovic (2008)	60.8	61.9	62.3	63.4	64.6	65.3
ANEMI simulated value	63.8	65	65.4	66.7	66.8	65.1

2.3.7 Discussion

In this report, the global version of the ANEMI version 2 model-simulated results are compared with the available historical observations and future projections of different models available in the literature. The comparison results showed a very promising features of ANEMI feedback based society-biosphere-climate-economy-energy system model. In case of future temperature simulations the ANEMI results are close to the upper boundary of the comparable values. Overall model performance is very encouraging, as this is a feedback based dynamic integrated assessment model, where no prescribed or endogenous data is used to navigate the model.

This ANEMI version 2 model, with a significant number of parameters, requires systematic way of parameter calibration. The individual sectors are calibrated first before assembling the whole model. In spite of the individual sectoral calibration, the combined model simulation values converge very fast.

The developed model also provides good simulation results of the future system behaviour. The satisfactory reproduction of the historical behaviour along with reasonable future simulations proves the model's robustness for use in climate change policy analyses. It is anticipated that the developed model is able to successfully handle different policy/scenario analyses by revelling its feedback mechanism while mimicking the near real-world system behaviour. This modeling effort is intended to capture the future behaviour under changing climate but not to forecast the exact magnitude of change.

2.4 Conclusions

The ANEMI version 2 model has nine sectors. Even though some of the sectors are taken from the earlier work, the closed loop feedback concept of nine sectors that forms endogenous model structure makes the model different from other Integrated Assessment Models.

The ANEMI model is unique in this field. Basically every integrated assessment model has its own area of focus, which dominates the model behaviour> In the case of ANEMI, water, energy-economy, and population sectors play dominant roles, where availability of water and climate change influence most of the other sectors.

It can be concluded that the ANEMI version 2 model describes the society-biosphere-climate-economy-energy system very closely and its simulations reproduce available observations and values from the literature to high level of satisfaction. Therefore, we conclude that there is a high utility of the closed feedback based model over the imposed exogenous trends based conventional models in the analyses of climate change policy options.

3 REGIONAL MODEL DESCRIPTION

The ANEMI version 2 model is replica that combines simplified representations of the socioeconomic determinants of greenhouse gas emissions, the atmosphere and oceans, and impacts on human activities and ecosystems on a global scale. The model is developed using a system dynamics simulation approach and version 2 has nine major sectors, all of which interact with one another through feedback relationships. The ANEMI version 2 shares important characteristics with climate-economy models, integrated assessment models, and hydrologic models at a global scale.

The major limitation of the global model is its inability to answer questions of importance at the regional and/or local scales. Development of climate-change adaptation and mitigation strategies for different regions of the world requires appropriate spatial resolution of the model that will be able to describe regional and local impacts of climate change. The second objective of the work presented in the report is regionalization of the global version of the ANEMI model. Focus of the regionalization effort was on the development of the regional version of ANEMI that allows investigation of global climate change effects on regional water resources, economic performance, energy supply and demand, population and land-use. The regional version of the model allows assessment of regional policy options for stabilizing global climate. The particular emphasis is on Canada. The regional version of ANEMI model separates Canada from the rest of the world (ROW). The climate, carbon and a portion of the hydrologic cycle sectors are dealing with global processes and remain on a global scale.

There are two different modelling approaches that can be used for downscaling global model to regional scale: bottom-up and top-down. The typical bottom-up approach focuses on individual sectors, not on the relationships within the combined system. Therefore, the implementation of such a model is relatively simple. The top-down modeling approach considers the system as

a whole irrespective of the number of sectors and subsectors by counting different imputes across the model domain. In this case top-down approach is followed while regionalizing the global ANEMI version 2 model.

In the next few sections of the report, the detailed explanation of the structure of each regionalized sector is provided. The presentation includes populations, land-use, water, food production, and energy-economy sectors. The focus of the regional model presentation is only on the main concepts and feedbacks since the rest of the details are already provided in the global model description. In order to address integration of sectors that function on the global scale with sectors on the regional scale, the presentation of implemented disaggregation procedure is provided. The chapter ends with the presentation of regional model performance.

3.1 Population Sector

Population sector represents the growth or decline of regional population under the influence of other sectors. The population change is derived from birth rate, death rate, and migration. In this model, fertility and life expectancy are affected by water-stress, defined as the ratio of 'desired surface water' and 'available surface water'.

The regional ANEMI model simulations start from 1980 and therefore initial regional distribution of the global population is required. The population sector initial value (1980) is regionalized based on the UN population data (DESA, 2011). The initial population growth rates for the two ANEMI model regions, Canada and ROW, are calculated based on the population growth from 1975 to 1980. The only external input to this sector is the water availability and the water-stress. They are the outputs of the water quality sector. The regionalized population sector simulates population distribution that matches UN predictions (up to 2050). International migration (between Canada and ROW) is also incorporated in the regional version

of ANEMI model, as the population in-migration to Canada a vital source of labour force. The model also has the capability of handling the environmental refugee/migration inflow based on the Canadian immigration policy.

The structure for the population sector in the regional version of ANEMI model is exactly the same as in the global model (presented in section 2.1.6). Therefore, the same governing equations and most of the parameter values are valid for both versions of the model. The initial values of the population in 1980 are shown in

Table **3.1**.

Table 3.1: Population by age-group of 1980 (DESA, 2011)

Age group (year)	**0-14**	**15-44**	**45-64**	**65 to 65+**
Canada (population in millions)	5.575	12.00	4.637	2.305
Rest of the world (population in millions)	1560	1940	6520	259

3.2 Land-Use Sector

The land-use sector is highly influenced by the population sector via forest clearing and burning activities. The land transfer rate is proportional to the population growth and highly dependent on the policy and population awareness of various environmental issues. In the model, only the population growth is considered as the variable that affects the change of existing land-use pattern.

In the regionalization process the main determining factor, population growth is directly connected with the regional version of the land-use sector. Therefore, the regionalization of the land transfer matrix is required. The regional transfer matrix is derived from the global value

(provided by Goudrian and Ketner, 1994) and available land area for each region. So the simple assumption used in the regionalization of land-use sector is that the land transformation rate is only the function of regional total land area. This type of regionalization inherits some setbacks, as the data limitation at the regional scale introduced uncertainty into the land transfer matrix. However, the reduction in uncertainty has been obtained through multiple attempts made to calibrate the model output.

In the regional model, the land-use model structure and parameter values remain unchanged from the global model (presented in section 2.1.5), except the initial transfer matrix, which is given in Table 3.2. This matrix is calculated based on the ratio of land area of Canada and the world. Therefore, the land transfer matrix for the ROW is obtained by deducting the land transfer value in Table 3.2 from the value in Table 2.5.

Table 3.2: Initial land transfer matrix for Canada (Mha yr^{-1}, in 1980)

From(j): / **To (i):**	Tropical Forest	Temperate Forest	Grassland	Agricultural Land	Human Area	Semi-Desert and Tundra
Tropical Forest	0.814148	0	0	0	0	0
Temperate Forest	0	0.1	0	0	0	0
Grassland	0.05	0.05	21.7106	0	0	0
Agricultural Land	0.12	0	0	21.7106	0	0.015
Human Area	0.01	0.01	0.04828	0.04828	0	0
Semi-Desert and Tundra	0	0	0	0	0	0

3.3 Water Sectors

One of the main strengths of ANEMI is presence of three water sectors that (a) link climate change with other socio-economic sectors and (b) provide for assessment of impacts caused by water deficiency and quality degradation on population, industrial output, and food production.

Three major water sectors incorporated in the ANEMI model dealing with global and regional water resources include: hydrologic cycle, water demand, and water quality.

3.3.1 Hydrologic Cycle

This sector is basically dealing with hydrologic cycle that describes the interactions among land, water and atmosphere. The objective of the hydrologic cycle sector is also to estimate the balance between water supply and water demand within each region, and the effects of water deficiency on other sectors. The current version of the regional ANEMI model is not well equipped to address the effects of excess water (flooding) on other socio-economic sectors.

The atmospheric and oceanic portions of the hydrologic cycle (except precipitation) are the same as in the global version of the model. The regionalization of this sector is not able to produce regional atmospheric water content but it's definitely able to disaggregate regional discharge/surface water availability based on long term observations of rainfall and land characteristics. As the atmospheric water content and temperature cannot be separated for Canada and ROW, the disaggregation is done based on historical data. The rainfall and temperature are disaggregated using outputs of 17 GCM models (discussed in section 3.7). However, the ANEMI model is not able to capture the expected shifting of rainfall pattern at desired spatial resolution over the globe.

3.3.2 Water Demand

The main sources of water demand are industrial use, agricultural use and municipal use. The water demand sector is closely linked with the population, energy-economy, hydrologic cycle, and water quality sectors by water demand, consumption, water use intensity, wastewater treatment and water availability respectively.

Regionalization of the water demand sector is carried out in a simple way. Waste-water treatment and desalination capacity are playing a big role in the water demand part, where water is a scare resource. The regional distribution of the desalinated water supply capacity is obtained from the World's Water 2006-2007 (Pacific Institute, 2007). While distributing the capacity, only those countries/regions are considered which posses more than one percent of the world's desalination capacity. Waste water treatment data is not available from all countries/regions and this report relies on the data from FAO database (http://faostat.fao.org/, last accessed August 2011).

In respect to water demand sector structure and relevant equations both the regional and global versions are the same except the initial conditions for the irrigated area and electricity production (presented in section 2.1.7.2). The irrigated area for 1980 is calculated based on the information published in World's Water 2008-2009 (Pacific Institute, 2009). The electricity production for Canada and ROW is obtained from EIA database (EIA, 2006). The initial information used in the regional model is shown in **Table 3.3**. For Canada, no desalination capacity is considered up to the present time, but the model has the capability to incorporate the desalination facilities if required.

Table 3.3: Initial value for irrigated area and electricity production (1980)

	Irrigated area (thousand hectare)	**Electricity Production (billion KWh)**
Canada	573.703	367.8
Rest of the world	208430	2649.56

3.3.3 Water Quality

Problems related to the quality of water are aggravated in industrially developed and densely populated regions of the world where no efficient wastewater treatment takes place. The

water quality sector of the regional version of ANEMI model needs to describe the dynamic influence of water quality on human life on a regional scale. However, comprehensive chemical composition, and other local scale characteristics of water quality are not modeled, as their local effects are of low significance on the regional scale. Hence, the regional version of ANEMI model is not capable to handling any local issue, such as: local industrial pollution, algae bloom and so on, but at regional scale it is able to point out the overall health of the water resources including the availability of sufficient water supply for human survival with the 'water stress' parameter. In general 'water quality' sector deals with the water quality issues those are addressed by determining the necessary clean water requirement to maintain the standard water quality, dilution requirement.

Water quality sector is connected with the water demand sector by negative causal relationship. The modeling comprises of domestic, industrial and agricultural wastewater components. In the regionalization of this sector, the initial industrial treatment percentage is considered the same for all the regions (no data is available). Initial Irrigated area (in 1980) for each region is calculated from World Bank online database (http://databank.worldbank.org/, last accessed August 2011).

The structure of the regional ANEMI model water quality sector remains the same as the global model (presented in section 2.1.7.3). In the regional model, most of the parameter values are the same as in the global model, except initial treatment percentage. The values for Canada are: for domestic waste 70% and industrial waste 65%. The values for the 'rest of the world' are the same as in the global model.

3.4 Food Production Sector

Food production sector of the regional ANEMI model is connected to the large number of other sectors, which makes this sector more interactive and complex. On the contrary, the regionalization of the sector is not very complex, as most of the inputs are obtained from other sectors already as regional values. Therefore, the sector model structure remains the same as the global model structure (presented in section 2.1.4). The parameter values from connected sectors are determining the regional model behaviour. Other initial stocks like 'initial total erodible land' do not require regionalization, as they are starting with zero value. However, for 'land yield technological development' two initial parameter values of 1.5 and 1.25 are used for Canada and ROW, respectively.

3.5 Energy-Economy Sector

The energy-economy sector of the regional ANEMI model is considering two regions: Canada and RWO. Canada region is considered as a small open economy that takes energy prices and the global mean temperature as given. That is, fossil fuel prices and the global mean temperature are endogenous variables in the ROW region, but exogenous to the Canada region energy-economy sector. It is assumed that the energy consumption and greenhouse gas emissions of Canada do not impact the world, as Canada contributes about 2% of total global greenhouse gas emissions. The structure of the Canada region is almost identical to the global energy economy sector. The main difference is that the regional energy economy allows for a simple representation of trade in fossil fuels.

The extraction decision in the regional energy economy is based on the fossil fuel price functions from the global version of the ANEMI energy sector. As the price of fossil fuel is assumed exogenous to Canada, the desired amount of fossil fuel to extract by finding the inverse of the price functions:

$$F_{TE,i,t} = R_{i,t} + D_{i,t} - \upsilon_i R_{i,t=1980} \left(\frac{\overline{P_F}_{i,t}}{P_{F\,i,t=1980}} \right)^{1/\rho} \quad (3.1)$$

where $F_{TE,i}$ is the total extraction of fossil fuel type i at time t, given the current world price $\overline{P_F}_{i,t}$. $R_{i,t}$ is the current reserve value, $R_{i,t=1980}$ is the reserve value at the base year, $D_{i,t}$ is new discoveries, and $P_{F\,i,t=1980}$ is the world price of fossil fuel i at the base year. ρ is an elasticity parameter, and υ_i is a calibration parameter adjusting the level of extraction.

Given the exogenous world price, demand for fossil fuels in the regional model is given. It is assumed that net exports of fossil fuel i, $NX_{i,t}$, is the difference between demand and total extraction each period. That is, net exports of fossil fuel type *i* is equal to total extraction minus fuel used for the production of heat energy and electric energy:

$$NX_{i,t} = F_{TE,i,t} - F_{H,i,t} - F_{El,i,t} \quad (3.2)$$

The structure for the production of energy in the regional model is exactly the same as in the global model (presented in section 2.1.3). The model uses the same production functions for heat energy and electricity production, and aggregation into total energy services. Given the world price, the representative firms' demand for fossil fuels can be derived.

Given that the prices of fossil fuels are exogenous, there is no mechanism to clear the market for fossil fuels in the regional energy economy. Demand and supply are determined separately. If supply is greater than demand, the excess supply is exported. Vice versa, the excess demand is met with imports.

In the regional model, the parameter values for the production functions of energy and energy aggregation are the same as in the global model. The differences in parameter values are in the reserve values and discoveries of fossil fuel sources, and the price functions for fossil fuel sources. As in the global ANEMI model version of the energy economy the assumed future discovery of fossil fuels in Canada is presented in Table 3.4.

Table 3.4: Assumed future fossil fuel discovery (Canada) in billion GJ

	1980 Assumed Initial Reserves	1980 Reserves (EIA & Statistics Canada)	1980-2005 Discoveries (EIA & Statistics Canada)	2006 - Assumed Discoveries
Coal	140	90	50	-
Oil	2500	40	1180	1280
Natural Gas	400	77	133	190

Canada has a vast reserve of oil sands; however, economical, political, and technological constraints make it very difficult to make a prediction about what share of the oil sands will actually be extracted. Given these constraints, it is assume here that the total recoverable oil in Canada is about 410 billion barrels - approximately 25% of the oil estimated to be in the Alberta's oil sands (conversion factor from the EIA is 1 barrel of oil = 6.119 GJ). In 2007, the Alberta Energy and Utilities Board estimated that about 10% of the oil was recoverable given the economic conditions and technology available at that time. The natural gas discoveries follow a similar assumption about improvement in technology or increase in prices.

3.6 Disaggregation Procedure

Climate change processes are interacting over various temporal and spatial scales. One of the main requirements of the integrated assessment modelling is their ability to model various impacts across various scales. Disaggregation methodologies are used very often to assist in the process of transferring information across the scales. Harms and Campbell (1967) were

among the first researchers to formalize the disaggregation approach and apply it to temporal disaggregation of streamflow. Lane (1979) was among the first to transfer the same dissagreggation principles into the spatial domain. Regionalization of ANEMI model requires disaggregation of spatial and temporal information. The implemented procedures are described in the following sections of the report.

3.6.1 Temporal Disaggregation

The main objective of any disaggregation technique is to allow the prevention of the statistical properties at more than one level (for example maintaining statistical properties of the annual streamflow data in generating monthly streamflow for water resources management purposes). Mean, variances, probability distribution and covariance's can be designated as desired statistical properties in this type of disaggregation approach. In addition, the disaggregation allows reduction in the number of parameters with little or no corresponding loss of desirable properties in the generated data.

Because disaggregation is one step beyond the very basic time series modeling, such as autoregressive (AR) modeling, its application is more difficult. However, disaggregation approaches do eliminate many common problems that practitioners have with the stochastically generated data. The added benefits are well worth the effort required (Salas et al, 2009).

Disaggregation process provides new time series based on the available data series. The generation of disaggregated series (monthly or daily data, for example), based on the original series may be done with the help of a linear model designed to preserve important statistical properties of the original series. Disaggregation can be implemented in time and space.

In general all disaggregation models can be articulated in terms of linear dependence model as:

$$Y = AX + B\varepsilon \tag{3.3}$$

where Y is the current observation of the time series that will be generated, X is the original series or independent series, ε represents the current value from a completely random series (stochastic term). A and B are matrices of parameters.

It should be noted that in this approach each of the time series that make up X and Y must follow the normal distribution with zero mean. This condition could be secured by taking the original data series and transforming the individual values to normally distributed values and then subtracting the mean from the transformed values. The stochastic terms in matrix ε are assumed to be normal with zero mean and variance of one. The advantage of this disaggregation model is its very clean structure.

Mejia et al, (1976) introduced the following form of temporal disaggregation procedure:

$$Y = AX + B\varepsilon + CZ \tag{3.4}$$

where C is a parameter matrix with the same dimensions as Y, Z is a column matrix containing monthly values from the previous year.

From the above equation, Lane (1979) developed a condensed form of disaggregation model, where numbers of parameters are reduced by declaring zero value to the unimportant parameters. The condensed model can be expressed as:

$$Y_t = A_t X + B_t \varepsilon + C_t Z_{t-1} \tag{3.5}$$

where t and $t-1$ denotes the current time and immediate previous year respectively.

3.6.2 Spatial Disaggregation

Disaggregation provides an easy to apply and very efficient method for developing high resolution data (regional level) for climate change impact analyses. The disaggregation methods usually keep the overall patterns and are less likely to alter the original global data. The ANEMI version 2 model is a lumped model with a complex and sophisticated climate sector that are not easy to apply in regional impacts and policy experimentation. Hay et al (1992) proposed a disaggregation approach, which can be used to study regional impacts of climate change.

In the regionalization of ANEMI model, the disaggregation approach of Lane (1979) is used to establish a link between global and regional scales. The mathematical description of the disaggregation process is:

$$V = EU + F\varepsilon + GW \tag{3.6}$$

where *V* is a column matrix of regional values being generated, *U* is a column matrix of current global values, *W* is a column matrix of the previous regional values. *E*, *F,* and *G* are parameter matrices.

The approach is designed to preserve directly three sets of moments: lag-zero moments among the regions, lag-one moments among the regions and lag-zero moments between the global and regional values (Salas et al, 2009). Like the temporal disaggregation approach, the spatial

disaggregation can be staged in different steps. So, the global value can be disaggregated into regional value in the first step and then can be further disaggregated to local value.

3.6.3 Disaggregation Data Description

As the climate sector of the ANEMI version 2 model remains global, the current version of the model is not able to provide regional temperature change. In this study both, regional rainfall and temperature change need to be computed, since they are the driving force for other sectors, such as: economy-energy, hydrologic cycle, food production, etc. An attempt is taken to establish a relationship between global and regional temperature and rainfall data based the results from various GCM models. Due to the scarcity of long term historical observations, outputs from seventeen GCM models were used in the study (

Table 3.5).

From

Table 3.5, it is noticed that different model comes with its own resolution, which makes the analysis difficult. To avoid such resolution discrepancy a course resolution (10.0 long, 10.0 lat) is chosen. At the very beginning, all of these 17 GCMs data are averaged over 10°X10° grid size (Figure 3.1), so that they can represent the same grid area, with a time span of 99 years (from

1901 to 1999). Then the ensemble mean for each of the individual cells (10°X10°) are computed by averaging the 17 sets of data. The whole process reduces 17 sets of individual datasets in to a single (ensemble mean) 10°X10° dataset. Since the objective of the whole disaggregation process is to produce representative data sets for Canada and ROW (rest of the world), therefore rainfall and temperature for the 2 regions needs to be separated. Thiessen polygon method is implemented over the computed ensemble mean data to calculate the weight of each of the cells located within Canada and ROW. As a final step, areal average data for the two individual regions are computed for the 99 years for further analysis.

Table 3.5: GCM models used for the regionalization of the temperature and rainfall data

Originating Group	Country	ID	Additional info.
National Center for Atmospheric Research	USA	CCSM3	2.8X2.8
Canadian Centre for Climate Modelling & Analysis	Canada	CGCM3.1(T47)	2.8X2.8
Canadian Centre for Climate Modelling & Analysis	Canada	CGCM3.1(T63)	1.9X1.9
CSIRO Atmospheric Research	Australia	CSIRO-CCSM3Mk3.0	1.9X1.9
CSIRO Atmospheric Research	Australia	CSIRO-Mk3.5	1.9X1.9
Max Planck Institute for Meteorology Meteorological Institute of the University of Bonn	Germany	ECHAM5/MPI-OM	1.9X1.9
Meteorological Research Institute of KMA, and Model and Data group	Germany/Korea	ECHO-G	3.9X3.9
US Dept. of Commerce / NOAA / Geophysical Fluid Dynamics Laboratory	USA	GFDL-CM2.0	2.5 long, 2.0 lat
NASA / Goddard Institute for Space Studies	USA	GISS-AOM	4.0 long, 3.0 lat
NASA / Goddard Institute for Space Studies	USA	GISS-EH	5.0 long, 4.0 lat
NASA / Goddard Institute for Space Studies	USA	GISS-ER	5.0 long, 4.0 lat
Institute for Numerical Mathematics	Russia	INM-CM3.0	5.0 long, 4.0 lat
Institute Pierre Simon Laplace	France	IPSL-CM4	3.75 long, 2.5 lat
Meteorological Research Institute	Japan	MRI-CGCM2.3.2	2.8X2.8
National Center for Atmospheric Research	USA	PCM	2.8X2.8

Originating Group	Country	ID	Additional info.
Hadley Centre for Climate Prediction and Research / Met Office	UK	UKMO-HadCM3	3.75 long, 2.75 lat
Hadley Centre for Climate Prediction and Research / Met Office	UK	UKMO-HadGEM1	1.875 long, 1.25 lat

Equation 3.6 represents the basic model equation for the spatial disaggregation modeling, where, parameter matrices *E, F,* G and *Ɛ* are generated with the help of R (http://www.r-project.org/, last accessed July, 2011), which is a language and environment for statistical computing and graphics. The customized R model is capable of handling both the temporal and spatial data sets, and the associated programming codes are available at ANEMI User's Manual (Akhtar et al, 2011). For the temporal disaggregation (yearly temperature to monthly temperature), parameter matrices *A, B,* C and *Ɛ* are also generated in the same way as spatial disaggregation with help customized R software. In this case ANEMI version 2 utilizes the Equation 3.4, where the yearly temperature value *U* is endogenously feed into the model from the climate sector.

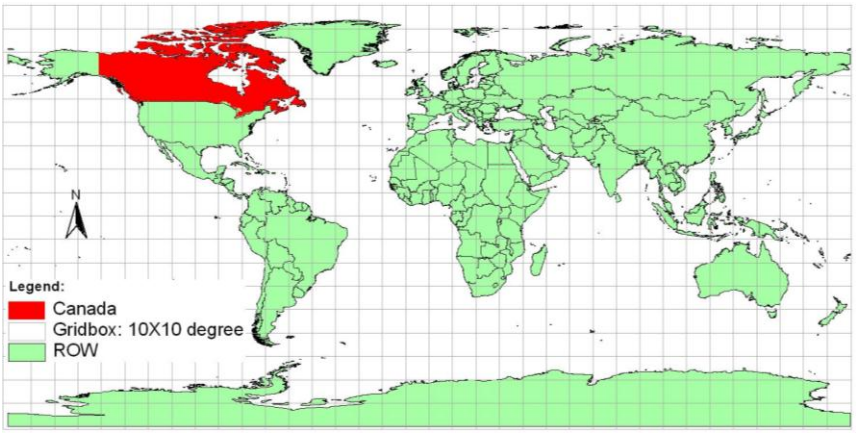

Figure 3.1: Map showing Canada and rest of the world (ROW) with 10 by 10 greed

3.7 Regional Model Performance

The Canada version of the ANEMI model is developed to evaluate the driving feedback structure and policy scenarios within nine sectors of the model. The regional model is verified by comparing the simulated value with the observation along a few established model simulations. The simulation time horizon is from 1980 until 2100. The model performance evaluation period is selected to be first 30 years (from 1980 to 2010). Because of continuous data scarcity, in many cases single or multiple discrete observations are considered in the evaluation of model performance.

3.7.1 Water Sectors

The main processes within the water sectors (hydrologic cycle, water demand and water quality) of Canada version of the ANEMI model are developed using temporal and spatial disaggregation.

The water withdrawals for various uses (domestic, industry, and agriculture) are driven by the economic activities, size of population, climatic conditions, irrigation requirements and so on. Pacific Institute (full name: Pacific Institute for Studies in Development, Environment, and Security, is a non-profit research institute created in 1987 to provide independent research and policy analysis on issues at the intersection of development, environment, and security. It is located in Oakland, California, USA) calculated water consumption of Canada for the year 2006, whereas Shiklomanov and Rodda (2003) gathered a decadal data starting from 1980. In addition, Shiklomanov and Rodda (2003) also projected the future water consumption until 2030.

The validation comparison graphs (Figures 3.2, 3.3 and 3.4) show that the estimation of the Pacific Institute is not analogous to the data analysed by Shiklomanov and Rodda (2003). Water withdrawal for agricultural use is not available in Shiklomanov and Rodda's (2003) publication.

The regional ANEMI model produces values much closer to the Pacific Institute than to Shiklomanov and Rodda's (2003).

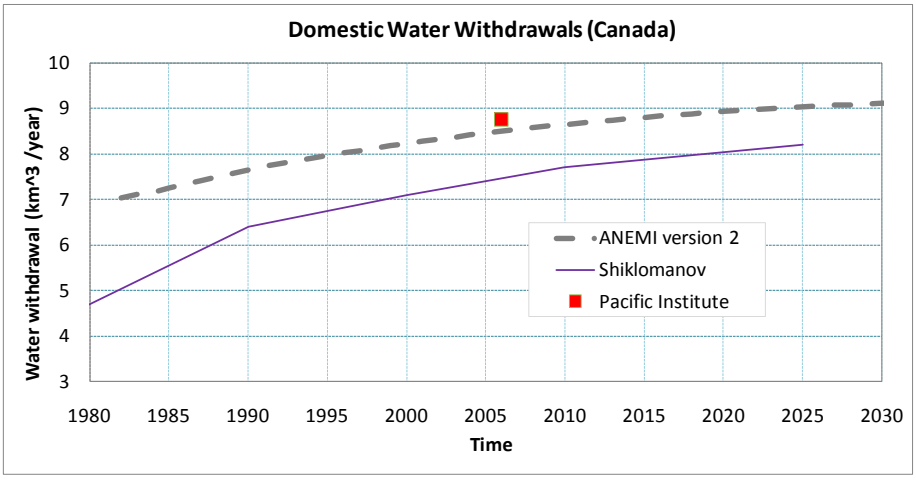

Figure 3.2: Domestic water withdrawals (Canada) validation

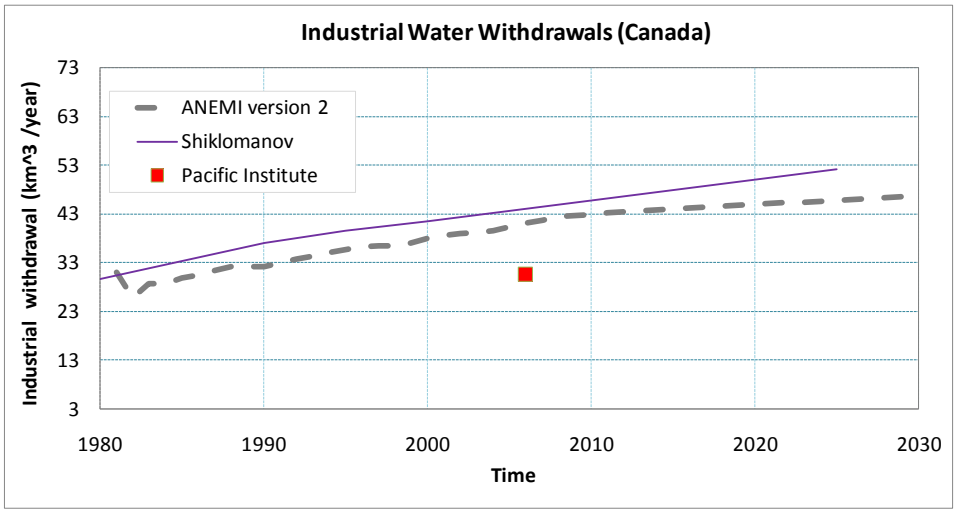

Figure 3.3: Industrial water withdrawals (Canada) validation

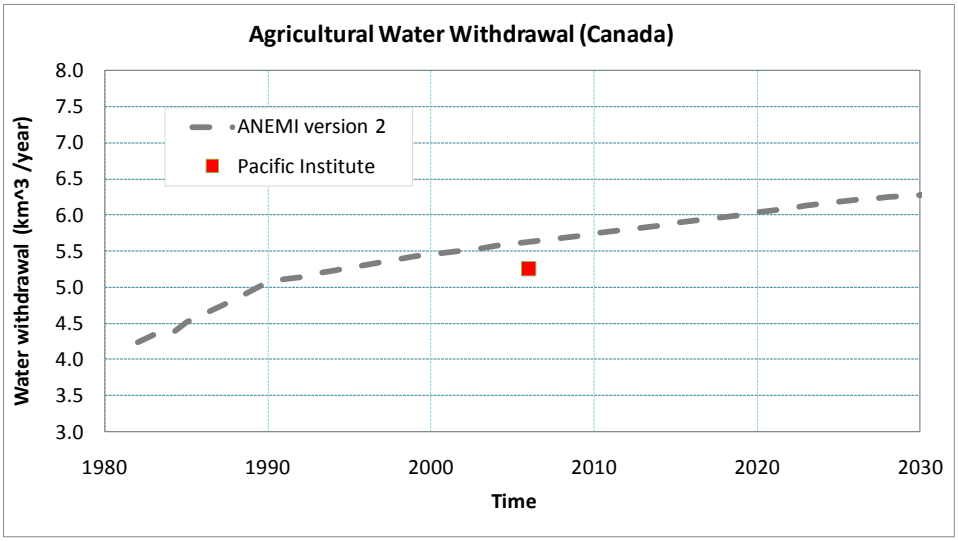

Figure 3.4: Agricultural water withdrawals (Canada) validation

3.7.2 Population

The regional version of the ANEMI model includes a very detailed population sector. The simulated results match perfectly with the observed UN population data (for Canada region) until 2005. The UN data after 2005 are from their own modeling projections, not from the observations. It is also noticeable that the IIASA (International Institute for Applied Systems Analysis) data sets are not agreeable with the observations, the whole data set is basically projected (projection is done in 2007). The Figure 3.5 also shows that the two projections (UN and IIASA) are very different in respect to population size. The ANEMI simulated results follow an average path indicating (a) a very good agreement with observed information (until 2005); and (b) some deviation from IIASA future projections.

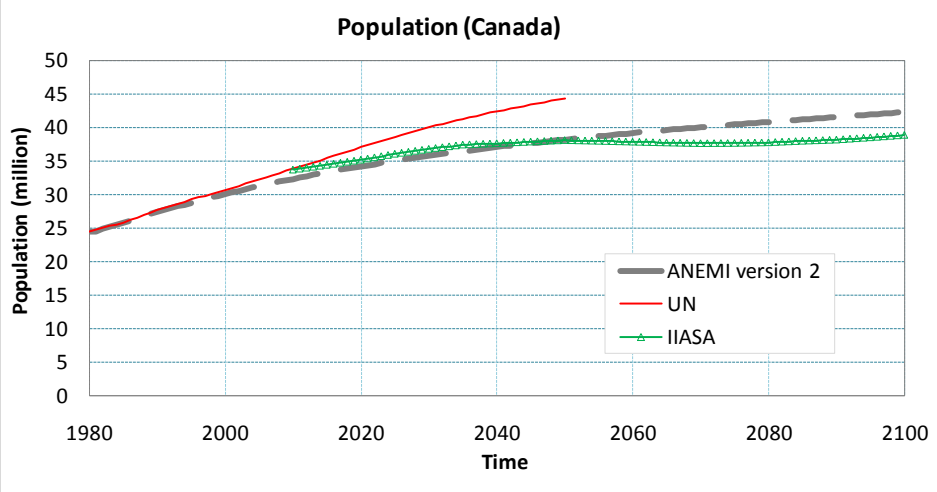

Figure 3.5: Population (Canada) validation

3.7.3 Land-Use

Canada contains over one-third of the world's boreal forest, one-fifth of the world's temperate rainforest, and one-tenth of the total global forest cover. Canada's relatively undisturbed forest areas are sufficiently large to maintain all of their native biodiversity. However, with the increasing demand, forest areas are being converted into either agricultural land or human settlements. Land-use sector of the regional ANEMI (Canada region) model has the capability to generate land conversion based on the population growth. Two verification graphs (Figures 3.6 and 3.7) are presented to show the future land-use change in respect to forest and cultivated/agricultural area. The simulated results are also compared with the WDI database (World Development Indicators, The World Bank, http://databank.worldbank.org, last accessed, August 2011). The ANEMI performance shows a good agreement with the observations. The observed data for agricultural area are not showing any trend. The ANEMI simulations are showing a rising trend, as expected by the majority of the scientific communities.

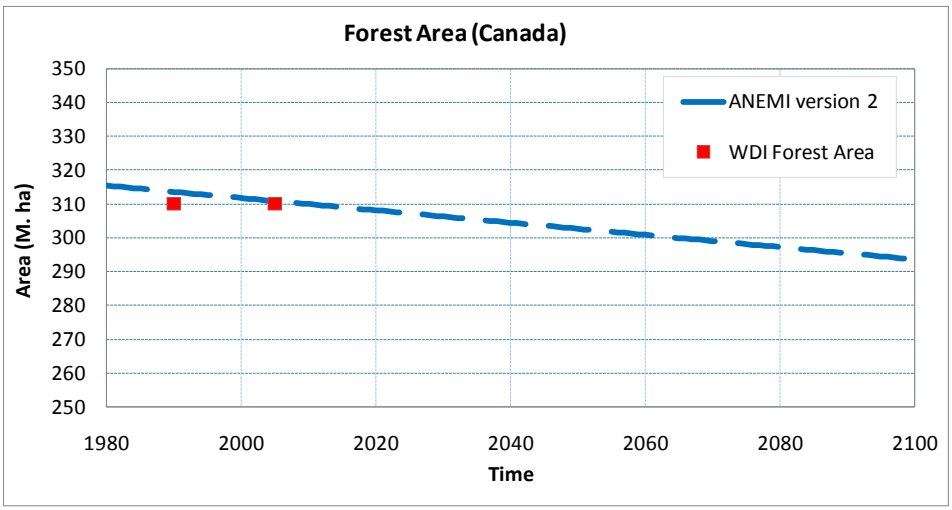

Figure 3.6: Forest area (Canada) validation

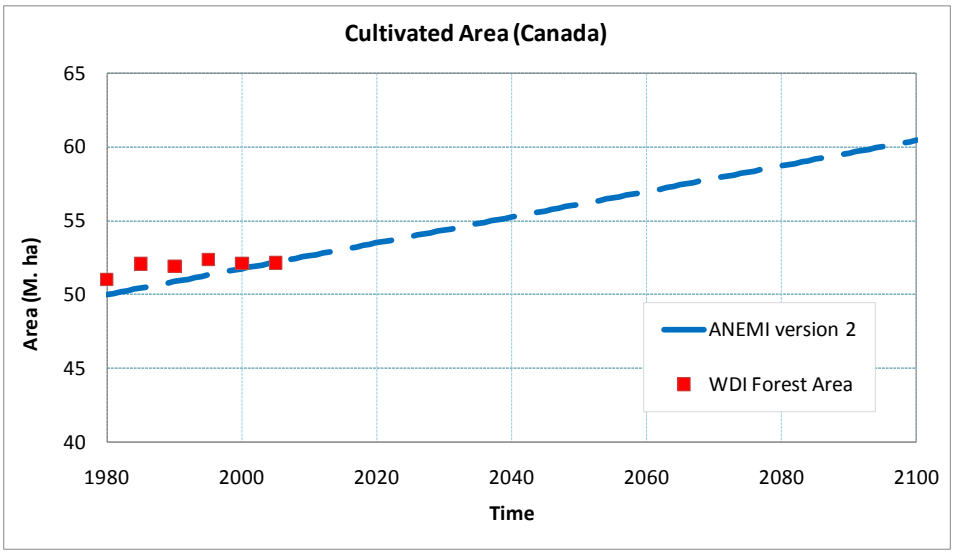

Figure 3.7: Cultivated area (Canada) validation

From the comparison graphs, it can be concluded that the regional version of the ANEMI model is performing satisfactorily and is capable of handling different policy scenario in the context of Canada.

3.7.4 Energy-Economy

The Gross Domestic Product (GDP) in Canada expanded 1% in the first quarter of 2011 over the previous quarter. From 1961 until 2010, Canada's average quarterly GDP growth was 0.84% reaching historical high of 3.33% in December of 1963 and a record low of -1.80% in March of 2009. Canada's economy is diversified and highly developed. The foundation of Canada's economy is foreign trade and The United States is by far the nation's largest trade partner. Foreign trade is responsible for about 45% of the nation's gross domestic product (GDP).

It seems difficult to find any good projections of GDP for Canada. In most cases, 1% change relative to baseline is reported for policy experimentation. The regional ANEMI simulated results seem close to the WDI data (here, GDP is expressed in constant 2005 international dollar value) from the World Bank (http://databank.worldbank.org, last accessed, August 2011) satisfying the calibration of energy-economy sector of Canada model (Figure 3.8).

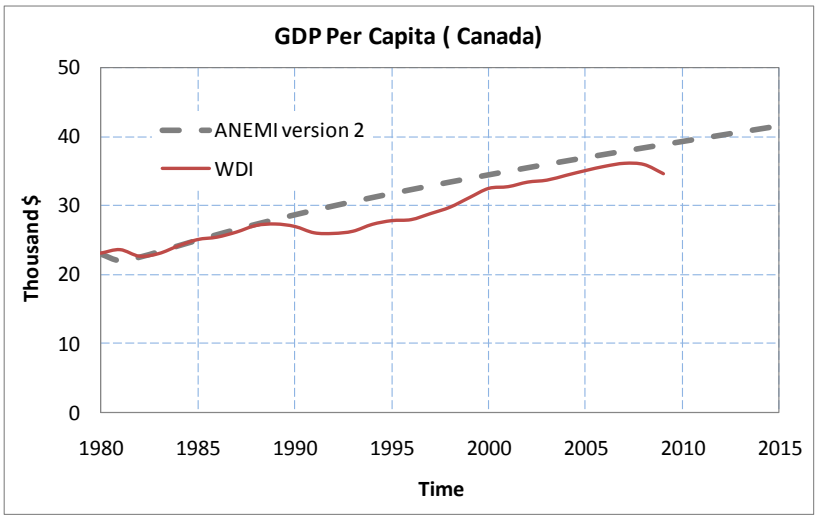

Figure 3.8: Real GDP per capita for Canada

4 MODEL USE

Both, the global and the regional versions of the ANEMI model which are developed by combining individual sectors together, are verified using historical observations as well as available published literature. Initially, all the individual sectors are calibrated separately and are then connected together to form the integrated model, which can satisfactorily represent the society-biosphere-climate-economy-energy system.

The purpose of the ANEMI model is not to forecast the future but to assist in understanding the complexity of the whole system and provide insight in the possible behaviour of the system and its components under changing climate. The integrated assessment model like ANEMI provides policymakers and scientists with the tool that can answer many 'what if' questions. This chapter of the report demonstrates the implementation of ANEMI version 2 model to simulation of policy scenarios developed in cooperation with project partners. The set of scenarios presented here is selected from comprehensive in-person communication with project partners. The detailed report on scenario development is available in Popovich et al (2010) that is available on the same CD-ROM.

4.1 Description of Scenarios

Detailed process of communication with the climate change policy community (represented by the project partners) resulted in the identification of seven policy scenarios. In the second phase of the ANEMI model implementation these scenarios were aggregated into three general scenarios presented in following sections of the report.

4.1.1 Carbon Tax Scenario

The assessment reports from the Intergovernmental Panel on Climate Change (IPCC, 2007b; Trenberth et al, 2007; Schneider et al 2001) have identified the key potential impacts of climate change. Furthermore, these reports point to human-induced increases in the atmospheric concentration of greenhouse gasses (GHGs) as a likely cause of climate change. There is a relatively strong consensus in the scientific community that GHGs emissions need to be cut in order to reduce the impacts of climate change.

Various policy options are available to reduce GHG emissions (Popovitch et al, 2010). Three of them are tested with the ANEMI model. The first, and the easiest policy to implement is carbon tax. In the energy-economy sector, the carbon tax is implemented as a tax per unit of CO_2 emissions, effectively raising the price of fossil fuel. Selected results from the carbon tax scenario are presented later in this chapter. The carbon tax is implemented in 2012 and slowly ramped up to $100 per tonne of CO_2 emission over 30 years**.** The carbon tax has a significant impact on energy input into heat energy production as it is primarily produced from fossil fuel. The impact on electricity production is less severe as nuclear and hydro power are not impacted by the carbon tax.

4.1.2 Increase Water Use Scenario

Water is crucial not only for human survival but it also work as a fuel for growing economy. With the increasing population and rising global temperature, the total demand for water is rising irrespective of the individual water uses (domestic, industrial and agricultural). Such an increase in water demand results in the demand for additional infrastructure (dams, reservoirs, and diversions). Many watersheds now have their water resources fully allocated and greater irrigation efficiency will be required if irrigated area is to expand in the future, while maintaining acceptable stream flows for other uses. Decreasing water availability, declining

water quality, and growing water demand are posing significant challenges to human population and health of ecosystems as well. Intergovernmental Panel on Climate Change (Kundzewicz et al, 2007) states that global warming will lead to "changes in all components of the freshwater system," and concludes that "water and its availability and quality will be the main pressures on, and issues for, societies and the environment under climate change'' (Bates et al, 2008). In some areas, improved irrigation efficiencies may actually dictate an increase in irrigation water used per unit of land, where crops are now receiving insufficient water for optimum growth. For example, in Alberta and British Columbia, evaluation of irrigation system practices found that for some crops, producers were under-irrigating and could improve production by increasing the amount of water applied. At the same time, continued improvement in irrigation and conveyance efficiency will free up some water for other uses.

Climate change projections for Canada indicate a 37% increase in irrigation water demand in the Okanagan Valley, B.C. (Neilsen et al, 2001). In addition, due to global warming the area where crops require irrigation may increase in the Prairies, Ontario, Quebec and the Atlantic Provinces. Therefore, the second policy scenario included in this study focuses on increased water use. An assumed amount of 15% increase across all water uses is tested to demonstrate the ANEMI model response to the increase in need for water.

4.1.3 Food Production Increase Scenario

In a news release by the Food and Agriculture Organization of the United Nations, it stated that "Producing 70 percent more food for an additional 2.3 billion people by 2050 while at the same time combating poverty and hunger, using scarce natural resources more efficiently and adapting to climate change are the main challenges world agriculture will face in the coming decades" (FAO, 2009).

This scenario is closely related to the previous one, in which the demand for water is expected to increase. Whereas previous scenario experimented with the impact of increasing irrigation to cope with rising food demand, this scenario tests the impact of redistributing land-use, by converting more land from forest to agriculture. This scenario also uses the global version of the ANEMI model, making a more general set of conclusions for the world's capacity to meet global food demand. It also shows the sink capacity of the land, and produces output in various sectors, including: population, hydrologic cycle, water quality, energy-economy, climate, carbon, and food production.

4.2 Global Model Analyses

In the following three sections, the main results of ANEMI simulations of three policy scenarios are presented.

4.2.1 Global Carbon Tax Scenario

The carbon tax is implemented in 2012 and slowly ramped up to $100 per tonne of CO_2 over 30 years. Figures 4.1 and Figure **4.2** show how are electric and heat energy production impacted by the implementation of the carbon tax. The dashed line in these two figures show ANEMI simulation results without the carbon tax and full line shows results with the carbon tax in place. The carbon tax has a significant impact on energy input into heat energy production as it is primarily produced from the fossil fuel. The impact on electricity production is less severe as nuclear and hydro power are not impacted by the carbon tax.

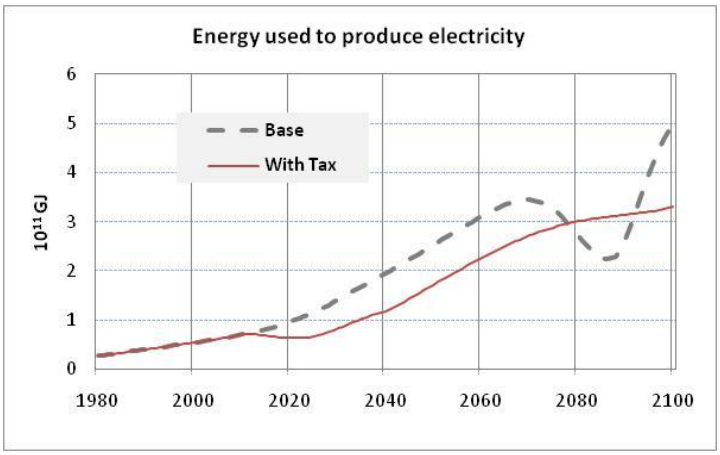

Figure 4.1: Energy used to produce electricity

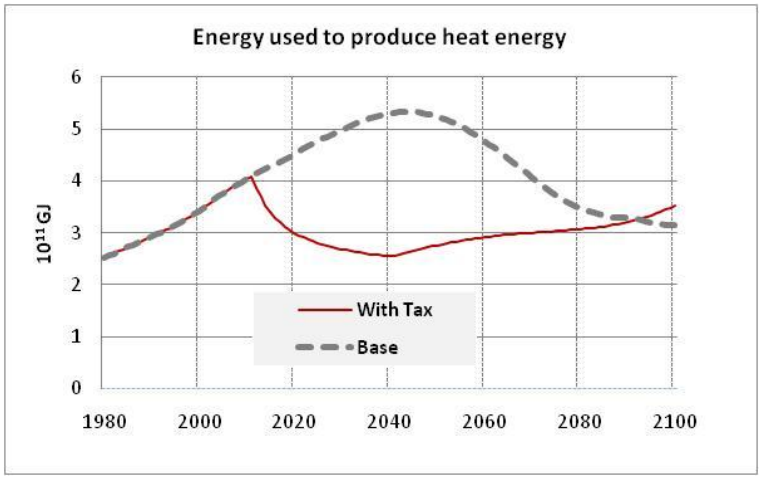

Figure 4.2: Energy used to produce heat energy

The implemented carbon-tax policy creates significant pressure on different fossil fuel pricing based on the carbon emission amount to produce unit amount of energy. Following the elasticity of substitution the share of each fossil fuel type is automatically adjusted to produce the low cost energy. Not only this type of adjustment (a certain combination of coal, oil and natural gas to produce cost effective energy) but mostly a dramatic drop in energy consumption (Figure 4.3**Error! Reference source not found.**) change the whole dynamics of the global energy-economy sector. The initial reduction of the fossil fuel based energy

consumption, just immediate after the implementation of the carbon-tax helps to maintain a relatively stable supply of the fossil fuel based energy throughout the 21st century. Such behaviour is driven by the availability of the fossil fuel reserve. In the base simulation, fossil fuel price started to climb up, as the reserve tends to decline and after 2080 the world is mostly running out of fossil fuel to produce heat and electric energy. On the other hand, under the carbon tax scenario, initial reduction in energy consumption saves a significant portion of fossil fuel to burn later. As the fossil fuel based energy consumption decreases significantly, so the fossil fuel based emissions follow the same trend (**Error! Reference source not found.**). However, after 2040 there is a change in trend for energy consumption path because of the introduction of carbon capture and storage technology.

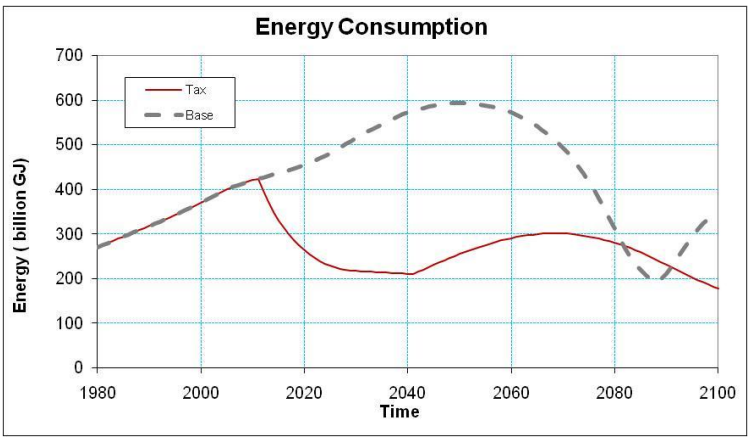

Figure 4.3: Global energy consumption

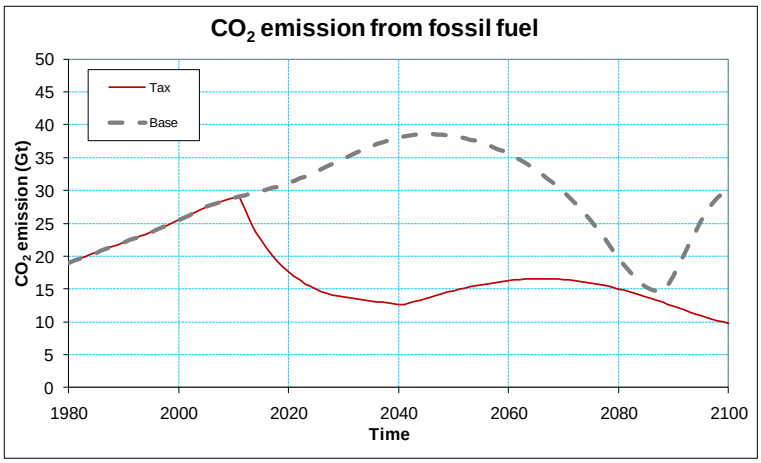

Figure 4.4: Global CO_2 emissions from fossil fuel

The main source of anthropogenic emissions is the burning of fossil fuel and forest cutting/burning. Under this scenario, the fossil fuel based emissions are reduced by almost half, which significantly lowers the atmospheric CO_2 concentration increment rate and by 2100 the global atmospheric concentration could be well below 500ppm (Figure 4.5). Atmospheric CO_2 concentration is considered as one of the sources of increased radiative forcing, which works as a driving force for increase in global temperature. The model also shows around 0.5 ^{0}C drop in atmospheric temperature by 2100, compared to base condition (Figure 4.6). Due to its positive correlation, the sea-level rising rate slows down relative to the base (no carbon tax) run (Figure 4.7).

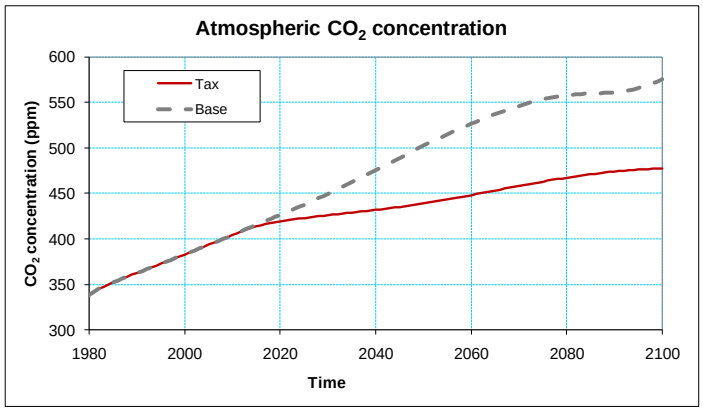

Figure 4.5: Global atmospheric CO_2 concentration

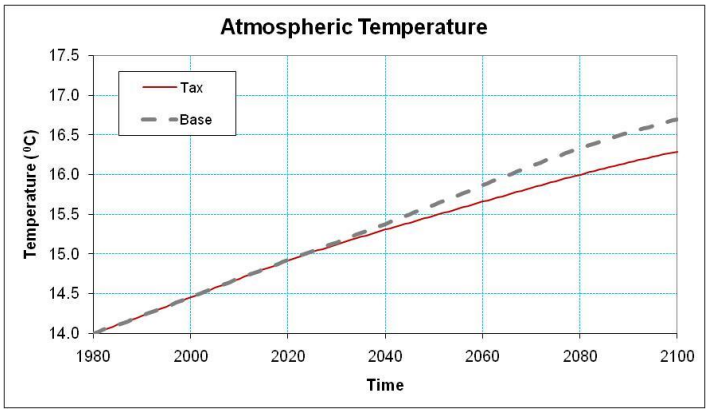

Figure 4.6: Global atmospheric temperature change

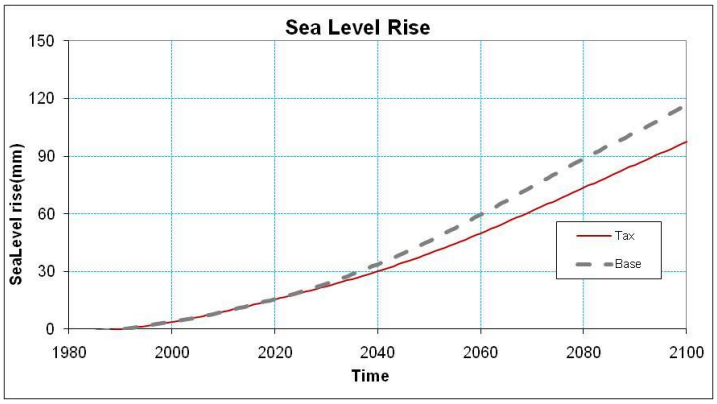

Figure 4.7: Global sea-level rise

The suitable temperature and less pollution result in increase of human life expectancy a bit after the implementation of carbon tax policy and thereby global population increase by almost 10% compared to the base condition for more than 50 years (Figure 4.8). Such population increase demands more food production (Figure 4.9), leading to higher water demand for irrigation. As more irrigation produces higher pollution of water and requires more fresh water for dilution, the water-stress starts to increase (Figure 4.10) and eventually acts as a negative feedback force in food production and population sectors. The global GDP also exhibits 13% increase from the base conditions in 2100 (Figure 4.11).

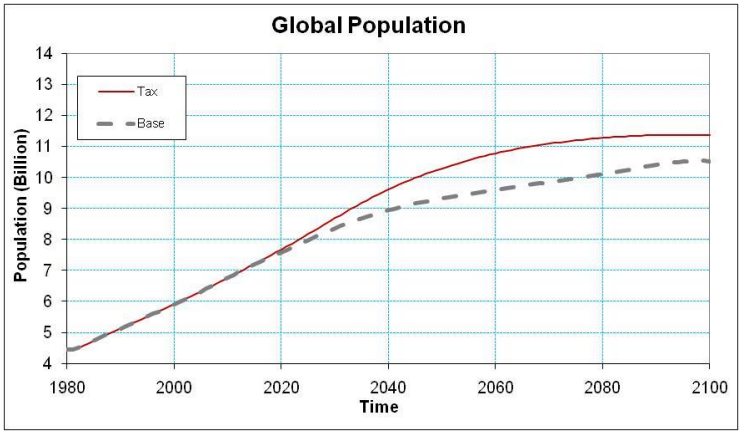

Figure 4.8: Global population

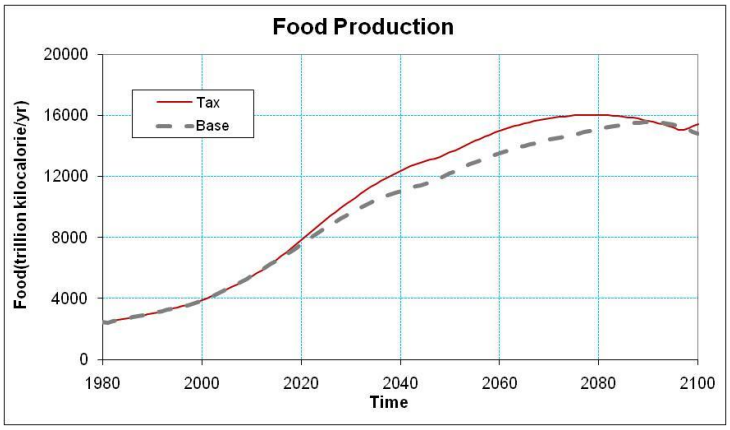

Figure 4.9: Global food production

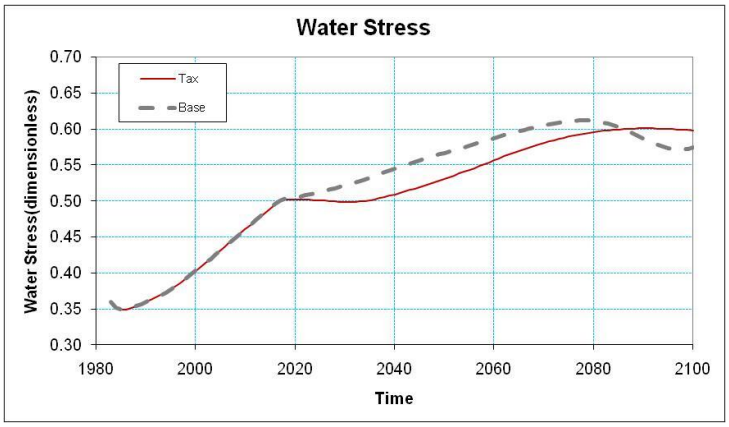

Figure 4.10: Global water-stress

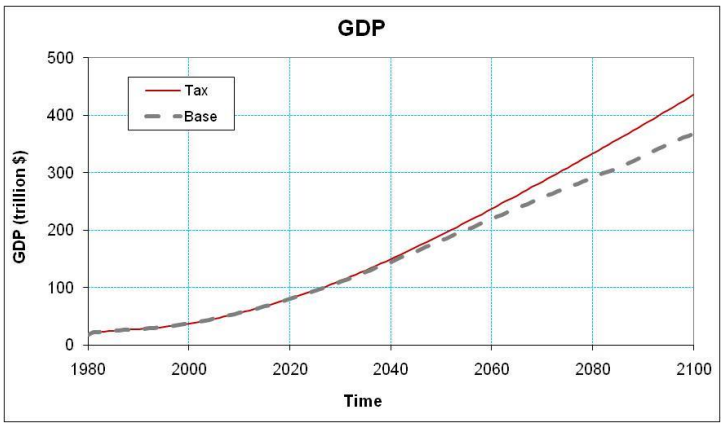

Figure 4.11: Global GDP change

The impact of the carbon tax on GDP per capita is first negative (minor) impact, because of the distortion created by the tax policy (Figure 4.11). Eventually, all the benefits from reduction of climate damage and price effects for fossil fuel suppress the tax distortion effect. The price effect for fossil fuel is showing some benefit from delaying depletion of the reserves. In the ANEMI model, fossil fuel prices are a function of the reserve level relative to the base year. That is, when reserves decrease, the price starts to increase, and the benefits from delaying the price increase are significant.

4.2.2 Global Water Use Scenario

The second scenario is tested using the global version of the ANEMI version 2 model, with 15% increase in water use for all uses. The intension of this scenario is to identify the probable impacts of increased water use on other sectors of the model and find how the multiple feedbacks determine the system response, not to forecast the future.

The main impact of 15% increase in water consumption from the base conditions (without the increase), decreases the available surface water by 1% (Figure 4.12). This value may seem negligible on global scale but if translated onto agriculture and human use, then it could vary from 0 to 50%. Therefore, it is very difficult to compute the actual water-stress, which the world may face by 2100. The model computations indicate around 6% increase in water-stress (Figure 4.13).

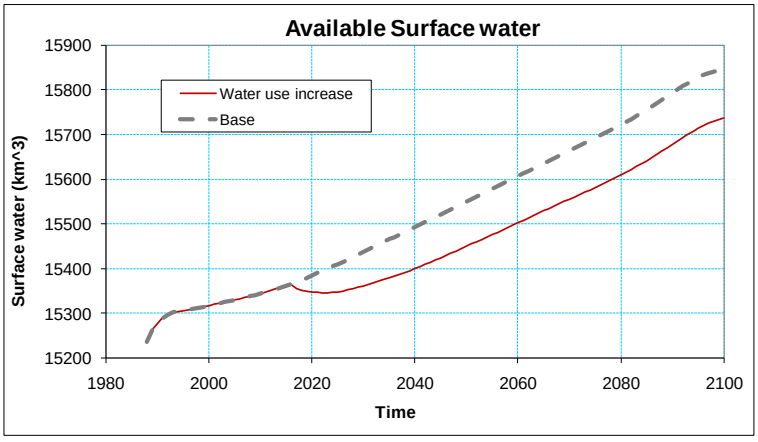

Figure 4.12: Global available surface water

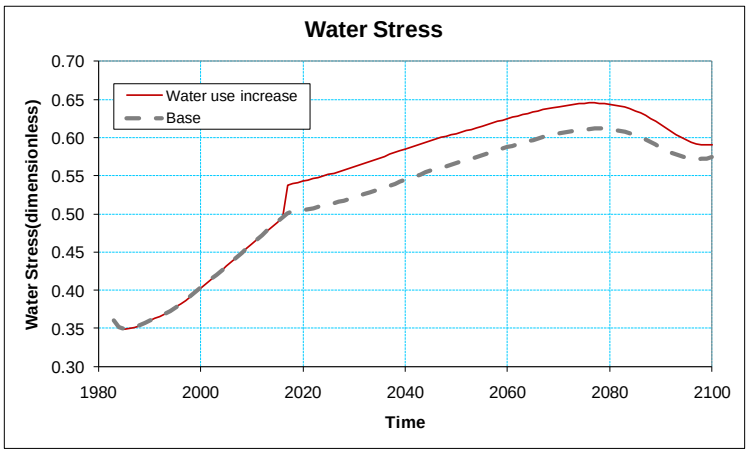

Figure 4.13: Global water-stress

The increase in water withdrawals is manifested in decrease of water quality and eventually produces even higher water-stress (due to increased dilution requirements). The agricultural sector faces higher water scarcity and loses productivity by more than 5% (Figure 4.14).

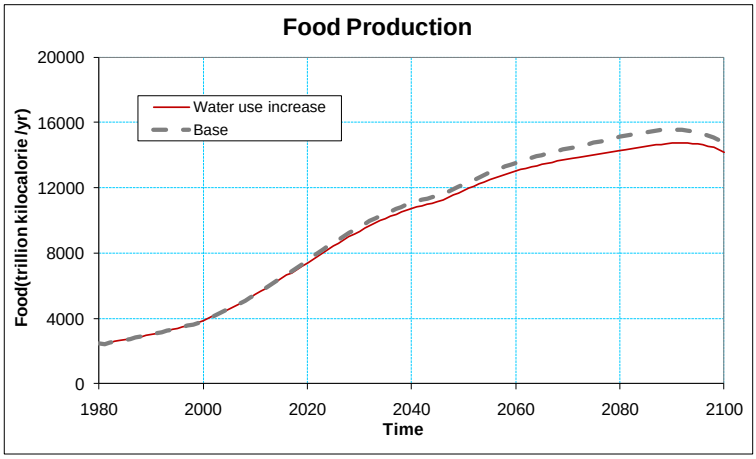

Figure 4.14: Global food production

The increase in water-stress increases a threat to human survival, especially in terms of life expectancy. The reduction of the per capita food production becomes a challenge. Unfortunately these two combined feedbacks result in 7.5% reduction of the overall population

by the end of this century (Figure 4.16). The global GDP also decreases (Figure 4.19) but at a very nominal level (2.5%) due to decrease in the population.

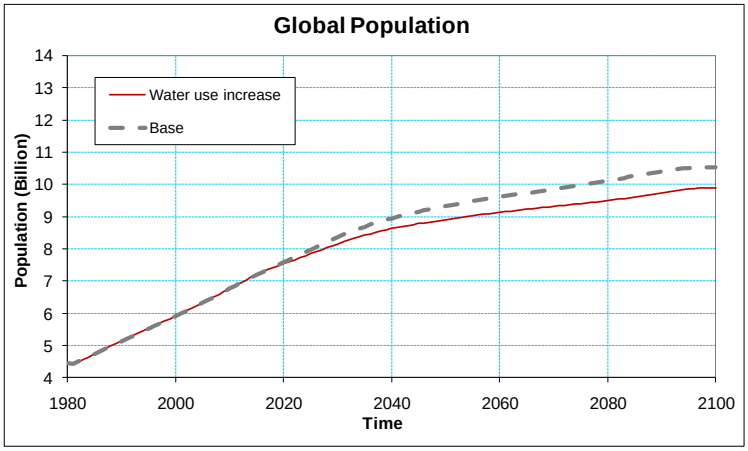

Figure 4.15: Global population

With the reduction of the global population, the CO_2 production from the fossil fuel along with atmospheric CO_2 concentration decreases (Figures 4.16 and 4.17). Atmospheric CO_2 concentration is one of the major driving sources of radiative forcing, responsible for the global temperature rise. Since the atmospheric CO_2 concentration exhibits negligible change, the model is not showing any significant change in atmospheric temperature (Figure 4.20), as well as the sea-level rise (**Error! Reference source not found.**).

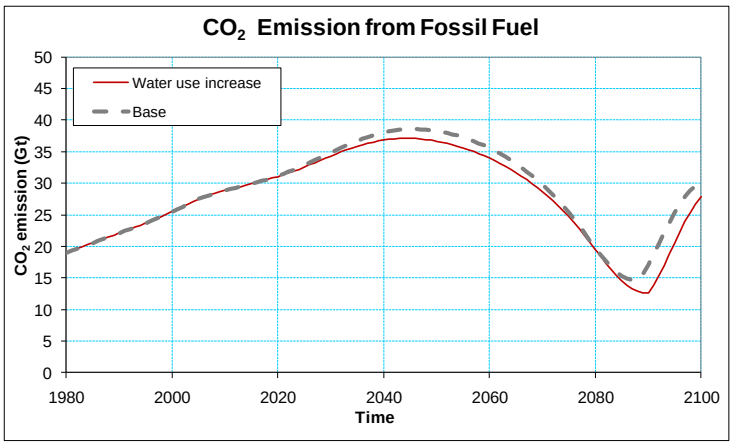

Figure 4.16: Global CO_2 emissions from fossil fuel

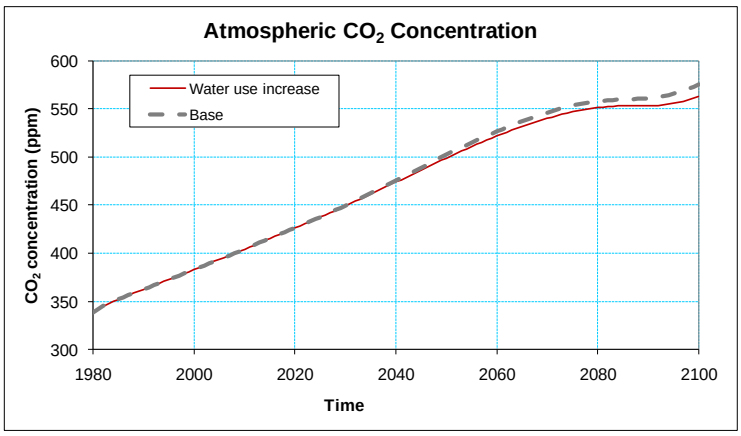

Figure 4.17: Global atmospheric CO_2 concentration

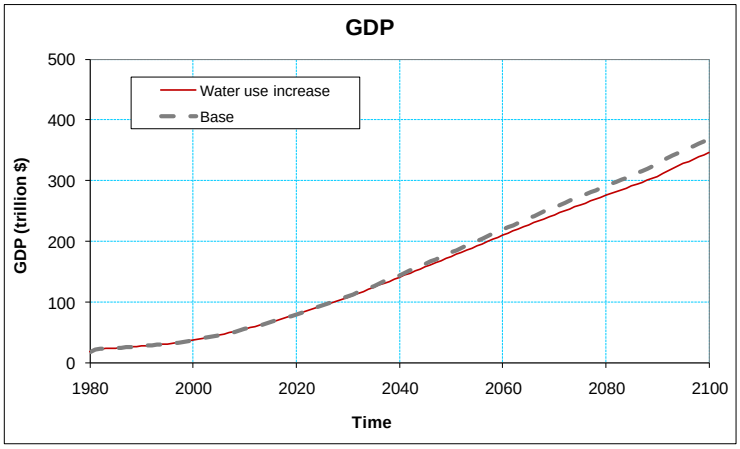

Figure 4.18: Global GDP

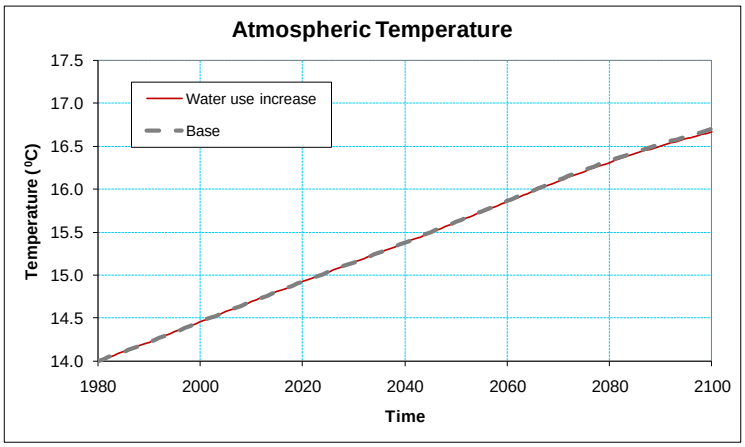

Figure 4.19: Global atmospheric temperature

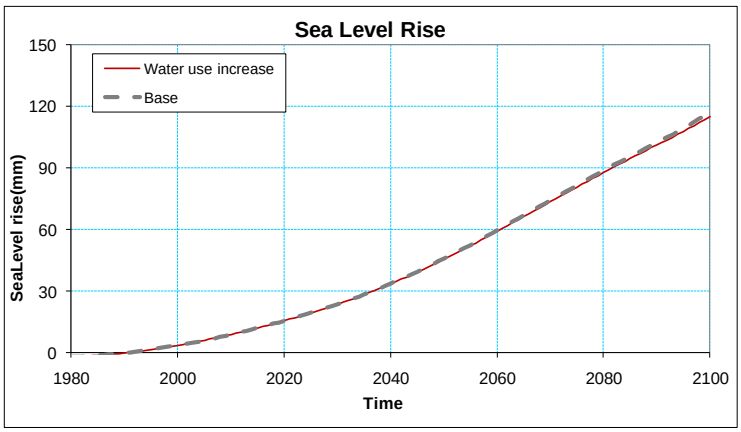

Figure 4.20: Global sea-level rise

4.2.3 Global Food Production Scenario

Simulations of the third scenario are focused on finding how is increase in agricultural land going to affect the total food production. In the global ANEMI version 2 model, land conversion rate (from forest to agriculture) is increased by 15% to allow for increase in food production and identification of the probable impacts on the other model sectors. For this investigation few important parameter and variables are analysed, such as: food production, available surface water, water-stress, global population, CO_2 concentration, etc.

The simulation results (Figure 4.21) demonstrate that the conversion of extra 15% of land into agricultural land increases the food production for about 1% at the beginning of the policy implementation period but after a while the extra production starts to decline because of the water shortage. Not only that the extra production from the increase in agricultural area diminishes, but the total food production falls below the base conditions (no increase in land conversion) after 2090 (Figure 4.21). It is important to note that more than 80% of the projected land expansion is expected to take place in sub-Sharan Africa and Latin America. By contrast, in South Asia and Near East/North Africa, where almost all the suitable land is already in use, there is a little room for expansion of the agricultural area. One fourth of the expanded agricultural land is assumed to be under irrigation, which increases the agricultural water consumption and thereby reduces the available water by 0.6% (Figure 4.22). The increase in water consumption also increases the total volume of polluted water, thereby requiring more fresh water for dilution purposes. This positive feedback structure causes continuation in water stress rise up to around 7% above the base case (Figure 4.23). The considerable increase in agricultural land failed to produce similar increase in food production.

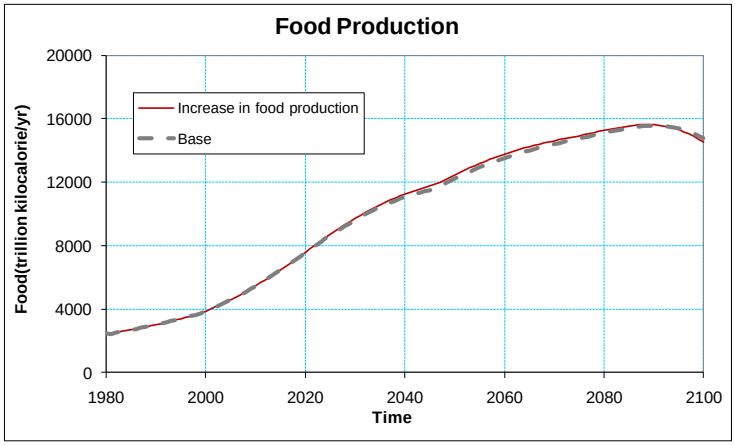

Figure 4.21: Global food production

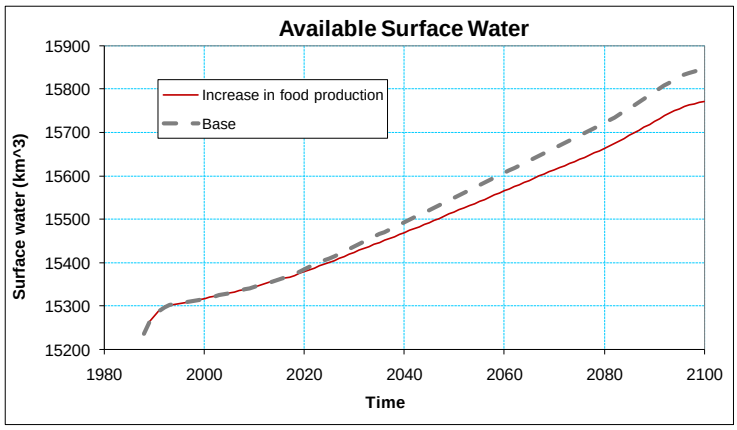

Figure 4.22: Global available surface water

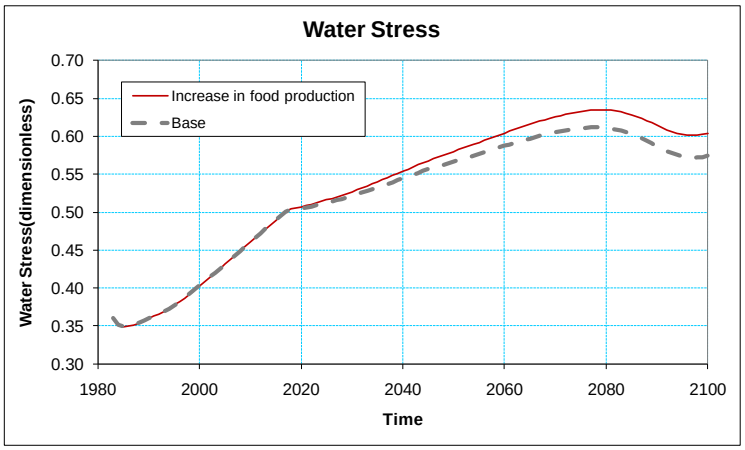

Figure 4.23: Global water stress

The increase in water stress generates inverse impact on food production that has positive impact on the life expectancy. Figure 4.24 shows population change which is judged insignificant in respect to total population.

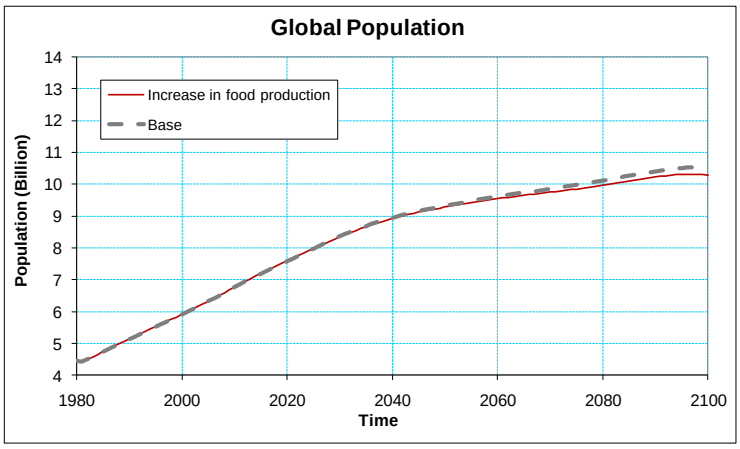

Figure 4.24: Global population

CO_2 emissions from the fossil fuel and GDP are directly related to the population. The simulated results show very small change in this case (Figures 4.25 and 4.26). However, the model results show nearly 1% increase in global CO_2 concentration (Figure 4.27), which may be a significant finding. In reality, the atmospheric concentration does not only originate in fossil fuel burning but a significant portion of carbon is coming from the change in land-use. In this simulation the extra amount of atmospheric CO_2 concentration is the consequence of 15% increase in land conversion (specifically forest cutting/burning) to expand the agricultural land.

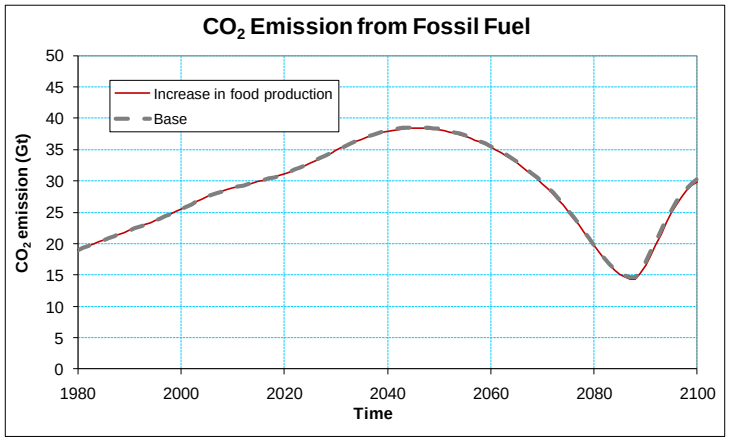

Figure 4.25: Global CO_2 emissions from fossil fuel

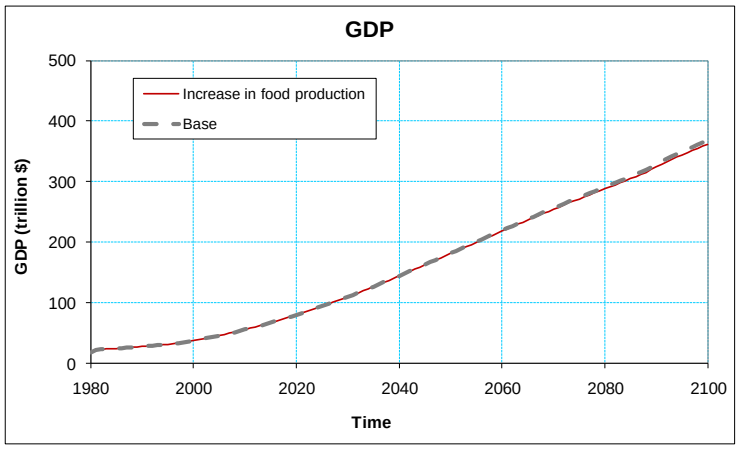

Figure 4.26: Global GDP

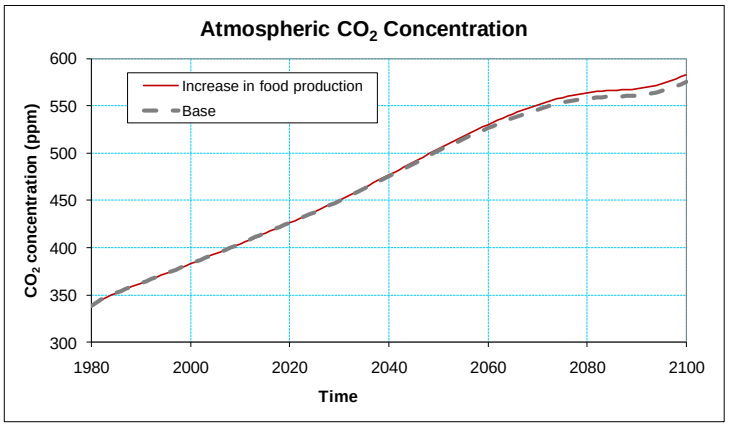

Figure 4.27: Global atmospheric CO_2 concentration

A minor change in atmospheric CO_2 concentration contributes to a small increase in radiative forcing that affects the global temperature change (Figure 4.28). As the forcing from solar radiation and other gases remain unchanged, only 1% increases in CO_2 concentration dampens further. Since, sea-level change is only a function of temperature, the model produces the same trend for sea-level change (Figure 4.29).

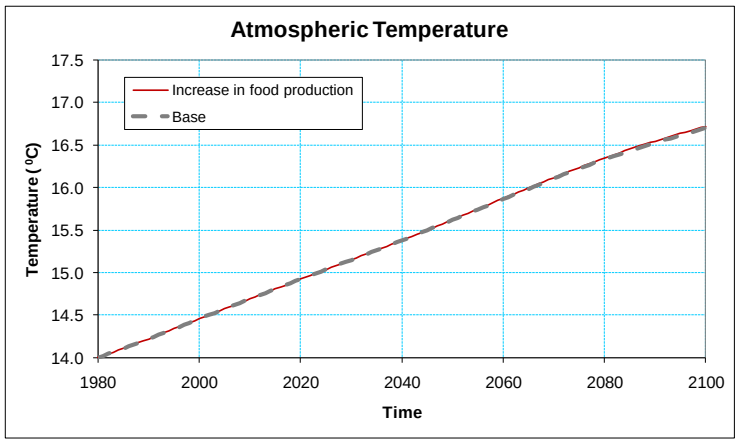

Figure 4.28: Global atmospheric temperature

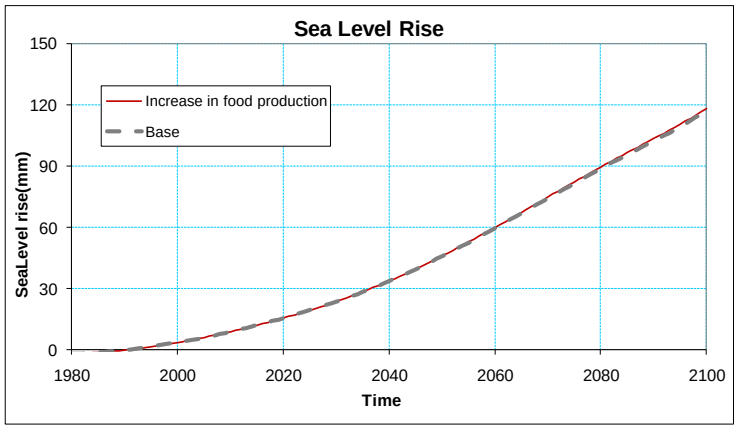

Figure 4.29: Sea-level rise

4.3 Regional (Canada) Model Analyses

One of the project objectives of this study was to develop a regional model for Canada that will provide support for national climate change policy analyses. The disaggregation method is applied to develop and calibrate the regional version of ANEMI model. Three selected policy scenarios are analyzed using the regional version of ANEMI and the following sections present the results.

4.3.1 Canada Carbon Tax Scenario

In this section, some selected results are shown from the regional model analyses. Each figure used for illustration of the results includes the baseline (no carbon tax applied) and the carbon-tax policy alternatives. The carbon-tax policy simulations assumes that Canada and the world implement the same carbon-tax policy - a carbon tax implemented in 2012 and slowly ramped up to $100 per tonne of CO_2 over 30 years.

Figure 4.30 shows GDP per capita for the baseline run and the carbon tax scenario. As in the global model the tax distortion initially reduces GDP- however, eventually the reduction in climate damages and the fossil fuel price effects take over and GDP increases relative to the baseline. The benefit from the carbon tax is somewhat offset in the regional model as fossil fuel exports decrease under the tax policy.

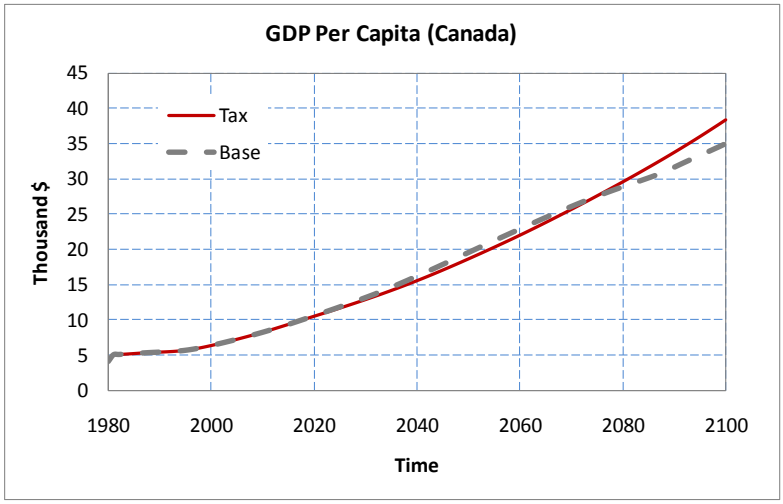

Figure 4.30: GDP per capita (Canada)

Figure 4.31 shows the total energy input used in the production of aggregate energy services in the regional model. For the baseline (no tax implemented), the hump shape in total energy

input is a result of increasing fossil fuel prices, which are exogenously given, from the global model. With the carbon tax, there is a significant impact on energy consumption in the regional model. This effect is also visible in the simulations of the global model.

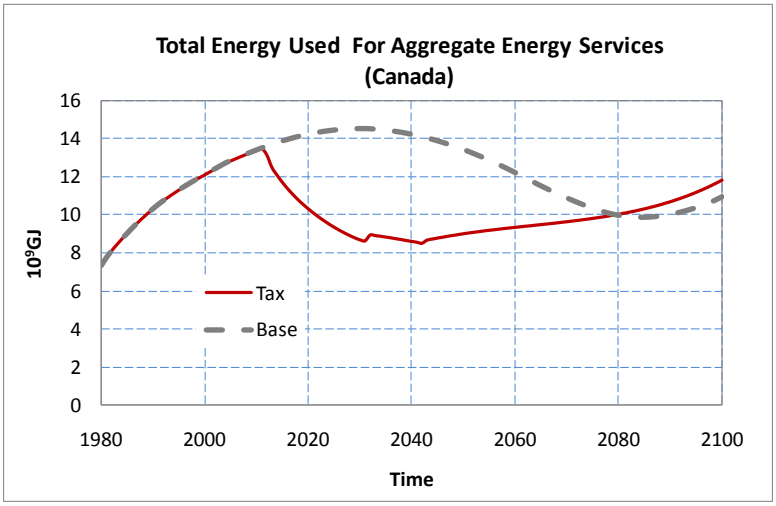

Figure 4.31: Total energy used in the production of aggregate energy services (Canada)

Error! Reference source not found. shows total industrial emission from the regional model. This emission is closely linked with the total energy consumption. Similar to the results of global model simulations, the carbon tax has a significant impact on fossil fuel consumption and industrial emission.

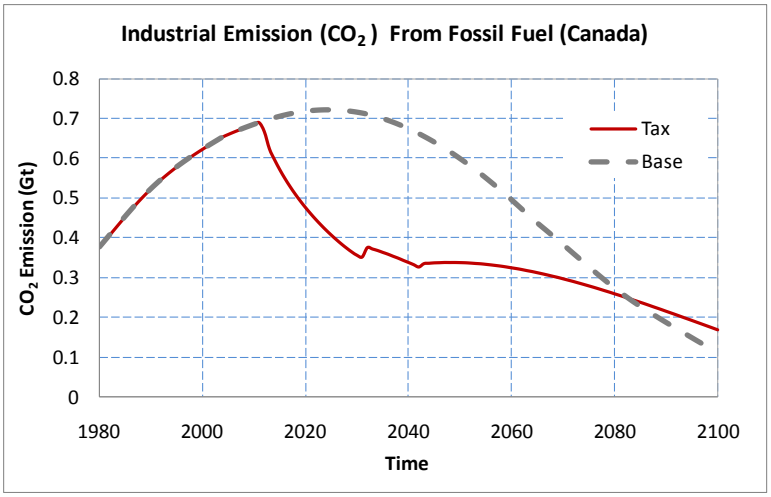

Figure 4.32: Industrial emission from fossil fuel (Canada)

4.3.2 Canada Water Use Scenario

To demonstrate the regional impact of the water use scenario, 15% increase in water use in Canada is assumed. It is already mentioned that the agricultural water use in Canada would require 37% more water due to increasing trend in temperature. However, regional simulations are performed using 15% increase in order to demonstrate the model performance and to maintain the consistency with the global model investigations.

Since Canada's water resources are abundant and water consumption small, the increase of 15% in consumption barely changes the total volume of available water compared to the base conditions (Figure 4.33). However, water-stress increases by more than 10% at the end of the century (Figure 4.34) still staying below the threshold level (0.4). Because of such comfortable position, food production (Figure 4.35) and other water intensive activities remain uninterrupted.

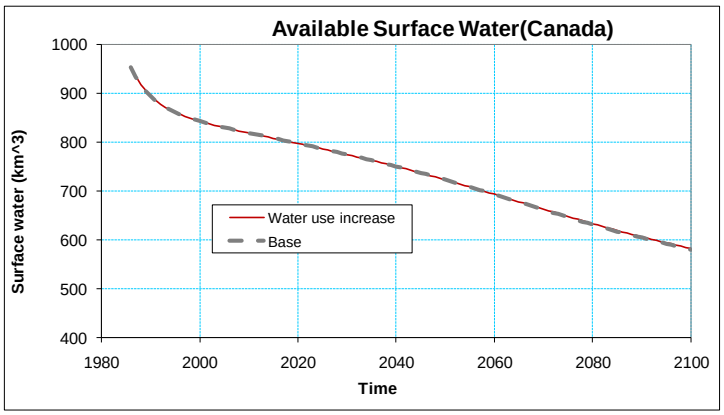

Figure 4.33: Available surface water (Canada)

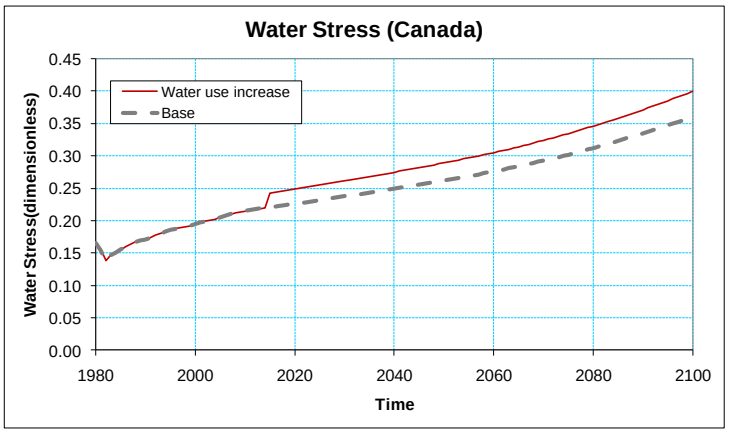

Figure 4.34: Water-stress (Canada)

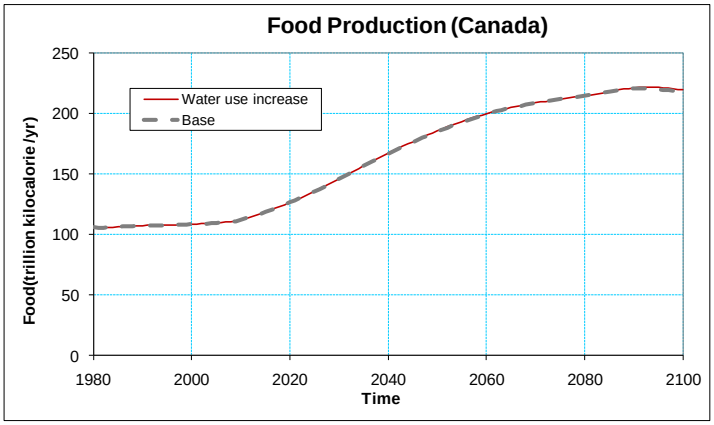

Figure 4.35: Food production (Canada)

It is well known that increased water-stress is a great threat for human survival and because of Canada's sufficient water resources human life expectancy is not decreasing by year 2100. Therefore, plenty of food stock and large water resources provide Canada with conditions for a very stable population (Figure 4.36).

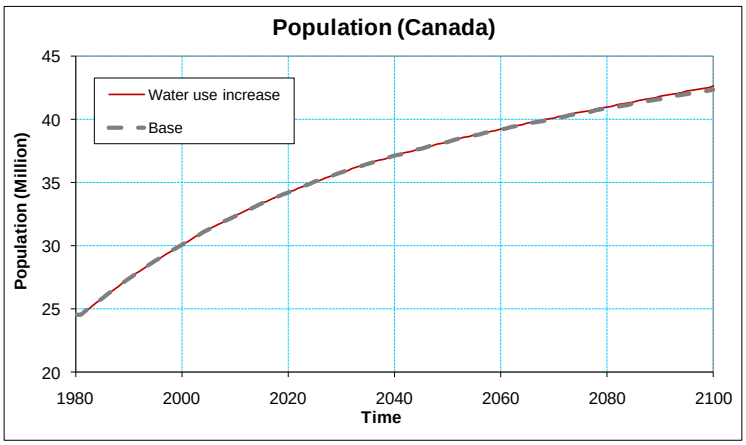

Figure 4.36: Population (Canada)

Since the population of Canada remains almost unchanged (0.5% increase) with the 15% increase in water consumption, the CO_2 emissions from fossil fuel and GDP also remains nearly unchanged (Figure 4.37 and Figure 4.38).

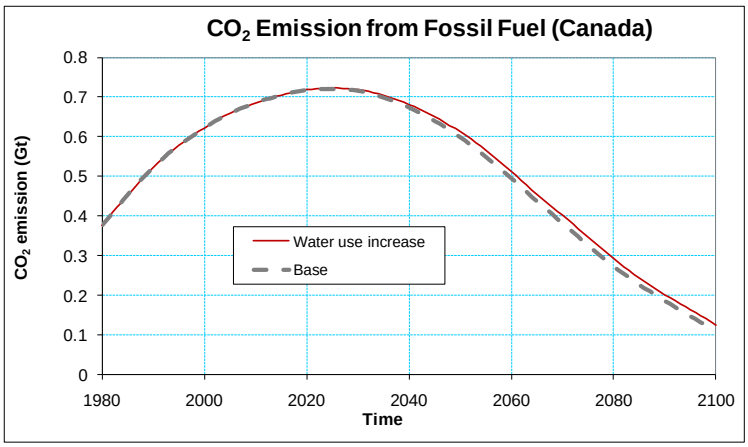

Figure 4.37: CO_2 emission from fossil fuel (Canada)

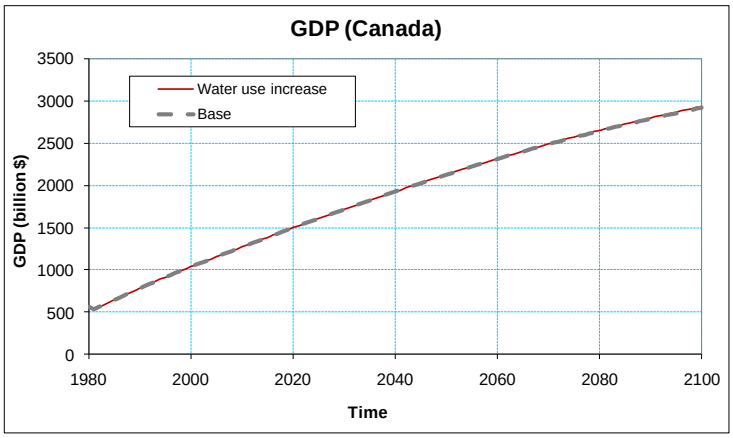

Figure 4.38: GDP (Canada)

4.3.3 Canada Food Production Increase Scenario

Over the past 40 years, the number of farms in Canada has declined, but the remaining farms have become larger and more productive. Greater use of mechanization, mineral fertilizers and pesticides, new and better crop varieties, and innovative farming practices keep the food production on increase. Over time, some of these advances have clearly compromised environmental health, including water quality. Agricultural impacts on water resources are

caused by: need for additional water (semi-arid landscapes), use of additional nutrients, use of pesticides and so on.

Even though it is expected that Canada would remain food sufficient country by the end of 21st century, as a part of the global community Canada may need to produce more food to meet the needs of the rest of the world. In this scenario analyses agricultural land conversion rate in Canada is increased by 15% (same as in global analyses) for model utility demonstrations and comparison with global model analyses.

In this scenario the results of simulations are not the same at the regional and global scales. Increase of 15% in land conversion provides for more than 13% increase in food production (Figure 4.39), whereas at the global scale, the increase was around 1%. However, this 15% extra agricultural land and practice requires more water. High availability and low water demand in Canada still make the effect of increased water consumption barely distinguishable (Figure 4.40). However, the water-stress increases around 7% at the end of this century (Figure 4.41), still remaining below the critical threshold level.

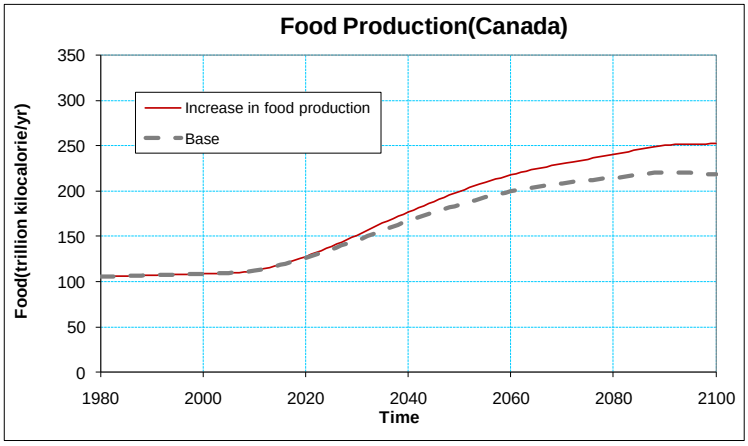

Figure 4.39: Food production (Canada)

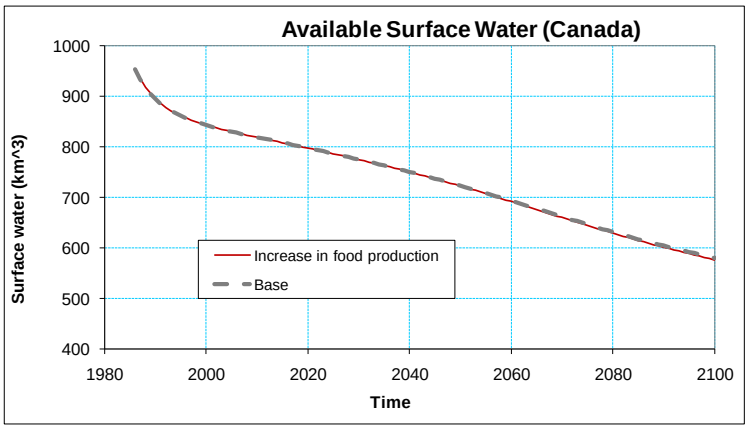

Figure 4.40: Available surface water (Canada)

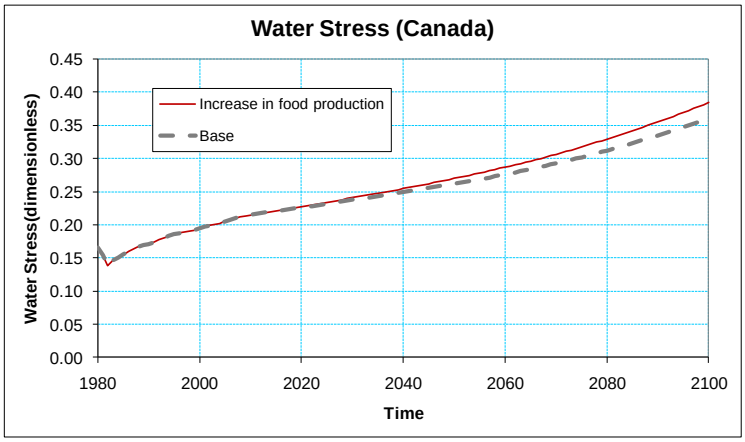

Figure 4.41: Water-stress (Canada)

Freshwater is essential for human survival, healthy ecosystems and sustainable development. Canada as a region has plenty of water resources to support its population. The total population shows slight increase by the end of this century. Surprisingly, the regional model results do not show any population growth (Figure 4.42). This behaviour can be explained by sufficient food production and/or the optimum availability of per capita food-energy. So, further increase in per capita food production does not change the life expectancy in Canada.

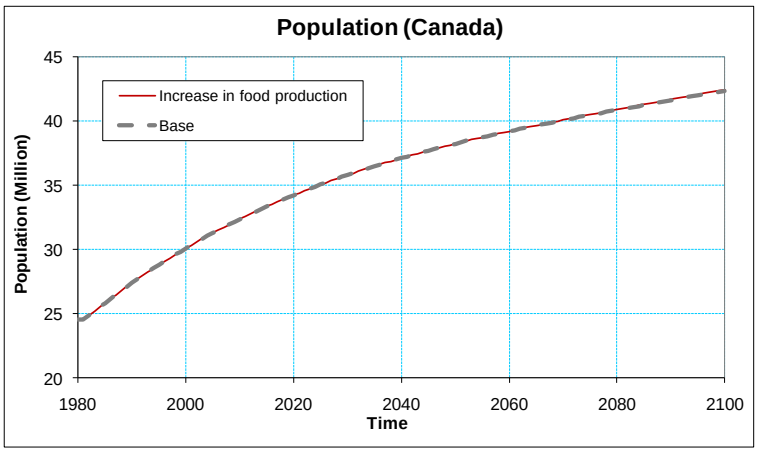

Figure 4.42: Population (Canada)

The total population in Canada remains almost unchanged even with 13% increase in food production. With no change in population, there is no increase in human induced fossil fuel based emissions and GDP. They both remain almost unchanged (Figure 4.43 and Figure 4.44).

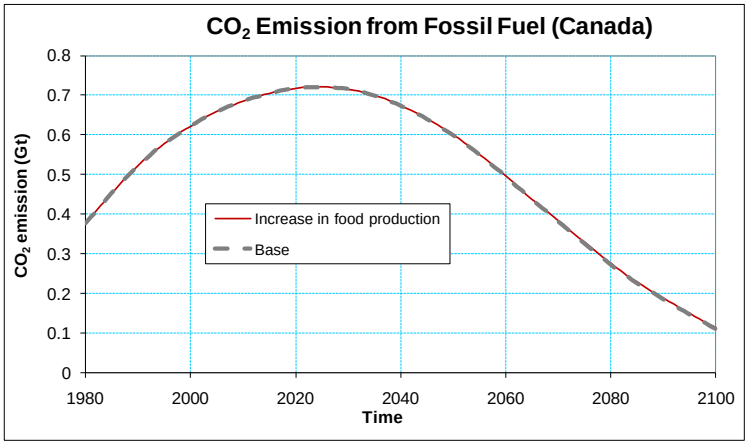

Figure 4.43: CO_2 emission from fossil fuel (Canada)

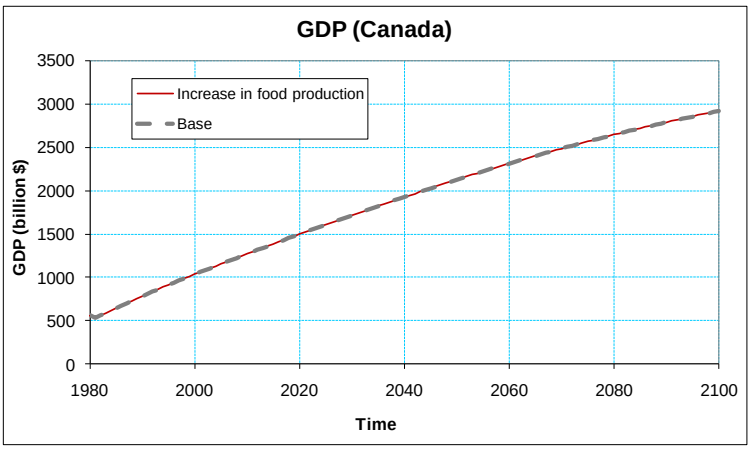

Figure 4.44: GDP (Canada)

4.4 Conclusions

Three different climate change policy scenarios are simulated using global and regional (Canada) versions of the ANEMI version 2 model. Scenarios are either related to emerging problems (shortage in food production, shortage in water availability, etc) or preventive climate change mitigation measures such as emissions reductions. However, the quantitative values used with all three scenarios were arbitrarily selected to investigate performance of the models and help understand better impacts of model structure on the complex system behaviour. The investigated scenarios include:

- Implementation of carbon tax as well as carbon capture and storage technology
- 15% increase in overall water use; and
- 15% increase in agricultural land conversion.

Simulations of the same scenarios are not showing the same results on global and local scales due to the spatial distribution of resources and climate impacts.

The water use increase scenario shows increase in global water-stress to an alarming stage and reduction in the food production. These two unfavourable conditions threaten the current

population growth and demonstrate a small decrease in future population. Contrary, the extra pressure on Canada's water resources couldn't change the population path due to the water-stress level that remains high above the threshold. Changes in GDP, atmospheric CO_2 concentration, and atmospheric temperature are insignificant.

In the land increase scenario, the 15% conversion rate to agricultural land is only affecting food production, approximately 1% increase at the global scale. A closer investigation reviled that the extra agricultural activities (a) add more pressure on already scarce water resources and (b) increase fresh water demand for dilution. The feedback structure of the model restricts the productivity because of water scarcity. On the other hand, food production in Canada increases by 13% due to the added agricultural land. This contrasting value is due to lower level of water stress in Canada. Other related model sectors are showing minor changes. The only visible change is in atmospheric CO_2 concentration, which is contributed by forest clearing/burning required for the development of new agricultural land.

In case of carbon tax scenario, carbon capture and storage technology is introduced. After implementing a moderate tax policy, the model shows a significant reduction in CO_2 emissions from fossil fuel and stabilization of the atmospheric CO_2 concentration. Carbon capture and storage technology can be implemented to lower the atmospheric CO_2 concentration below 500 ppm level. These combined efforts lower the global temperature and sea-level rise when compared to current policy environment. Rest of the model sectors are not significantly affected by this scenario.

The performed analyses are demonstrating model robustness and readiness for the application in investigation of various climate change mitigation and adaptation policy options.

REFERENCES

Akhtar, M. K., S. P. Simonovic, J. Wibe, J. MacGee, and J. Davies, (2011). An integrated system dynamics model for analyzing behaviour of the social-energy-economic-climatic system: User's Manual. *Water Resources Research Report no. 076* Facility for Intelligent Decision Support, Department of Civil and Environmental Engineering, London, Ontario, Canada, 148 pages

Alcamo, J. and T. Henrichs (2002) Critical regions: A model-based estimation of world water resources sensitive to global changes. *Aquatic Sciences*, 64: 352-362.

Alcamo, J., G. J. J. Kreileman, J. C. Bollen, G. J. van den Born, R. Gerlagh, M. S. Krol, A. M. C. Toet and H. J. M. de Vries. (1996).Baseline scenarios of global environmental change. *Global Environmental Change*, 6: 261-303.

Alcamo, J., G. J. J. Kreileman, M. S. Krol and G. Zuidema. (1994). Modeling the global society-biosphere-climate system: Part 1: Model description and testing. *Water, Air and Soil Pollution*, 76: 1-35.

Alcamo, J., P. Döll, T. Henrichs, F. Kaspar, B. Lehner, T. Rösch and S. Siebert. (2003a). Development and testing of the WaterGAP 2 global model of water use and availability. *Hydrologic Sciences Journal*, 48: 317-337.

Alcamo, J., P. Döll, T. Henrichs, F. Kaspar, B. Lehner, T. Rösch and S. Siebert. (2003b). Global estimates of water withdrawals and availability under current and future "business-as-usual" conditions. *Hydrologic Sciences Journal*, 48: 339-348.

AQUASTAT, (2010). FAO's Information System on Water and Agriculture, Food and Agriculture Organization of the Unites Nations. Available fromhttp://www.fao.org/nr/water/aquastat/main /index.stm, Last accessed December 12, 2010.

Arnell, N. W. (1999a). A simple water balance model for the simulation of streamflow over a large geographic domain. *Journal of Hydrology*, 217: 314-335.

Arnell, N. W. (1999b). Climate change and global water resources. *Global Environmental Change*, 9: S31-S49.

Atjay, G. L., P. Ketner and P. Duvigneaud. (1979). Terrestrial primary production and phytomass, in *The Global Carbon Cycle*, edited by B. Bolin, E. T. Degens, S. Kempe and P. Ketner, pp. 129-181, John Wiley and Sons, Chichester, U.K.

Bates, B.C. , Z.W. Kundzewicz, S. Wu and J.P. Palutikof, Eds. (2008). "Climate Change and Water," Technical Paper VI of the Intergovernmental Panel on Climate Change, IPCC Secretariat, Geneva, 210 pp.

Berthelot, M., P. Friedlingstein, P. Ciais, P. Monfray, J. L. Dufresne, H. Le Treut and L. Fairhead, (2002). Global response of the terrestrial biosphere to CO_2 and climate change using a coupled climate-carbon cycle model. *Global Biogeochemical Cycles*, 16(4), 1084, doi:10.1029/2001GB001827.

Brohan, P., J. J. Kennedy, I. Harris, S. F. B. Tett, and P. D. Jones (2006). Uncertainty estimates in regional and global observed temperature changes: A new data set from 1850*, Journal of Geophysical Research,* 111, D12106, doi:10.1029/2005JD006548

Chahine, Moustafa T.,(1992). The Hydrologic Cycle and Its Influence on Climate, Review Article, *Nature* 359: 373 – 380.

Chapagain, AK, Hoekstra, AY, Savenije, HHG, and Gautam, R, 2006, The water footprint of cotton consumption: An assessment of the impact of worldwide consumption of cotton products on the water resources in the cotton producing countries, *Ecological Economics*, vol. 60, no. 1, pp. 186-203.

Clarke, L., J. Edmonds, H. Jacoby, H. Pitcher, J. Reilly, R. Richels, (2007). Scenarios of Greenhouse Gas Emissions and Atmospheric Concentrations. Sub-report 2.1A of Synthesis and Assessment Product 2.1 by the U.S. Climate Change Science Program and the Subcommittee on Global Change Research. Department of Energy, Office of Biological & Environmental Research, Washington, DC., USA, 154 pp.

Cosgrove, W. J. and F. R. Rijsberman. (2000). *World Water Vision: Making Water Everybody's Business*. Earthscan Publications Ltd., London, U.K.

Cox, P. M., R. A. Betts, C. D. Jones, S. A. Spall and I. J. Totterdell. (2000). Acceleration of global warming due to carbon-cycle feedbacks in a coupled climate model. *Nature*, 408: 184-187. doi:10.1038/35041539

Cramer, W., A. Bondeau, F. I. Woodward, I. C. Prentice, R. A. Betts, V. Brovkin, P. M. Cox, V. Fisher, J. A. Foley, A. D. Friend, C. Kucharik, M. R. Lomas, N. Ramankutty, S. Sitch, B. Smith, A. White and C. Young-Molling. (2001). Global response of terrestrial ecosystem structure and function to CO2 and climate change: Results from six dynamic vegetation models. *Global Change Biology*, 7: 357-373.

Cramer, W., D. W. Kicklighter, A. Bondeau, B. Moore, C. Churkina, B. Nemry, A. Ruimy and A. L. Schloss. (1999). Comparing global models of terrestrial net primary productivity (NPP): overview and key results. *Global Change Biology*, 5(Suppl. 1): 1-15.

Dabrowski, J.M., K. Murray, P.J. Ashton, J.J. Leaner (2009). Agricultural impacts on water quality and implications for virtual water trading decisions. *Ecological Economics*, 68: 1074-1082.

Dasgupta, S., B. Laplante, C. Meisner, D. Wheeler, and J. Yan, (2009). The impact of sea level rise on developing countries: a comparative analysis, *Climatic Change,* 93:379–388.

Davies, E. G. R. (2007). Modelling Feedback in the Society-Biosphere-Climate System. Doctoral Dissertation. Department of Civil and Environmental Engineering, the University of Western Ontario, London, Ontario, Canada.

Davies, E. G. R. and S. P. Simonovic, (2008). An Integrated System Dynamics Model for Analyzing Behaviour of the Social-Economic-Climatic System: Model Description and Model Use Guide. *Water Resources Research Report no. 059*, Facility for Intelligent Decision Support, Department of Civil and Environmental Engineering, London, Ontario, Canada, 233 pages. ISBN: (print) 978-0-7714-2679-7; (online) 978-0-7714-2680-3.

Davies, E. G. R. and S. P. Simonovic, (2009). Energy Sector for the Integrated System Dynamics Model for Analyzing Behaviour of the Social-Economic-Climatic Model. *Water Resources Research Report no. 063*, Facility for Intelligent Decision Support, Department of Civil and Environmental Engineering, London, Ontario, Canada, 191 pages. ISBN: (print) 978-0-7714-2712-1; (online) 978-0-7714-2713-8.

Davies, E. G. R., and S. P. Simonovic, (2011) Global water resources modeling with an integrated model of the social-economic-environmental system. *Advances in Water Resources,* 34(6): 684-700.

Davies, Evan G. R. and S. P. Simonovic, (2010). ANEMI: A new model for integrated assessment of global change. *Interdisciplinary Environmental Review,* 11(2/3): 127-161.

Döll, P. (2002). Impact of climate change and variability on irrigation requirements: A global perspective. *Climatic Change*, 54: 269-293.

Energy Information Administration (EIA) (2006). Official Energy Statistics from the U.S. Government. U.S. Department of Energy, Washington, D.C. Available at http://www.eia.doe.gov/emeu/international/contents.html, last accessed Oct. 21, 2010.

Energy Information Administration (EIA) (2008). Carbon Dioxide Emission Factors (1980 -2006). U.S. Department of Energy, Washington, D.C. Available at http://www.eia.doe.gov/oiaf/1605/ggrpt/excel/CO2_coeff.xls, last accessed July, 2011.

Falkenmark, M. (2005). Water usability degradation – Economist wisdom or societal madness? *Water International,* 30: 136-146.

Falkowski, P., R. J. Scholes, E. Boyle, J. Canadell, D. Canfield, J. Elser, , N. Gruber, K. Hibbard, P. Hoegberg, S. Linder, F.T. Mackenzie, B. Moore III, T. Pedersen, Y. Rosenthal, S. Seitzinger, V. Smetacek and W. Steffen, (2000). The global carbon cycle: A test of our knowledge of earth as a system. *Science,* 290: 291-296

FAO (2009). Global agriculture towards 2050, High Level Expert Forum - How to Feed the World in 2050 Office of the Director, Agricultural Development Economics Division Economic and Social Development Department, Rome, Italy. Available from http://www.fao.org/fileadmin/templates/wsfs/docs/Issues_papers/HLEF2050_Global_Agriculture.pdf, Last accessed May.30, 2011.

Fauresa, J. M., J. Hoogeveena, and J. Bruinsmab (2003). "The FAO Irrigated Area Forecast for 2030", FAO, Rome, Italy. Available from http://www.anafide.org/doc/HTE%20125/125-3.pdf, Last accessed May.30, 2011.

Fiddaman, T. S. (1997). Feedback complexity in integrated climate-economy models. Doctoral Thesis. Alfred P. Sloan School of Management, Massachusetts Institute of Technology, Boston, Massachusetts, U.S.A.

Fiddaman, T. S. (2002). Exploring policy options with a behavioral climate-economy model. *System Dynamics Review*, 18: 243-267.

Forster, P. M. d. F. and J. M. Gregory. (2006). The climate sensitivity and its components diagnosed from Earth radiation, *Journal of Climate*, 19: 39-52.

Fujino, J., R. Nair, M. Kainuma, T. Masui, Y. Matsuoka, (2006). Multi-gas mitigation analysis on stabilization scenarios using AIM global model. Multigas Mitigation and Climate Policy. *The Energy Journal*, Special Issue #3.

Geider, R. J., E. H. Delucia, P. G. Falkowski, A. C. Finzi, J. P. Grime, J. Grace, T. M. Kana, J. La Roche, S. P. Long, B. A. Osborne, T. Platt, I. C. Prentice, J. A. Raven, W. H. Schlesinger, V. Smetacek, V. Stuart, S. Satyendranath, R. B. Thomas, T. C. Vogelmann, P. Williams and F. I. Woodward. (2001). Primary productivity of planet Earth: Biological determinants and physical constraints in terrestrial and aquatic habitats. *Global Change Biology*, 7: 849-882.

Gleick, P. H. (2000a). The changing water paradigm: A look at twenty-first century water resources development. *Water International*, 25: 127-138.

Gleick, P. H. (2000b). *The world's water: the biennial report on freshwater resources*. Island Press, Washington, D.C., U.S.A.

Goldewijk, K. K., J. G. van Minnen, G. J. J. Kreileman, M. Vloedbeld and R. Leemans. (1994). Simulating the carbon flux between the terrestrial environment and the atmosphere. *Water, Air and Soil Pollution*, 76: 199-230.

Goudriaan, J. and P. Ketner. (1984). A simulation study for the global carbon cycle, including man's impact on the biosphere. *Climatic Change*, 6: 167-192.

Greenhouse Gas Inventories Programme, Eggleston H.S., Buendia L., Miwa K., Ngara T., and Tanabe K. (eds). Published: IGES, Japan.

Hansen, J., D. Johnson, A. Lacis, S. Lebedeff, P. Lee, D. Rind, and G. Russell,(1981). Climate impact of increasing atmospheric carbon dioxide. *Science*, 213: 957-966, doi:10.1126/science.213.4511.957.

Hansen, J., R. Ruedy, J. Glascoe, and Mki. Sato, (1999): GISS analysis of surface temperature change. *Journal of Geophysical Research*, 104(D24): 30997-31022.

Hansen, J.E., R. Ruedy, Mki. Sato, M. Imhoff, W. Lawrence, D. Easterling, T. Peterson, and T. Karl, (2001). A closer look at United States and global surface temperature change. *Journal of Geophysical Research*, 106: 23947-23963.

Hansen, M.C., and B. Reed, (2000). A comparison of the IGBP DISCover and University of Maryland 1km global land-cover products, *International Journal of Remote Sensing*, 21:1365–1373.

Harms, A. A., and T. H. Campbell, (1967). An extension to the Thomas- Fiering model for the sequential generation of stream flow, *Water Resour. Res*., 3(3): 653–661.

Harvey, L. D. D. (2000). Box models of the terrestrial biosphere, in *The Carbon Cycle*, edited by T. M. L. Wigley and D. S. Schimel, pp. 238-247, Cambridge University Press, Cambridge, U.K.

Harvey, L. D. D. and S. H. Schneider. (1985a). Transient climate response to external forcing on 10^0–10^4 year time scales. Part I: Experiments with globally averaged, coupled, atmosphere and ocean energy balance models. *Journal of Geophysical Research*, 90(D1): 2191-2205.

Harvey, L. D. D. and S. H. Schneider. (1985b). Transient Climate Response to External Forcing on 10^0–10^4 Year Time Scales. Part 2: Sensitivity Experiments With a Seasonal, Hemispherically Averaged, Coupled Atmosphere, Land, and Ocean Energy Balance Model. *Journal of Geophysical Research*, 90(D1): 2207–2222.

Harvey, L. D. D. and Z. Huang. (2001). A quasi-one-dimensional coupled climate-change carbon-cycle model 1. Description and behaviour of the climate component. *Journal of Geophysical Research*, 106(C10): 22339-22353.

Hastings, D.A. and P.K. Dunbar, (1998). Development and assessment of the Global Land One-km Base Elevation Digital Elevation Model (GLOBE). International Society of Photogrammetry and Remote Sensing, Archives, 32: 218-221.

Hay, L., G. McCabe Jr., D. Wolock, and M. Ayers (1992). Use of weather types to disaggregate general circulation model predictions, *Journal of Geophysical Research*, 97(D3): 2781-2790.

Hijioka, Y., Y. Matsuoka, H. Nishimoto, M. Masui, and M. Kainuma, (2008). Global GHG emissions scenarios under GHG concentration stabilization targets. *Journal of Global Environmental Engineering,* 13: 97-108.

Hoekstra, A. Y., A. H. W. Beusen, H. B. M. Hilderink and M. B. A. van Asselt. (1997). Water in crisis?, in *Perspectives on Global Change: The TARGETS Approach*, edited by J. Rotmans and B. de Vries, pp. 291-317. Cambridge University Press, Cambridge, U.K.

Hoffert, M. I., A. J. Callegari and C. T. Hsieh (1981). A box-diffusion carbon dioxide model with upwelling, polar bottom water formation and a marine biosphere, in *Carbon Cycle Modelling*, edited by B. Bolin, pp. 287-305. John Wiley and Sons, Chichester, U.K.

Houghton, J. T., Y. Ding, D. J. Griggs, M. Noguer, P. J. van der Linden, X. Dai, K. Maskell and C. A. Johnson. (2001). Climate Change 2001: The Scientific Basis. Contribution of Working Group I to the Third Assessment Report of the Intergovernmental Panel on Climate Change. Cambridge University Press, Cambridge, U.K.

Houghton, J.T., L.G. Meira Filho, J. Bruce, Hoesung Lee, B. A. Callander, E. Haites, N. Harris, and K. Maskell (eds.), (1995). Climate Change 1994: Radiative Forcing of Climate Change and an Evaluation of the IPCC IS92 Emissions Scenarios. Cambridge University Press, Cambridge.

Huntington, T. G. (2006). Evidence for intensification of the global water cycle: Review and synthesis. *Journal of Hydrology*, 319: 83-95.

IGBP Terrestrial Carbon Working Group, (1998). The terrestrial carbon cycle: implications for the Kyoto Protocol. *Science*, 280: 1393–1394.

Intergovernmental Panel on Climate Change (IPCC) (2008). Database on greenhouse gas emission factors. National Greenhouse Gas Inventories Programme, Institute for Global Environmental Strategies, Hayama, Kanagawa, Japan. Available at http://www.ipcc-nggip.iges.or.jp/efdb/main.php, last accessed Aug. 10, 2011.

International Hydrologic Programme (IHP) (2000). World Freshwater Resources, CD-ROM prepared by I.A. Shiklomanov, International Hydrologic Programme, UNESCO International, 25: 11-32.

IPCC (2006), 2006 IPCC Guidelines for National Greenhouse Gas Inventories, Prepared by the National

IPCC, (2000). *Emissions Scenarios - A Special Report of Working Group III of the Intergovernmental Panel on Climate Change* [N. Nakicenovic and R. Swart (eds.)], Cambridge: Cambridge University Press, 599 pp.

IPCC, (2007a). Climate Change 2007: The Physical Science Basis. Contribution of Working Group I to the Fourth Assessment Report of the Intergovernmental Panel on Climate Change [Solomon, S., D. Qin, M. Manning, Z. Chen, M. Marquis, K.B. Averyt, M. Tignor and H.L. Miller (eds.)]. Cambridge University Press, Cambridge, United Kingdom and New York, NY, USA, 996 pp.

IPCC, (2007b). Summary for Policymakers. In: *Climate Change 2007: Impacts, Adaptation and Vulnerability. Contribution of Working Group II to the Fourth Assessment Report of the Intergovernmental Panel on Climate Change,* M.L. Parry, O.F. Canziani, J.P. Palutikof, P.J. van der Linden and C.E. Hanson, Eds., Cambridge University Press, Cambridge, UK, 7-22.

IPCC, (2007c). Climate Change 2007: Synthesis Report. Contribution of Working Groups I, II and III to the Fourth Assessment Report of the Intergovernmental Panel on Climate Change [Core Writing Team, Pachauri, R.K and Reisinger, A. (eds.)]. IPCC, Geneva, Switzerland, 104 pp.

J.A. Renwick, M. Rusticucci, B. Soden and P. Zhai, (2007). Observations: Surface and Atmospheric Climate Change. In: *Climate Change 2007: The Physical Science Basis. Contribution of Working Group I to the Fourth Assessment Report of the Intergovernmental Panel on Climate Change* [Solomon, S., D. Qin, M. Manning, Z. Chen, M. Marquis, K.B. Averyt, M. Tignor and H.L. Miller (eds.)]. Cambridge University Press, Cambridge, United Kingdom and New York, NY, USA.

Joos, F., J. C. Orr, and U. Siegenthaler. (1997). Ocean carbon transport in a box-diffusion versus a general circulation model. *Journal of Geophysical Research*, 102(C6): 12367-12388.

Keyfutz, N., W. Flieger , (1971). *Population: facts and methods of demography*. W.H. Freeman, San Franciso:

Kundzewicz, Z.W., L.J. Mata, N.W. Arnell, P. Döll, P. Kabat, B. Jiménez, K.A. Miller, T. Oki, Z. Sen and I.A. Shiklomanov, (2007): Freshwater resources and their management. Climate Change 2007: Impacts, Adaptation and Vulnerability. Contribution of Working Group II to the *Fourth Assessment Report of the Intergovernmental Panel on Climate Change*, M.L. Parry, O.F. Canziani, J.P. Palutikof, P.J. van der Linden and C.E. Hanson, Eds., Cambridge University Press, Cambridge, UK, 173-210.

Kusukawa, A., (1967). Social and Economic Factors in Mortality in Developing Countries. In United Nations, Department of Economic and Social Affairs, *Proceedings of the World Population Conference* 2:337. New York

Lambin, E. F., B. L. Turner, H. J. Geist, S. B. Agbola, A. Angelsen, J. W. Bruce, O. T. Coomes, R. Dirzo, G. Fischer, C. Folke, P. S. George, K. Homewood, J. Imbernon, R. Leemans, X. B. Li, E. F. Moran, M. Mortimore, P. S. Ramakrishnan, J. F. Richards, H. Skanes, W. Steffen, G. D. Stone, U. Svedin, T. A. Veldkamp, C. Vogel and J. C. Xu. (2001). The causes of land-use and land-cover change: moving beyond the myths. *Global Environmental Change*, 11: 261-269.

Lane, W. L., (1979). *Applied stochastic techniques (LAST computer package), user manual*. Division of Planning Technical Services, Bureau of Reclamation, Denver, Colorado.

Larryn, W. Diamond, and Nikolay N. Akinfiev, (2003). Solubility of CO_2 in water from -1.5 to 100 °C and from 0.1 to 100 MPa: evaluation of literature data and thermodynamic modelling*, Fluid Phase Equilibria*, 208 (1-2): 265-290.

Lowe, P. R. (1977). An approximating polynomial for the computation of saturation vapour pressure. *Journal of Applied Meteorology*, 16: 100-103.

Manabe, S., and R. J. Stouffer, (1980). Sensitivity of a global climate model to an increase of CO_2 concentration in the atmosphere. *Journal of Geophysical Research*, 85: 5529-5554.

Marland, G., T. A. Boden and R. J. Andres (2008). Global, Regional, and National CO_2 Emissions. In *Trends: A Compendium of Data on Global Change*. Carbon Dioxide Information Analysis Center, Oak Ridge National Laboratory, U.S. Department of Energy, Oak Ridge , Tenn., U.S.A.

Math Works,(2011). MATLAB® 7, Getting Started Guide (on line). The Math Works, Inc., Natick, MA. Available from http://www.mathworks.com/help/pdf_doc/matlab/getstart.pdf. Last accessed June 20, 2011.

McGuffie, K. and A. Henderson-Sellers. (2005). *A Climate Modelling Primer*, 3rd Edition. John Wiley and Sons, Ltd., Chichester, U.K.

Meadows, D. H., D. Meadows and J. Randers, (1992). *Beyond the Limits: Confronting Global Collapse, Envisioning a Sustainable Future.* Chelsea Green Publishing Company, Mills, Vermont, U.S.A.

Meadows, Dennis L., William W. Behrens, Donella H. Meadows, Roger F. Naill, Jorgen Randers, and Erich K. O. Zahn, (1974). *Dynamics of Growth in a Finite World*. Wright-Allen Press, Inc. Cambrigde, Massachusetts.

Meehl, G. A., T. F. Stocker, W. D. Collins, P. Friedlingstein, A. T. Gaye, J. M. Gregory, A. Kitoh, R. Knutti, J. M. Murphy, A. Noda, S. C. B. Raper, I. G. Watterson, A. J. Weaver and Z.-C. Zhao. (2007). Global climate projections, in *Climate Change 2007: The Physical Science Basis. Contribution of Working Group I to the Fourth Assessment Report of the Intergovernmental Panel on Climate Change*, edited by S. Solomon, D. Qin, M. Manning, Z. Chen, M. Marquis, K. B. Averyt, M. Tignor and H. L. Miller, pp. 747-846. Cambridge University Press, Cambridge, U.K.

Mejia, J.M., and J. Rousselle (1976). Disaggregation Models in Hydrology Revisited, *Water Resources Research*, *12(2): 185–186*

Metcalf and Eddy Inc. (2003). *Wastewater engineering: treatment and reuse*. 4th Edition. McGraw-Hill, Boston.

Meyer, R.F., E. D. Attanasi, and P. A.Freeman, (2007). Heavy oil and natural bitumen resources in geological basins of the world: U.S. Geological Survey Open-File Report 2007-1084, available online at http://pubs.usgs.gov/of/2007/1084/.

Microsoft, (1998). Guide to Visual Studio 6.0(professional edition), Visual Studio: Developing for Windows and the Web. Microsoft Corporation, USA.

Miller, G. W. (2006). Integrated Concepts in Water Reuse: Managing Global Water Needs. *Desalination*, 187: 65-75.

Moss,R., Mustafa Babiker, Sander Brinkman, Eduardo Calvo, Tim Carter, Jae Edmonds , Ismail Elgizouli, Seita Emori, Lin Erda, Kathy Hibbard, Roger Jones, Mikiko Kainuma, Jessica Kelleher, Jean Francois Lamarque, Martin Manning, Ben Matthews, Jerry Meehl, Leo Meyer, John Mitchell, Nebojsa Nakicenovic, Brian O'Neill, Ramon Pichs, Keywan Riahi, Steven Rose,Paul Runci, Ron Stouffer, Detlef van Vuuren, John Weyant, Tom Wilbanks, Jean Pascal van Ypersele, and Monika Zurek, (2008). *Towards New Scenarios for Analysis of Emissions, Climate Change, Impacts, and Response Strategies*. Technical Summary. Intergovernmental Panel on Climate Change, Geneva, 132 pp.

Neilsen, D., S. Smith, W. Koch, G. Frank, J. Hall and P. Parchomchuk, (2001). Impact of climate change on crop water demand and crop suitability in the Okanagan Valley, British Columbia. Technical Bulletin 01-15. Pacific Agri-Food Research Centre, Summerland, BC 32 p. Available from http://www.obwb.ca/obwrid/docs/005_2001_Climate_Change_on_Crop_Water.pdf, Last accessed July.30, 2011.

Nicholls, R.J., (2002). Analysis of global impacts of sea-level rise: A case study of flooding. *Physics and Chemistry of the Earth*, 27:1455–1466.

Nicholls, R.J., (2004). Coastal flooding and wetland loss in the 21st century: Changes under the SRES climate and socioeconomic scenarios, *Global Environmental Change*, 14:69–86.

Nicholls, R.J., and R.S.J. Tol, (2006). Impacts and responses to sea-level rise: A global analysis of the SRES scenarios over the twenty-first century, *Philosophical Transactions of the Royal Society A*, 364:1073–1095.

Nicholls, R.J., F.M.J. Hoozemans, and M. Marchand, (1999). Increasing flood risk and wetland losses due to global sea-level rise: regional and global analyses, *Global Environmental Change*, 9:S69–S87.

Nordhaus W. D. (2007). *The Challenge of Global Warming: Economic Models and Environmental Policy*. New Haven, CT: Yale University. Available at http://nordhaus.econ.yale.edu/dice_mss_072407_all.pdf, last accessed July 10, 2011.

Nordhaus, W. D. (1994). *Managing the Global Commons: the economics of climate change*. Cambridge, MA: MIT Press.

Nordhaus, W. D. and J. Boyer, (2000). *Warming the world: Economic models of global warming*. The MIT Press, Cambridge, Massachusetts, U.S.A.

NRC (National Research Council (NRC), (2006). *Surface Temperature Reconstructions for the Last 2,000 Years*. National Academy Press, Washington, DC.

Pacific Institute, (2007). *World's Water 2006-2007: The Biennial Report on Freshwater Resources*. Island Press, Washington

Pacific Institute, (2009). *The World's Water 2008-2009: The Biennial Report on Freshwater Resources*. Island Press, Washington

Popovich, C.J., S. P. Simonovic and G. A. McBean (2010). "Use of an Integrated System Dynamics Model for Analyzing Behaviour of the Social-Economic-Climatic System in Policy Development". *Water Resources Research Report no. 067*, Facility for Intelligent Decision Support, Department of Civil and Environmental Engineering, The University of Western Ontario, 37 pages. ISBN: (print) 978-0-7714-2838-8; (online) 978-0-7714-2839-5.

Postel, S., (1999). *Pillar of Sand: can the irrigation miracle last?* W. W. Norton, New York, U.S.A.

Quillet, A., C. Peng, and M. Garneau, (2010). Toward dynamic global vegetation models for simulating vegetation–climate interactions and feedbacks: recent developments, limitations, and future challenges. *Environmental Reviews*, 18: 333-353

Rahmstorf Stefan, (2007). A Semi-Empirical Approach to Projecting Future Sea-Level Rise, *Science*, 315: 368-370.

Riahi, K., A. Grübler, and N. Nakicenovic, (2007). "Scenarios of long-term socio-economic and environmental development under climate stabilization". *Technological Forecasting and Social Change*, 74(7): 887-935

Rost, S., D. Gerten, A. Bondeau, W. Luncht, J. Rohwer, and S. Schaphoff, (2008), Agricultural green and blue water consumption and its influence on the global water system, *Water Resour. Res*., 44, W09405, doi:10.1029/2007WR006331.

Salas, J.D., J.W.Delleur, V. Yevjevich and W.L.Lane, (2009). *Applied Modelling of Hydrologic Time Series*. Water Resources Publications, LLC. Michigan, USA

Schimel, D., I.G. Enting, M. Heimann, T.M.L. Wigley, D. Raynaud, D. Alves, and U. Siegenthaler, (1994). CO_2 and the Carbon Cycle. In: J.T. Houghton , L.G.M. Filho, J. Bruce, H. Lee, B.A. Callander, E. Haites, N. Harris, and K. Maskell (eds.). *Climate Change 1994: Radiative Forcing of Climate Change and An Evaluation of the IPCC IS92 Emission Scenarios*. Cambridge University Press, Cambridge, UK.

Schneider, S, J. Sarukhan, J. Adejuwon , C. Azar, W. Baethgen, C. Hope, R. Moss, N. Leary, R. Richels, J.P. van Ypersele, (2001). Overview of Impacts, Adaptation, and Vulnerability to Climate Change. In*: Climate Change 2001: Impacts, Adaptation and Vulnerability. Contribution of Working Group II to the Third Assessment Report of the Intergovernmental Panel on Climate Change.* Cambridge University Press, Cambridge, United Kingdom and New York, NY, USA.

Shiklomanov, I. A. and J. Rodda. (2003). *World water resources at the beginning of the 21st century*. Cambridge University Press, Cambridge, U.K.

Shiklomanov, I. A., (2000). Appraisal and assessment of world water resources. *Water International*, 25(1): 11-32.

Siegenthaler, U. and F. Joos., (1992). Use of a simple model for studying oceanic tracer distributions and the global carbon cycle*. Tellus*, 44B: 186-207.

Simonovic, S. P., (2002). World water dynamics: Global modeling of water resources, *Journal of Environmental Management*, 66(3): 249-267.

Smith, S.J. and T.M.L. Wigley, (2006). Multi-Gas Forcing Stabilization with the MiniCAM. *Energy Journal*, 27(Special Issue: 3): 373-391.

Smith, T. M. and R. W. Reynolds, (2005). A global merged land-air-sea surface temperature reconstruction based on historical observations (1880-1997), *Journal of Climate*, 18: 2021-2036.

Stern, Nicholas (2007). *The Economics of Climate Change: The Stern Review*. Cambridge, UK: Cambridge University Press. Available from http://www.hm-treasury.gov.uk/independent_reviews/stern_review_economics_climate_change/sternreview_index.cfm, l*ast accessed August 12, 2011.*

Thompson, S. L., and S. H. Schneider, (1979). A seasonal zonal energy balance climate model with an interactive lower layer, *Journal of Geophysical Research*, 84: 2401-2414.

Trenberth, K.E., P.D. Jones, P. Ambenje, R. Bojariu, D. Easterling, A. Klein Tank, D. Parker, F. Rahimzadeh, United Nations Department of Economic and Social Affairs(UNESA), (2006). World Population Prospects: the 2006 Revision Population Database (on line), UNESA Population Division, New York, New York, U.S.A. Available from http://esa.un.org/unpp. Last accessed Nov. 1, 2007.

United Nations Department of Economic and Social Affairs, Population Division (DESA), (2011). World Population Prospects: The 2010 Revision, CD-ROM Edition. Available from http://esa.un.org/unpd/wpp/Excel-Data/population.htm, last accessed July 10, 2011.

van Vuuren, D., M. den Elzen, P. Lucas, B. Eickhout, B. Strengers, B. van Ruijven, S. Wonink, R. van Houdt, (2007). Stabilizing greenhouse gas concentrations at low levels: an assessment of reduction strategies and costs. *Climatic Change*, 81(2): 119-159

van Vuuren, D.P., B. Eickhout, P.L. Lucas, and M.G.J. den Elzen, (2006). Long-term multi-gas scenarios to stabilise radiative forcing - Exploring costs and benefits within an integrated assessment framework. *Energy Journal*, 27(Special Issue: 3): 201-233.

Vassolo, S. and P. Döll. (2005). Global-scale gridded estimates of thermoelectric power and manufacturing water use, *Water Resources Research*, 41, W04010, doi:10.1029/2004WR003360.

Veldkamp, A. and E. F. Lambin. (2001). Predicting land-use change. *Agriculture, Ecosystems and Environment*, 85: 1-6.

Ventana Systems. (2010a). Vensim DSS Software (on line). Ventana Systems, Inc., Harvard, Massachusetts, U.S.A. Available from http://www.vensim.com/documentation.html. Last accessed April.20, 2011.

Ventana Systems. (2010b). Vensim Referenc e Manual (on line). Ventana Systems, Inc., Harvard, Massachusetts, U.S.A. Available from http://www.vensim.com/documentation.html, last accessed January 12, 2011.

Vinnikov, K. Y., N. C. Grody, A. Robock, R. J. Stouffer, P. D. Jones and M. D. Goldber,. (2006). Temperature trends at the surface and in the troposphere. *Journal of Geophysical Research*, 111, D03106, doi:10.1029/2005JD006392.

Vörösmarty, C. J. ,(2002a). Global change, the water cycle, and our search for Mauna Loa. *Hydrologic Processes*, 16: 135-139.

Vörösmarty, C. J., (2002b). Global water assessment and potential contributions from Earth Systems Science. *Aquatic Sciences*, 64: 328-351.

Vörösmarty, C. J., P. Green, J. Salisbury and R. B. Lammers, (2000). Global water resources: Vulnerability from climate change and population growth. *Science*, 289: 284-288.

Watson, R. T., I. R. Noble, B. Bolin, N. H. Ravindranath, D. J. Verardo and D. J. Dokken, (2000). *Land Use, Land-Use Change, and Forestry*. Cambridge University Press, Cambridge, U.K.

William D. Williams, (2001). Lakes and Reservoirs, the Watershed: Water from the Mountains into the Sea. Volume: 2, United Nations Environment Programme, Division of Technology, Industry and Economics. Available from http://www.unep.or.jp/ietc/publications/short_series/lakereservoirs-2/2.ASP, last accessed July12, 2011.

Wise, MA, KV Calvin, AM Thomson, LE Clarke, B Bond-Lamberty, RD Sands, SJ Smith, AC Janetos, JA Edmond, (2009). Implications of Limiting CO2 Concentrations for Land Use and Energy. *Science*. 324:1183-1186.

Xingong Li, Rex J. Rowley, John C. Kostelnick, David Braaten, Joshua Meisel, and Kalonie Hulbu, (2009). GIS Analysis of Global Impacts from Sea Level Rise, *Photogrammetric Engineering & Remote Sensing*, 75(7): 807–818

APPENDIX A: PREVIOUS REPORTS IN THE SERIES

ISSN: (print) 1913-3200; (online) 1913-3219

(1) Slobodan P. Simonovic (2001). Assessment of the Impact of Climate Variability and Change on the Reliability, Resiliency and Vulnerability of Complex Flood Protection Systems. Water Resources Research Report no. 038, Facility for Intelligent Decision Support, Department of Civil and Environmental Engineering, London, Ontario, Canada, 91 pages. ISBN: (print) 978-0-7714-2606-3; (online) 978-0-7714-2607-0.

(2) Predrag Prodanovic (2001). Fuzzy Set Ranking Methods and Multiple Expert Decision Making. Water Resources Research Report no. 039, Facility for Intelligent Decision Support, Department of Civil and Environmental Engineering, London, Ontario, Canada, 68 pages. ISBN: (print) 978-0-7714-2608-7; (online) 978-0-7714-2609-4.

(3) Nirupama and Slobodan P. Simonovic (2002). Role of Remote Sensing in Disaster Management. Water Resources Research Report no. 040, Facility for Intelligent Decision Support, Department of Civil and Environmental Engineering, London, Ontario, Canada, 107 pages. ISBN: (print) 978-0-7714-2610-0; (online) 978-0-7714- 2611-7.

(4) Taslima Akter and Slobodan P. Simonovic (2002). A General Overview of Multiobjective Multiple-Participant Decision Making for Flood Management. Water Resources Research Report no. 041, Facility for Intelligent Decision Support, Department of Civil and Environmental Engineering, London, Ontario, Canada, 65 pages. ISBN: (print) 978-0-7714-2612-4; (online) 978-0-7714-2613-1.

(5) Nirupama and Slobodan P. Simonovic (2002). A Spatial Fuzzy Compromise Approach for Flood Disaster Management. Water Resources Research Report no. 042, Facility for Intelligent Decision Support, Department of Civil and Environmental Engineering, London, Ontario, Canada, 138 pages. ISBN: (print) 978-0-7714-2614-8; (online) 978-0-7714-2615-5.

(6) K. D. W. Nandalal and Slobodan P. Simonovic (2002). State-of-the-Art Report on Systems Analysis Methods for Resolution of Conflicts in Water Resources Management. Water Resources Research Report no. 043, Facility for Intelligent Decision Support, Department of Civil and Environmental Engineering, London, Ontario, Canada, 216 pages. ISBN: (print) 978-0-7714-2616-2; (online) 978-0-7714-2617-9.

(7) K. D. W. Nandalal and Slobodan P. Simonovic (2003). Conflict Resolution Support System – A Software for the Resolution of Conflicts in Water Resource Management. Water Resources Research Report no. 044, Facility for Intelligent Decision Support, Department of Civil and Environmental Engineering, London, Ontario, Canada, 144 pages. ISBN: (print) 978-0-7714-2618-6; (online) 978-0-7714-2619-3.

(8) Ibrahim El-Baroudy and Slobodan P. Simonovic (2003). New Fuzzy Performance Indices for Reliability Analysis of Water Supply Systems. Water Resources Research Report no. 045, Facility for Intelligent Decision Support, Department of Civil and Environmental Engineering, London, Ontario, Canada, 90 pages. ISBN: (print) 978-0-7714-2620-9; (online) 978-0-7714- 2621-6.

(9) Juraj Cunderlik (2003). Hydrologic Model Selection for the CFCAS Project: Assessment of Water Resources Risk and Vulnerability to Changing Climatic Conditions. Water Resources Research Report no. 046, Facility for Intelligent Decision Support, Department of Civil and Environmental Engineering, London, Ontario, Canada, 40 pages. ISBN: (print) 978-0-7714- 2622-3; (online) 978-0-7714- 2623-0.

(10) Juraj Cunderlik and Slobodan P. Simonovic (2004). Selection of Calibration and Verification Data for the HEC-HMS Hydrologic Model. Water Resources Research Report no. 047, Facility for Intelligent Decision Support, Department of Civil and Environmental Engineering, London, Ontario, Canada, 29 pages. ISBN: (print) 978-0-7714-2624-7; (online) 978-0-7714-2625-4.

(11) Juraj Cunderlik and Slobodan P. Simonovic (2004). Calibration, Verification and Sensitivity Analysis of the HEC-HMS Hydrologic Model. Water Resources Research Report no. 048, Facility for Intelligent Decision Support, Department of Civil and Environmental Engineering, London, Ontario, Canada, 113 pages. ISBN: (print) 978- 0-7714-2626-1; (online) 978-0-7714- 2627-8.

(12) Predrag Prodanovic and Slobodan P. Simonovic (2004). Generation of Synthetic Design Storms for the Upper Thames River basin. Water Resources Research Report no. 049, Facility for Intelligent Decision Support, Department of Civil and Environmental Engineering, London, Ontario, Canada, 20 pages. ISBN: (print) 978- 0-7714-2628-5; (online) 978-0-7714-2629-2.

(13) Ibrahim El-Baroudy and Slobodan P. Simonovic (2005). Application of the Fuzzy Performance Indices to the City of London Water Supply System. Water Resources Research Report no. 050, Facility for Intelligent Decision Support, Department of Civil and Environmental Engineering, London, Ontario, Canada, 137 pages. ISBN: (print) 978-0-7714-2630-8; (online) 978-0-7714-2631-5.

(14) Ibrahim El-Baroudy and Slobodan P. Simonovic (2006). A Decision Support System for Integrated Risk Management. Water Resources Research Report no. 051, Facility for Intelligent Decision Support, Department of Civil and Environmental Engineering, London, Ontario, Canada, 146 pages. ISBN: (print) 978-0-7714-2632-2; (online) 978-0-7714-2633-9.

(15) Predrag Prodanovic and Slobodan P. Simonovic (2006). Inverse Flood Risk Modelling of The Upper Thames River Basin. Water Resources Research Report no. 052, Facility for Intelligent Decision Support, Department of Civil and Environmental Engineering, London, Ontario, Canada, 163 pages. ISBN: (print) 978-0-7714-2634-6; (online) 978-0-7714-2635-3.

(16) Predrag Prodanovic and Slobodan P. Simonovic (2006). Inverse Drought Risk Modelling of The Upper Thames River Basin. Water Resources Research Report no. 053, Facility for Intelligent Decision Support, Department of Civil and Environmental Engineering, London, Ontario, Canada, 252 pages. ISBN: (print) 978-0-7714-2636-0; (online) 978-0-7714-2637-7.

(17) Predrag Prodanovic and Slobodan P. Simonovic (2007). Dynamic Feedback Coupling of Continuous Hydrologic and Socio-Economic Model Components of the Upper Thames River Basin. Water Resources Research Report no. 054, Facility for Intelligent Decision Support, Department of Civil and Environmental Engineering, London, Ontario, Canada, 437 pages. ISBN: (print) 978-0-7714-2638-4; (online) 978-0-7714-2639-1.

(18) Subhankar Karmakar and Slobodan P. Simonovic (2007). Flood Frequency Analysis Using Copula with Mixed Marginal Distributions. Water Resources Research Report no. 055, Facility for Intelligent Decision Support, Department of Civil and Environmental Engineering, London, Ontario, Canada, 144 pages. ISBN: (print) 978-0-7714-2658-2; (online) 978-0-7714-2659-9.

(19) Jordan Black, Subhankar Karmakar and Slobodan P. Simonovic (2007). A Web-Based Flood Information System. Water Resources Research Report no. 056, Facility for Intelligent Decision Support, Department of Civil and Environmental Engineering, London, Ontario, Canada, 133 pages. ISBN: (print) 978-0-7714-2660-5; (online) 978-0-7714-2661-2.

(20) Angela Peck, Subhankar Karmakar and Slobodan P. Simonovic (2007). Physical, Economical, Infrastructural and Social Flood Risk – Vulnerability Analyses in GIS. Water Resources Research Report no. 057, Facility for Intelligent Decision Support, Department of Civil and Environmental Engineering, London, Ontario, Canada, 80 pages. ISBN: (print) 978-0- 7714-2662-9; (online) 978-0-7714-2663-6.

(21) Predrag Prodanovic and Slobodan P. Simonovic (2007). Development of Rainfall Intensity Duration Frequency Curves for the City of London Under the Changing Climate. Water Resources Research Report no. 058, Facility for Intelligent Decision Support, Department of Civil and Environmental Engineering, London, Ontario, Canada, 51 pages. ISBN: (print) 978-0- 7714-2667-4; (online) 978-0-7714-2668-1.

(22) Evan G. R. Davies and Slobodan P. Simonovic (2008). An integrated system dynamics model for analyzing behaviour of the social-economic-climatic system: Model description and model use guide. Water Resources Research Report no. 059, Facility for Intelligent Decision Support, Department of Civil and Environmental Engineering, London, Ontario, Canada, 233 pages. ISBN: (print) 978-0-7714-2679-7; (online) 978-0-7714-2680-3.

(23) Vasan Arunachalam (2008). Optimization Using Differential Evolution. Water Resources Research Report no. 060, Facility for Intelligent Decision Support, Department of Civil and Environmental Engineering, London, Ontario, Canada, 42 pages. ISBN: (print) 978-0-7714- 2689-6; (online) 978-0-7714-2690-2.

(24) Rajesh Shrestha and Slobodan P. Simonovic (2009). A Fuzzy Set Theory Based Methodology for Analysis of Uncertainties in Stage-Discharge Measurements and Rating Curve. Water Resources Research Report no. 061, Facility for Intelligent Decision Support, Department of Civil and Environmental Engineering, London, Ontario, Canada, 104 pages. ISBN: (print) 978-0-7714-2707-7; (online) 978-0-7714-2708-4.

(25) Hyung-Il Eum, Vasan Arunachalam and Slobodan P. Simonovic (2009). Integrated Reservoir Management System for Adaptation to Climate Change Impacts in the Upper Thames River Basin. Water Resources Research Report no. 062, Facility for Intelligent Decision Support, Department of Civil and Environmental Engineering, London, Ontario, Canada, 81 pages. ISBN: (print) 978-0-7714-2710-7; (online) 978-0-7714-2711-4.

(26) Evan G. R. Davies and Slobodan P. Simonovic (2009). Energy Sector for the Integrated System Dynamics Model for Analyzing Behaviour of the Social- Economic-Climatic Model. Water Resources Research Report no. 063. Facility for Intelligent Decision Support, Department of Civil and Environmental Engineering, London, Ontario, Canada. 191 pages. ISBN: (print) 978-0-7714-2712-1; (online) 978-0-7714-2713-8.

(27) Leanna King, Tarana Solaiman, and Slobodan P. Simonovic (2009). Assessment of Climatic Vulnerability in the Upper Thames River Basin. Water Resources Research Report no. 064, Facility for Intelligent Decision Support, Department of Civil and Environmental Engineering, London, Ontario, Canada, 61pages. ISBN: (print) 978-0-7714-2816-6; (online) 978-0-7714- 2817-3.

(28) Slobodan P. Simonovic and Angela Peck (2009). Updated Rainfall Intensity Duration Frequency Curves for the City of London under Changing Climate. Water Resources Research Report no. 065, Facility for Intelligent Decision Support, Department of Civil and Environmental Engineering, London, Ontario, Canada, 64pages. ISBN: (print) 978-0-7714-2819-7; (online) 987-0-7714-2820-3.

(29) Leanna King, Tarana Solaiman, and Slobodan P. Simonovic (2010). Assessment of Climatic Vulnerability in the Upper Thames River Basin: Part 2. Water Resources Research Report no. 066, Facility for Intelligent Decision Support, Department of Civil and Environmental Engineering, London, Ontario, Canada, 72pages. ISBN: (print) 978-0-7714-2834-0; (online) 978-0-7714-2835-7.

(30) Christopher J. Popovich, Slobodan P. Simonovic and Gordon A. McBean (2010).Use of an Integrated System Dynamics Model for Analyzing Behaviour of the Social-Economic-Climatic System in Policy Development. Water Resources Research Report no. 067, Facility for Intelligent Decision Support, Department of Civil and Environmental Engineering, London, Ontario, Canada, 37 pages. ISBN: (print) 978-0-7714-2838-8; (online) 978-0-7714-2839-5.

(31) Hyung-Il Eum and Slobodan P. Simonovic (2009). City of London: Vulnerability of Infrastructure to Climate Change; Background Report 1 – Climate and Hydrologic Modeling.

Water Resources Research Report no. 068, Facility for Intelligent Decision Support, Department of Civil and Environmental Engineering, London, Ontario, Canada, 102pages. ISBN: (print) 978-0-7714-2844-9; (online) 978-0-7714-2845-6.

(32) Dragan Sredojevic and Slobodan P. Simonovic (2009). City of London: Vulnerability of Infrastructure to Climate Change; Background Report 2 – Hydraulic Modeling and Floodplain Mapping. Water Resources Research Report no. 069, Facility for Intelligent Decision Support, Department of Civil and Environmental Engineering, London, Ontario, Canada, 147 pages. ISBN: (print) 978-0-7714-2846-3; (online) 978-0-7714-2847-0.

(33) Tarana A. Solaiman and Slobodan P. Simonovic (2011). Quantifying Uncertainties in the Modelled Estimates of Extreme Precipitation Events at the Upper Thames River Basin. Water Resources Research Report no. 070, Facility for Intelligent Decision Support, Department of Civil and Environmental Engineering, London, Ontario, Canada, 167 pages. ISBN: (print) 978-0-7714-2878-4; (online) 978-0-7714-2880-7.

(34) Tarana A. Solaiman and Slobodan P. Simonovic (2011). Assessment of Global and Regional Reanalyses Data for Hydro-Climatic Impact Studies in the Upper Thames River Basin. Water Resources Research Report no. 071, Facility for Intelligent Decision Support, Department of Civil and Environmental Engineering, London, Ontario, Canada, 74 pages. ISBN: (print) 978-0-7714-2892-0; (online) 978-0-7714-2899-9.

(35) Tarana A. Solaiman and Slobodan P. Simonovic (2011). Development of Probability Based Intensity-Duration-Frequency Curves under Climate Change. Water Resources Research Report no. 072, Facility for Intelligent Decision Support, Department of Civil and Environmental Engineering, London, Ontario, Canada, 89 pages. ISBN: (print) 978-0-7714-2893-7; (online) 978-0-7714-2900-2.

(36) Dejan Vucetic and Slobodan P. Simonovic (2011). Water Resources Decision Making Under Uncertainty. Water Resources Research Report no. 073, Facility for Intelligent Decision Support, Department of Civil and Environmental Engineering, London, Ontario, Canada, 143 pages. ISBN: (print) 978-0-7714-2894-4; (online) 978-0-7714-2901-9.

(37) Angela Peck, Elisabeth Bowering and Slobodan P. Simonovic (2010). City of London: Vulnerability of Infrastructure to Climate Change, Final Report - Risk Assessment. Water Resources Research Report no. 074, Facility for Intelligent Decision Support, Department of Civil and Environmental Engineering, London, Ontario, Canada, 66 pages. ISBN: (print) 978-0-7714-2895-1; (online) 978-0-7714-2902-6.

(38) Akhtar, M. K., S. P. Simonovic, J. Wibe, J. MacGee, and J. Davies, (2011). An integrated system dynamics model for analyzing behaviour of the social-energy-economic-climatic system:

User's Manual. Water Resources Research Report no. 076, Facility for Intelligent Decision Support, Department of Civil and Environmental Engineering, London, Ontario, Canada, 161 pages. ISBN: (print) 978-0-7714-2897-5; (online) 978-0-7714-2904-0.